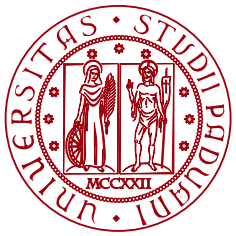

UNIVERSITÀ
DEGLI STUDI
DI PADOVA

DEPARTMENT OF PHYSICS AND ASTRONOMY "GALILEO GALILEI"
Master Degree in Astrophysics and Cosmology

MASTER'S THESIS

Measurement of the anisotropic gravitational wave background with a network of ground-based detectors

Candidate:
Giorgio Mentasti
Student ID 1238278

Thesis advisor:
Prof. Marco Peloso

Thesis co-advisor:
Prof. Carlo R. Contaldi

Academic year 2020-2021
22 September 2021

Colophon

This document was typeset in URW Palladio 11pt using LaTeX. The typographical style is modelled after ArsClassica and inspired to The Elements of Typographic Style by Robert Bringhurst. The cover page was made using the frontespizio package by Enrico Gregorio. The bibliography was produced with Biber.

Mail: giorgio.mentasti@studenti.unipd.it

Abstract

In this thesis we study how to measure the anisotropies of the Stochastic Gravitational Wave Background (SGWB) with a network of ground-based detectors. In particular, we investigate how to correlate measurements at planned third-generation gravitational wave detectors, such as Einstein Telescope, Cosmic Explorer, and a third generation of the LIGO detectors, to measure the coefficients of an expansion in spherical harmonics of the SGWB arriving from divergent directions of our sky. We also study the possibility of measuring different polarisations of the SGWB.

Contents

Introduction

Scientific interest in Gravitational Wave Background

On 14 September 2015, the Laser Interferometer Gravitational-wave Observatory (LIGO) and the Virgo collaboration made the first direct detection of a gravitational wave (GW) signal sourced by a binary black hole merger, named *GW150914* [1]. This event came after a huge experimental effort of more than 50 years and about one hundred years after Einstein's first theoretical prediction. From that day, further observations and technological improvements led to an enrichment of the sample of GW detections. Soon the Japanese interferometer KAGRA joined the network, giving an important contribution to this newborn field of physics and other instruments are planned to be built in the next years. Gravitational wave astronomy has proved firstly to be an effective tool to investigate the astrophysics of compact objects evolutions, providing information on mass and spin parameters. Once we will own a set of measurements rich enough, we will we able also to have a better understanding of compact objects formation and to constrain several models of star evolution, since, as we know, astrophysical compact objects are the results of the last stages of a stellar life.

However, we expect GWs not to bring precious information just from the astrophysical perspective. In fact, the expected signals coming from compact objects mergers are excellent tests of General relativity, since the merging waveforms (i.e. the shape of the GW amplitude in time) are well known from Einstein theory. As a second important cosmological aspect of interest in this field of research, gravitational waves can also give an independent estimate of the Hubble rate H_0 value, strongly constraining several theoretical models. Furthermore, GWs are coupled with matter only via gravitational interaction, therefore being very weekly coupled with all the content of the universe (gravitation is the weakest among fundamental interactions). On one hand, this makes their detection very hard (so hard that it took a century to see them for the first time), but on the other hand for this reason all the GWs basically free stream from the source, without experiencing substantial alterations during their travel towards us. This means that GWs originated by early universe events (which we expect to exist from cosmology) may bring a faithful snapshot of the first stages of the universe history. These events are expected to be undetectable as single events like *GW150914* since they happened at extremely high redshift and therefore very weak in amplitude: we can only study the statistical properties of signal resulting from the superposition of all the primordial GW sources as a whole. This signal is what we call the Stochastic Gravitational Wave Background (SGWB).

We expect the SGWB background to be constituted by a cosmological and an astrophysical

primordial component. Among the cosmological sources, the amplification of quantum vacuum fluctuations during inflation is expected to be at an undetectable level for 3G detectors. However, several other mechanisms related to inflation could produce a detectable signal. [2, 3]. Other cosmological sources of the SGWB include pre-big-bang models, phase transitions, and topological defects (see [4] for a review). The astrophysical component originates instead from the superposition of a large number of unresolved sources that are too weak to be detected individually. In the frequency range probed by ground-based detectors, the strongest astrophysical SGWB is expected to be one due to the coalescence of black holes and neutron star binaries.

The most immediate step to disentangle the cosmological and astrophysical components of the SGWB is through the spectral dependence of its average (monopole) amplitude. Beside this, crucial information will be contained in its directionality dependence. The angular anisotropies (namely, the difference between the SGWB from any given direction, and the average monopole value) provide information about the angular distribution of the astrophysical sources [5] and might also become a tool to trace astrophysical or cosmological structures [6]. Anisotropies in the astrophysical background correlate with the Large Scale Structure distribution, due to both how the GW originate and on how they propagate to arrive to Earth [7]. Anisotropies in the cosmological component can also be inherent in their production mechanism [8, 9] or originate from the GW propagation in the perturbed cosmological background [10, 11]. This might also imprint a non-Gaussian statistics to the cosmological SGWB angular anisotropies, so that the SGWB might also be a new probe of primordial non-Gaussianity [11]. To characterize the anisotropies, one typically decomposes the SGWB in spherical harmonics $Y_{\ell m}$ (in one given chosen fixed cosmological frame), and then study the correlation between different multipoles of this decomposition.

Ground based detectors for gravitational waves detection

So far, the current network of GW experiments proved the existence of a SGWB. However, its observation has been the object of several studies concerning its possible detection by GW ground-based [12, 13], space-based [14] interferometry and PTA [15]. This thesis work is aimed to provide a general methodology to study an anisotropic SGWB with a network of ground-based detectors, taking into account the possibility to observe a polarized background, i.e. where the production of gravitational waves is not chiral symmetric.

A ground based detector is made of an Michelson-like interferometer, whose interference pattern can be affected by the presence of a gravitational wave signal. When a gravitational wave comes to the detector, its arm length shows a variation in time, accordingly to the frequency of the incoming gravitational wave. Therefore the resulting interference pattern varies periodically: the characterization of this interference pattern variation brings information

about the original gravitational signal. A possible design for a gravitational wave detector is the L-shaped, schematized in figure 1. In this case we have the two perpendicular arms travelled by two different light beams, which interfere in proximity of the photodetector. The two LIGOs, Virgo and KAGRA interferometers are L-shaped instruments.

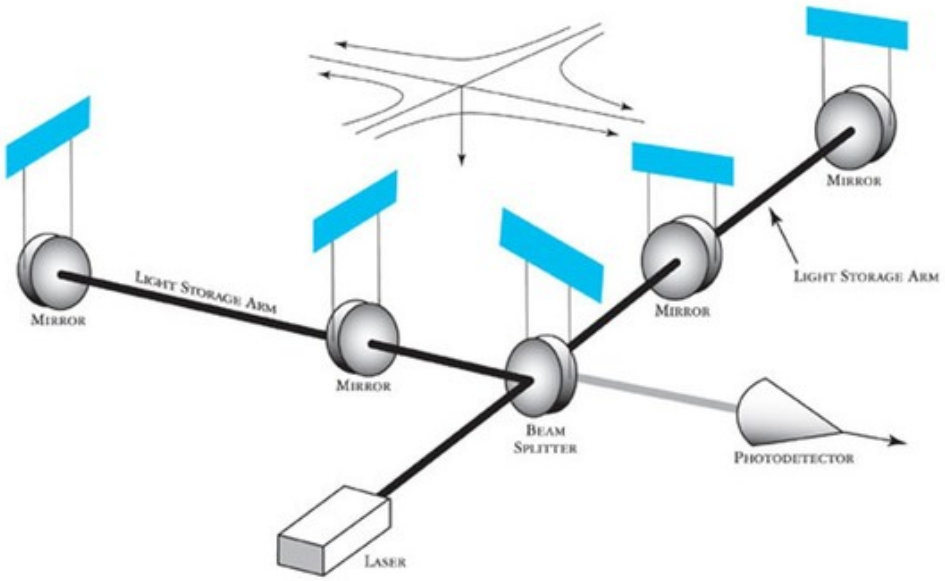

Figure 1: Scheme of an L-shaped gravitational wave interferometer. Image taken from the LIGO webpage: https://www.ligo.caltech.edu/page/what-is-interferometer

Another possibility to build a GW detector is the triangular-shaped configuration, obtained by superimposing three different Michelson-like interferometers, with an angle of 60° between their arms, in such a way that each couple of interferometers shares one of their two arm lengths. The configuration is schematized in figure 2 for Einstein Telescope (ET), which will be built as a triangular-shaped instrument.

Ref. [12] developed a formalism for the response to the anisotropic and unpolarized SGWB of two L-shaped detectors that are bound to the surface of the Earth, and that therefore have a regular scan pattern related to the daily rotation of our planet. The authors choose to expand the anisotropies in spherical harmonics and study the response of the two LIGO interferometers to the multipolar contributions of the SGWB, computing the SNR of this network. On the other hand, in [17] a useful formalism for the study of a polarized anisotropic background with two L-shaped detectors has been introduced.

The aim of this thesis work is to make advantage of the formalism introduced in [17] and extend the treatment of [12] to a more general level. The first improvement made by this work is to go beyond the hypothesis of an unpolarized background and to consider an asymmetry in polarizations of the SGWB, understanding how it can affect the detectability of the SGWB.

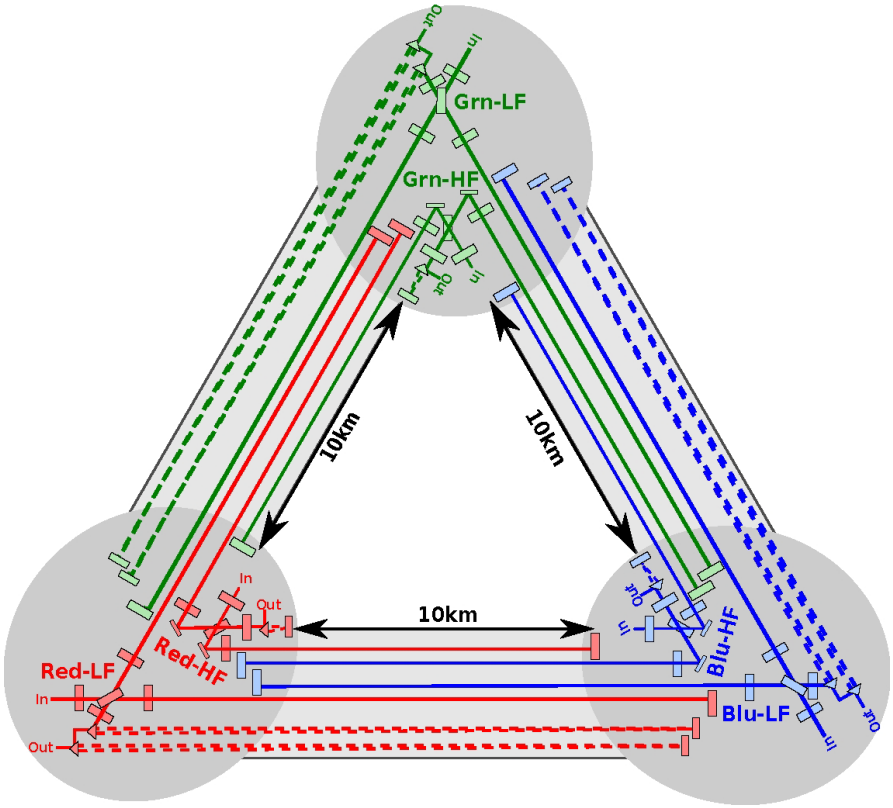

Figure 2: Scheme of an triangular-shaped gravitational wave interferometer, such as Einstein Telescope. The instrument is made of three Michelson-like interferometers (in figure, schematized in red, green and blue), which share an arm couple by couple. Image taken from [16]

As a second step, we generalize the results of [12] to a generic network of L-shaped and triangular-shaped detectors, while the authors considered just the two LIGO interferometers. Furthermore, we are able to provide explicit calculations for the response to the monopole, the dipole and the quadrupole of the spherical harmonics expansion for a network made of the two Advanced LIGOs, Advanced Virgo, KAGRA and Einstein Telescope (ET). In doing this we make advantage of the formalism introduced in [17] which provide analytic expressions useful for the computation to the response of two interferometers to the monopolar and the dipolar component of the SGWB. As a last improvement, we provide the analogous expressions aforementioned also for the quadrupolar component. As a last step, we study the response of the hypothetical network of two identical ET-like instruments to this SGWB. This network has been studied in [18], where an unpolarized SGWB has been considered and, thanks to the short distance between the instruments considered, further assumptions has been introduced: we show that our results agree with the ones of that paper.

Plan of the work

The plan of the thesis work is the following. In section 1 we introduce the fundamental quantities involved in the study of the SGWB, making assumptions on its power spectrum. In section 2 we study the data stream on a network of ground based detectors, which is influenced by both the action of gravitational waves and their noise. In section 3 we define what our signal is and we explain which are the conditions necessary to a SGWB to be detected by a generic network of ground based interferometers. In section 4 we apply the results of the previous section to a network made of the two Advanced LIGOs, Advanced Virgo, KAGRA and Einstein Telescope (ET). In section 5 we study an hypothetical network of two identical ETs located in the two sites currently under consideration for the building of the instrument. This section summarizes the publication [18]. In section 6 we present our conclusions. In appendix A we derive some useful properties of the GW polarization operators. Appendix B shows all the steps necessary to prove the results of section 3. In Appendix C we show that all odd terms in Φ do not contribute to the correlators that we have computed in section 5, so that the results of this section are corrected only to $O\left(|\Phi|^2\right)$. Appendix D provides the explicit analytical writing of the response functions introduced in section 3. Finally, In Appendix F we present the details of the analytic computation of the overlap functions in the small frequency regime.

Chapter 1

The stochastic gravitational wave background

We consider gravitational waves at the location of the detectors as small perturbations of the metric tensor on a Minkowski background, in such a way that

$$g_{\mu\nu}(x^\alpha) = \eta_{\mu\nu} + h_{\mu\nu}(x^\alpha) \tag{1.1}$$

where $\eta_{\mu\nu}$ is the (mostly positive signature) metric tensor for Minkowski spacetime and $h_{\mu\nu}$ the gravitational wave. Under our assumptions of weak perturbations of the metric

$$h \ll \eta \tag{1.2}$$

We move to traceless transverse gauge ($\partial_\mu h^{\mu\nu} = h^\mu_\mu = 0$) and solve the Einstein equations in the vacuum for this metric tensor, obtaining the plane wave solutions

$$\begin{aligned} h_{ab}(t, \boldsymbol{x}) &= \int_{-\infty}^{\infty} df \int d^2\hat{n}\, e^{2\pi i f(t - \hat{n}\cdot\boldsymbol{x})} \sum_{s=+,\times} h_s(f, \hat{n})\, e^s_{ab}(\hat{n}) = \\ &\equiv \sum_s h_{ab,s}(t, \boldsymbol{x}) \end{aligned} \tag{1.3}$$

where $\hat{n}$ is the unit vector in R^3, and $e^+_{ab}(\hat{n})$, $e^\times_{ab}(\hat{n})$ the two polarization tensors, defined by

$$e^+_{ab}(\hat{n}) = p_a p_b - q_a q_b \tag{1.4}$$

$$e^\times_{ab}(\hat{n}) = p_a q_b + q_a p_b \tag{1.5}$$

where

$$\hat{n} = \cos\varphi \sin\theta \hat{x} + \sin\varphi \sin\theta \hat{y} + \cos\theta \hat{z} \tag{1.6}$$

is the direction of propagation of the plane wave (θ, φ are polar angular coordinates, while $\hat{x}, \hat{y}, \hat{z}$ are unit vectors along the three Cartesian axes), while $\hat{p}$ and $\hat{q}$ are two directions perpendicular

to $\hat{n}$ and to each other, that are conventionally chosen as in [12]

$$\hat{p} = \sin\varphi\hat{x} - \cos\varphi\hat{y} \tag{1.7}$$

$$\hat{q} = \cos\varphi\cos\theta\hat{x} + \sin\varphi\cos\theta\hat{y} - \sin\theta\hat{z} \tag{1.8}$$

One can also consider left-handed and right-handed polarizations starting with $+$ and $\times$ polarization tensors (see Appendix A for more details) and rewrite (1.3) as

$$h_{ab}(t,\boldsymbol{x}) = \int_{-\infty}^{\infty} df \int d^2\hat{n}\, e^{2\pi i f(t-\hat{n}\cdot\boldsymbol{x})} \sum_{\lambda=R,L} h_\lambda(f,\hat{n})\, e^{\lambda}_{ab}(\hat{n}) \tag{1.9}$$

The plane wave solution of equation (1.9) is defined in a reference system fixed with respect to the cosmological fluid and in which the spatial pattern of the perturbations of the stochastic background is assumed to be statistically time-independent. The $\hat{z}$ vector of this system is chosen to point along the direction of the earth rotation axis. To describe a stochastic source, we treat the complex amplitude $h_\lambda(f,\hat{n})$ as a random Gaussian variable with zero mean and with statistics therefore completely specified by its variance. The dependence of the stochastic background on frequency and direction may be stated therefore in terms of the expectation value of the two point correlator for the random variable $h_\lambda(f,\hat{n})$ as

$$\left\langle h^*_\lambda(f,\hat{n})\, h_{\lambda'}\left(f'\hat{n}'\right)\right\rangle = \delta_{\lambda\lambda'}\delta^{(2)}_D\left(\hat{n}-\hat{n}'\right)\delta_D\left(f-f'\right)\mathcal{H}_\lambda\left(|f|,\hat{n}\right) \tag{1.10}$$

where $\delta^{(2)}_D\left(\hat{n}-\hat{n}'\right)$ is a covariant two-dimensional Dirac delta-function on the unit two-sphere and $\delta_D\left(f-f'\right)$ the Dirac delta function on the frequency space.

In principle, such a source has spectral properties which depends upon amplitude and frequency in an arbitrary way. For simplicity in this work we consider a factorized dependence

$$\mathcal{H}_\lambda\left(|f|,\hat{n}\right) = H_\lambda\left(|f|\right)P_\lambda\left(\hat{n}\right) \tag{1.11}$$

which amounts in assuming that sources of the SGWB situated along different line of sights emit with the same "average" spectrum in frequency.

1.1 – ENERGY DENSITY AND SPECTRUM

We know that gravitational waves have an average energy density (see [19])

$$\rho_{GW,\lambda} = \frac{c^2}{32\pi G}\langle \dot{h}^*_{ab,\lambda}\dot{h}^{ab,\lambda}\rangle \tag{1.12}$$

To compute it, we start from (1.9) taking its time derivative:

$$\dot{h}_{ab,\lambda}(t,\boldsymbol{x}) = 2\pi i \int_{-\infty}^{\infty} df \int_{S^2} d\hat{\Omega} f e^{2\pi i f(t-\hat{\Omega}\cdot\boldsymbol{x}/c)} h_\lambda(f,\hat{\Omega}) e^{\lambda}_{ab}(\hat{\Omega}) \tag{1.13}$$

and using (1.10), combined with the fact that the trace of each polarization matrix defined in (1.4) is equal to 2, we obtain

$$\begin{aligned}\langle \dot{h}^{*}_{ab,\lambda}(t,\boldsymbol{x}) \dot{h}^{ab,\lambda}(t,\boldsymbol{x})\rangle =& 4\pi^2 \int_{-\infty}^{\infty} df \int_{S^2} d\hat{\Omega} f e^{-2\pi i f(t-\hat{\Omega}\cdot\boldsymbol{x}/c)} e^{*\lambda}_{ab}(\hat{\Omega}) \\ & \int_{-\infty}^{\infty} df' \int_{S^{2,\prime}} d\hat{\Omega}' f' e^{2\pi i f'(t-\hat{\Omega}'\cdot\boldsymbol{x}/c)} e^{\lambda,ab}(\hat{\Omega}') \langle h_\lambda(f,\hat{\Omega}) h_\lambda(f',\hat{\Omega}')\rangle \\ =& 16\pi^2 \int_{S^2} d\hat{\Omega} P_\lambda(\hat{\Omega}) \int_0^{\infty} df f^2 H_\lambda(|f|)\end{aligned} \tag{1.14}$$

From Friedmann equations we know that the critical density assumes the following expression:

$$\rho_{crit} = \frac{3c^2 H_0^2}{8\pi G} \tag{1.15}$$

where H_0 is the Hubble rate. We define the fractional energy density in GW per logarithmic frequency interval and per polarisation as

$$\Omega^{\lambda}_{GW}(f) \equiv \frac{f}{\rho_{crit}} \frac{d\rho_{GW,\lambda}}{df} \tag{1.16}$$

and using (1.14) with (1.12) we obtain

$$\Omega^{\lambda}_{GW}(f) = \frac{4\pi^2}{3H_0^2} f^3 H_\lambda(|f|) \int d\hat{\Omega} P_\lambda(\hat{\Omega}) \tag{1.17}$$

Next, we decompose the angular power spectrum in terms of spherical harmonics, writing it as:

$$P_\lambda(\hat{\Omega}) = \sum_{\ell=0}^{+\infty} \sum_{m=-\ell}^{\ell} p_{lm,\lambda} Y_{lm}(\hat{\Omega}) \quad , \quad p_{00,\lambda} = \sqrt{4\,\pi} \tag{1.18}$$

where the value of $p_{00.\lambda}$ is set considering the convention for the monopole $Y_{00} = \frac{1}{\sqrt{4\pi}}$. The monopole only contributes to the energy density budget, and therefore

$$\Omega^{\lambda}_{GW}(f) = \frac{16\pi^3}{3H_0^2} f^3 H_\lambda(|f|) \quad \Rightarrow \quad H_\lambda(|f|) = \frac{3\,H_0^2\,\Omega^{\lambda}_{GW}(|f|)}{16\,\pi^3\,f^3} \tag{1.19}$$

The total SGWB energy density is obtained by summing (1.13) over the two polarisations. From it, one defines the fractional energy density in GW per logarithmic frequency interval

$$\rho_{GW} = \frac{c^2}{32\pi G}\langle \dot{h}_{ab}\dot{h}^{ab}\rangle \qquad\qquad \Omega_{GW}(f) \equiv \frac{f}{\rho_{crit}}\frac{d\rho_{GW}}{df} = \sum_{\lambda}\frac{f}{\rho_{crit}}\frac{d\rho_{GW,\lambda}}{df} \tag{1.20}$$

Therefore

$$\rho_{GW} = \sum_{\lambda}\rho_{GW,\lambda} \qquad\qquad \Omega_{GW}(f) = \sum_{\lambda}\Omega_{GW,\lambda} \tag{1.21}$$

using (1.10) and (1.19) we can then write

$$\Omega_{GW}(f) = \frac{16\pi^3}{3H_0^2}f^3\sum_{\lambda}H_{\lambda}(|f|) \tag{1.22}$$

Assuming a symmetric background, i.e. $H_R(|f|) = H_L(|f|) \equiv H(|f|)$, the last expression becomes

$$\Omega_{GW}(f) = \frac{32\pi^3}{3H_0^2}f^3 H(|f|) \tag{1.23}$$

Chapter 2

Data stream on ground based interferometers and their noise model

For the aim of this thesis, we consider a network of N L-shaped ground based detectors (as for instance LIGO, Virgo and KAGRA) and M ground based detectors with triangular configuration (as for instance Einstein Telescope). For each L-shaped interferometer of the network, we measure the difference ΔT of the time required by light to complete a return light across one interferometer arm and that to complete a return flight across the other arm. The measurement is affected by the instrument noise and possibly by a signal,

$$m_i(t) = \frac{\Delta T_i}{T_0} = n_i(t) + s_i(t) \quad , \quad i = 1, \dots, N \tag{2.1}$$

where T_0 is the time needed for a return flight in absence of signal and noise (namely, twice the unperturbed arm length).

In a similar fashion we can define the set of measurements made by each triangular-shaped interferometer of the network. In this case, each triangular detector has an equilateral triangular configuration with three Michelson interferometers at its vertices $\alpha = X, Y, Z$, therefore

$$m_{i\alpha}(t) = \frac{\Delta T_{i\alpha}}{T_0} = n_{i\alpha}(t) + s_{i\alpha}(t) \quad , \quad i = 1, \dots, M \quad , \quad \alpha = X, Y, Z \tag{2.2}$$

We then make the crucial assumption that the noise of each instrument of the network is not correlated with the one present in the others. We then assume that the noise of each detector is Gaussian with zero mean.

These assumptions imply a vanishing correlation between L-shaped and triangular-shaped detectors

$$\left\langle \tilde{n}^*_{i\alpha}(f)\, \tilde{n}_j(f') \right\rangle \equiv 0 \tag{2.3}$$

where $i = 1, \dots, M$ and $j = 1, \dots, N$. For the L-shape detectors, we can then write

$$\left\langle \tilde{n}^*_i(f)\, \tilde{n}_j(f') \right\rangle \equiv \frac{\delta_{ij}}{2} \delta_D(f - f')\, P_i(|f|) \tag{2.4}$$

where $i = 1, \dots, N$ and $j = 1, \dots, N$ and we assume that our noise is Gaussian with zero mean.

For what instead concerns the variance of the noise of the triangular-shaped detectors, due

to the fact that every interferometer shares one arm with each of the other two interferometers (of the same detector), we write

$$\left\langle \tilde{n}^*_{i\alpha}\left(f\right)\tilde{n}_{j\beta}\left(f'\right)\right\rangle \equiv \frac{\delta_{ij}}{2}\delta_D\left(f-f'\right)N_{\alpha\beta,i}\left(|f|\right) \tag{2.5}$$

where $i = 1,\ldots,M$, $j = 1,\ldots,M$. In the limit in which the i-th detector has an exact equilateral configuration, with identical instruments at the three vertices, the noise correlation matrix at each site is formally of the type

$$N_{\alpha\beta,i} = \begin{pmatrix} N_{d,i} & N_{o,i} & N_{o,i} \\ N_{o,i} & N_{d,i} & N_{o,i} \\ N_{o,i} & N_{o,i} & N_{d,i} \end{pmatrix} \tag{2.6}$$

This matrix can be diagnalized by the three channels

$$\begin{aligned} m_{iA} &\equiv \frac{2}{3\sqrt{3}}\left(2m_{iX}-m_{iY}-m_{iZ}\right) \\ m_{iE} &\equiv \frac{2}{3}\left(m_{iZ}-m_{iY}\right) \\ m_{iT} &\equiv \left(\frac{2}{3}\right)^{3/2}\left(m_{iX}+m_{iY}+m_{iZ}\right) \end{aligned} \tag{2.7}$$

These linear combinations were introduced in [20] for the LISA experiment, that has also an equilateral configuration (the explicit frequency dependence of $N_{d,i}$ and $N_{o,i}$ for LISA can be found for example in ref. [21]). More precisely, we change the normalization of each channel with respect to [20], so that the $A-$ and $E-$channels behave as 90° degrees interferometers at small frequency, with arm factors $d^{ab}_{iA,E}$ having a standard normalization, see eq. (E.5). The redefinition (2.7) can be written

$$m_{iO} = c_{O\alpha}\, m_{i\alpha} \quad , \quad c \equiv \begin{pmatrix} \frac{4}{3\sqrt{3}} & -\frac{2}{3\sqrt{3}} & -\frac{2}{3\sqrt{3}} \\ 0 & -\frac{2}{3} & \frac{2}{3} \\ \left(\frac{2}{3}\right)^{3/2} & \left(\frac{2}{3}\right)^{3/2} & \left(\frac{2}{3}\right)^{3/2} \end{pmatrix} \tag{2.8}$$

where the index O scans the three channels A, E, T, and where we stress that the same combinations $c_{O\alpha}$ are taken in each detector. Combining eqs. (2.5) and (2.7) one obtains

$$\left\langle \tilde{n}^*_{iO}\left(f\right)\tilde{n}_{jO'}\left(f'\right)\right\rangle = \frac{1}{2}\delta_D\left(f-f'\right)\,\delta_{ij}\,\delta_{OO'}\,N_{O,i}\left(|f|\right) \tag{2.9}$$

with

$$N_{A,i}\left(f\right) = N_{E,i}\left(f\right) = \frac{8}{9}\left[N_{d,i}\left(f\right)-N_{o,i}\left(f\right)\right] \qquad N_{T,i}\left(f\right) = \frac{8}{9}\left[N_{d,i}\left(f\right)+2N_{o,i}\left(f\right)\right] \tag{2.10}$$

We use these channels in this work, as they diagonalize the noise matrix, and this simplifies the computation of the SNR that we perform below. As already remarked, and as we explicitly verify in Section 5.2, the $A-$ and $E-$channels behave as 90° interferometers in the small frequency regime (which, as we show below, is the relevant one for the correlators that we are computing). Moreover, in the small frequency regime the $T-$channel vanishes, so we disregard it in our computations.

The discussion so far in this chapter assumed generic L-shaped and triangularly shaped detectors, with noise specified by eqs. (2.4), (2.3) and (2.5). Here we specify the noise model for the instruments that we consider in our analysis.

For what concerns the triangularly shaped detectors, we consider a noise model according to that of the proposed Einstein Telescope (ET). From the literature, we are aware of a computation of the ET sensitivity under the assumption that ET is a single 90° interferometer [22](that, as we remarked, is appropriate for the A and E channels in the small frequency limit). We show the sensitivity curve of [22] in Figure 3.

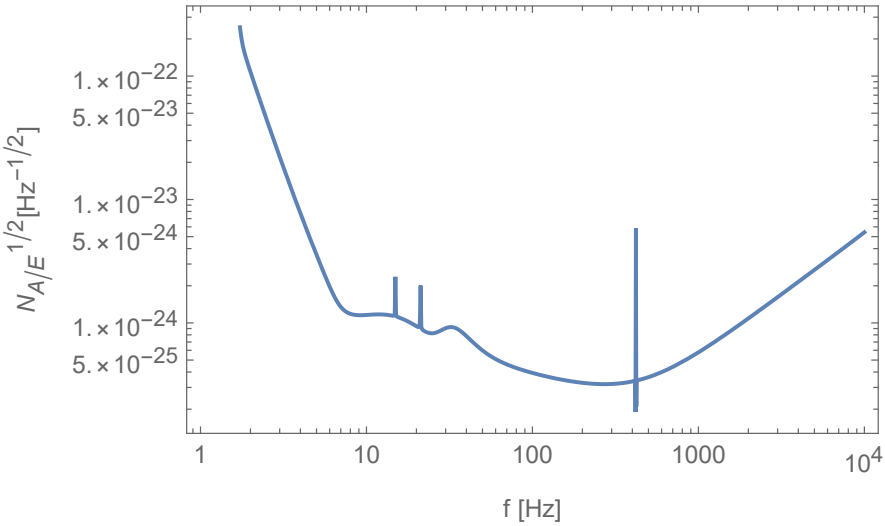

FIGURE 3: Predicted Power Spectral Density (PSD) of ET with data stored in [22]. On y axis we plot the square root of the PSD accordingly to (2.10), while on x axis we plot the frequency scale.

For what concerns instead the L-shaped detectors, we consider the noise functions of Advanced LIGO, Advanced Virgo and of KAGRA as in [23]. We show these functions in Figure 4

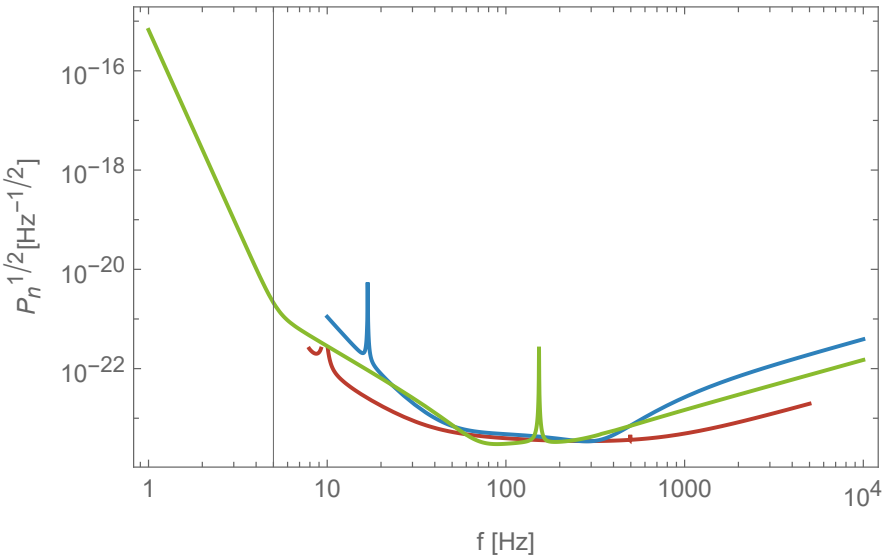

FIGURE 4: Predicted Power Spectral Density (PSD) of Advanced LIGO (red curve), Advanced Virgo (blue curve) and KAGRA (green curve), based on data stored in [23]. On y axis we plot the square root of the PSD, accordingly to (2.6), while on x axis we plot the frequency scale.

Chapter 3

Measurement in a network of interferometers

We proceed as in ref. [12], that studied the sensitivity of an Earth-based detector to a directionality dependent SGWB, introducing the time-dependent Fourier transform of (2.1) for L-shaped interferometers

$$\tilde{m}_i(f, t) = \int_{t-\tau/2}^{t+\tau/2} dt' e^{-2\pi i f t'} m_i(t') \tag{3.1}$$

Analogously, for triangular-shaped interferometers from the linear combinations (2.7) of the measurements (2.2) at the three vertices, we can define

$$\tilde{m}_{iO}(f, t) = \int_{t-\tau/2}^{t+\tau/2} dt' e^{-2\pi i f t'} m_{iO}(t') \tag{3.2}$$

where the integration is done on a timescale τ much greater than the inverse of the smallest frequency that we want to study, but sufficiently small that we can disregard the rotation of the Earth in this time. We introduce the Fourier transforms of the signals $\tilde{s}_{iO}$, $\tilde{s}_j$, and of the noises $\tilde{n}_{iO}$, $\tilde{n}_j$ in an analogous manner.

We can then define the estimator

$$\begin{aligned} \mathcal{C}(t) \equiv \int_{-\infty}^{+\infty} df \sum_{i=1}^{M} \sum_{j=i+1}^{M} \sum_{O,O'} \tilde{m}^*_{i,O}(f, t)\, \tilde{m}_{j,O'}(f, t)\, \tilde{Q}_{ij,OO'}(f) + \\ + \sum_{i=1}^{M} \sum_{j=1}^{N} \sum_{O} \tilde{m}^*_{i,O}(f, t)\, \tilde{m}_j(f, t)\, \tilde{Q}_{ij,O}(f) + \\ + \sum_{i=1}^{N} \sum_{j=i+1}^{N} \sum_{O,O'} \tilde{m}^*_i(f, t)\, \tilde{m}_j(f, t)\, \tilde{Q}_{ij}(f) \end{aligned} \tag{3.3}$$

where the functions $\tilde{Q}_{ij,OO'}(f)$, $\tilde{Q}_{ij,O}(f)$ and $\tilde{Q}_{ij}(f)$ are weights (in the sum over channels, interferometers of the network, and frequencies) that will be chosen later to maximize the signal-to-noise-ratio (SNR). We have that

$$\int_{-\infty}^{+\infty} \tilde{m}_{i,O}(f, t)\, \tilde{m}^*_{j,O'}(f, t) = \int_{-\infty}^{+\infty} \tilde{m}^*_{i,O}(f, t)\, \tilde{m}_{j,O'}(f, t) \tag{3.4}$$

and identically for the other two terms, as immediately follows from the substitution $f \to -f$

in equations (3.1) and (3.2). Furthermore, (see appendix B for details) we find that

$$\begin{aligned} Q_{ij,OO'}(f) &= Q^*_{ij,OO'}(-f) \\ Q_{ij,O}(f) &= Q^*_{ij,O}(-f) \\ Q_{ij}(f) &= Q^*_{ij}(-f) \end{aligned} \tag{3.5}$$

which implies that the estimator in (3.3) is a real number. Note that in the definition of the estimator (3.3) we do not consider the correlations between instruments located at the same site. This is done because it is difficult to properly characterize all the noise contributions when the distance between the couple of the instruments is very little.

We assume that the statistical properties of the signal and the noise do not change with time. Then for an anisotropic SGWB, the statistics of the measurement is periodic, with periodicity given by the rotation period $T_e = \frac{2\pi}{\omega_e}$ of the Earth

$$\mathcal{C}(t) = \sum_{m=-\infty}^{\infty} \mathcal{C}_m \, \mathrm{e}^{im\omega_e t} \quad , \quad \mathcal{C}_m \equiv \frac{1}{T}\int_0^T dt \, \mathrm{e}^{-im\omega_e t}\, \mathcal{C}(t) \tag{3.6}$$

where we take the observation time T to be an integer multiple of one day T_e.

For each coefficient $\mathcal{C}_m$, we compute the signal-to-noise ratio

$$\mathrm{SNR}_m \equiv \frac{\langle \mathcal{C}_m \rangle}{\sqrt{\langle \mathcal{C}_m^2 \rangle}} \tag{3.7}$$

3.1 – EXPECTATION VALUE OF THE SIGNAL

In appendix B we show that the expectation value of (3.6) is

$$\begin{aligned} \langle C_m \rangle = \sum_\lambda \frac{8\pi\,\tau}{5} \int_{-\infty}^{+\infty} df\, H_\lambda(|f|) \sum_{\ell=|m|}^{\infty} p_{\ell m,\lambda} \Bigg[\sum_{i=1}^{M}\sum_{j=i+1}^{M} \sum_{O,O'} \gamma_{\ell m,ij,OO',\lambda}(f)\, Q_{ij,OO'}(f) + \\ + \sum_{i=1}^{M}\sum_{j=i+1}^{N} \sum_{O} \gamma_{\ell m,ij,O,\lambda}(f)\, Q_{ij,O}(f) + \sum_{i=1}^{N}\sum_{j=1}^{N} \gamma_{\ell m,ij,\lambda}(f)\, Q_{ij}(f) \Bigg] \equiv \\ \equiv \sum_\lambda \langle C_{m,\lambda} \rangle \end{aligned} \tag{3.8}$$

where we defined, in a similar way to what has been done in [12], the overlap functions [1]

$$\begin{aligned}
\gamma_{\ell m,ij,OO',\lambda}(f) &\equiv \frac{5}{8\pi}\int d^2\hat{n}\mathrm{e}^{2\pi i f\hat{n}\cdot\Delta\boldsymbol{x}_{ij}}\,Y_{\ell m}\left(\hat{n}\right)e^{*\lambda}_{ab}\left(\hat{n}\right)e^{\lambda}_{cd}\left(\hat{n}\right)\,d^{ab}_{iO}\,d^{cd}_{jO'}\\
\gamma_{\ell m,ij,O,\lambda}(f) &\equiv \frac{5}{8\pi}\int d^2\hat{n}\mathrm{e}^{2\pi i f\hat{n}\cdot\Delta\boldsymbol{x}_{ij}}\,Y_{\ell m}\left(\hat{n}\right)e^{*\lambda}_{ab}\left(\hat{n}\right)e^{\lambda}_{cd}\left(\hat{n}\right)\,d^{ab}_{iO}\,d^{cd}_{j}\\
\gamma_{\ell m,ij,\lambda}(f) &\equiv \frac{5}{8\pi}\int d^2\hat{n}\mathrm{e}^{2\pi i f\hat{n}\cdot\Delta\boldsymbol{x}_{ij}}\,Y_{\ell m}\left(\hat{n}\right)e^{*\lambda}_{ab}\left(\hat{n}\right)e^{\lambda}_{cd}\left(\hat{n}\right)\,d^{ab}_{i}\,d^{cd}_{j}
\end{aligned}\tag{3.9}$$

It is useful to rewrite the γ coefficients of equation (3.9) as

$$\begin{aligned}
\gamma_{\ell m,ij,OO',\lambda}(f) &\equiv \gamma_{\ell m,\lambda,abcd}(\kappa_{ij},\hat{s}_{ij})\times d^{ab}_{iO}\,d^{cd}_{jO'}\\
\gamma_{\ell m,ij,O,\lambda}(f) &\equiv \gamma_{\ell m,\lambda,abcd}(\kappa_{ij},\hat{s}_{ij})\times d^{ab}_{iO}\,d^{cd}_{j}\\
\gamma_{\ell m,ij,\lambda}(f) &\equiv \gamma_{\ell m,\lambda,abcd}(\kappa_{ij},\hat{s}_{ij})\times d^{ab}_{i}\,d^{cd}_{j}
\end{aligned}\tag{3.10}$$

where we define the tensor

$$\begin{aligned}
d^{ab}_{i\alpha} &\equiv \frac{\hat{u}^a_{i\alpha}\hat{u}^b_{i\alpha}-\hat{v}^a_{i\alpha}\hat{v}^b_{i\alpha}}{2}\\
d^{ab}_{j} &\equiv \frac{\hat{u}^a_{j}\hat{u}^b_{j}-\hat{v}^a_{j}\hat{v}^b_{j}}{2}
\end{aligned}\tag{3.11}$$

with $\hat{u}_{i\alpha}$, $\hat{v}_{i\alpha}$ the arm directions of the triangular-shaped interferometers and $\hat{u}_i$, $\hat{v}_i$ the arm directions of the L-shaped interferometers (defined in appendix B). We also defined

$$\kappa_{ij}=2\pi f\left|\Delta\boldsymbol{x}_{ij}\right|\quad,\quad\hat{s}_{ij}=\frac{\Delta\boldsymbol{x}_{ij}}{\left|\Delta\boldsymbol{x}_{ij}\right|}\tag{3.12}$$

with

$$\Delta\boldsymbol{x}_{ij}=\boldsymbol{x}_i-\boldsymbol{x}_j\tag{3.13}$$

and where

$$\gamma_{\ell m,\lambda,abcd}(\kappa,\hat{s})\equiv\frac{5}{8\pi}\int d^2\hat{n}\mathrm{e}^{i\kappa\hat{n}\cdot\hat{s}}\,Y_{\ell m}\left(\hat{n}\right)e^{*\lambda}_{ab}\left(\hat{n}\right)e^{\lambda}_{cd}\left(\hat{n}\right)\tag{3.14}$$

This decomposition is motivated by the fact that the coefficients (3.14) can be evaluated once for all, independently of the pair of detectors under consideration. In Appendix D we provide the explicit analytic expressions for the monopole, dipole, and quadrupole contributions[2], and we explain how this computation can be extended to higher multipoles.

[1] The factor $\frac{5}{8\pi}$ is conventional, and it has the purpose of eliminating the overall factor in the last of (A.1) in the monopole term.

[2] The expressions for the monopole and dipole can be found in [17], while the expression for the quadrupole is an original result of this thesis.

3.2 – VARIANCE OF THE NOISE AND SNR

We evaluate the denominator of eq. (3.7) under the assumption of a weak signal, namely assuming that the variance of the signal is negligible with respect to that of the noise. This assumption is valid if one is interested in obtaining the minimum signal that produces an SNR of order 1. After some algebraic steps shown in appendix B we find

$$\left\langle |\mathcal{C}_m|^2 \right\rangle = \frac{\tau^2}{4T} \int_{-\infty}^{+\infty} df \left[\sum_{i=1}^{M} \sum_{j=i+1}^{M} \sum_{OO'} N_{i,O}\left(|f|\right) N_{j,O'}\left(|f|\right) \left| Q_{ij,OO'}\left(f\right) \right|^2 + \right.$$
$$+ \sum_{i=1}^{M} \sum_{j=1}^{N} \sum_{O} N_{i,O}\left(|f|\right) P_j\left(|f|\right) \left| Q_{ij,O}\left(f\right) \right|^2 +$$
$$\left. + \sum_{i=1}^{N} \sum_{j=i+1}^{N} P_i\left(|f|\right) P_j\left(|f|\right) \left| Q_{ij}\left(f\right) \right|^2 \right] \tag{3.15}$$

Eventually, we insert eqs. (3.8) and (3.15) into the ratio (3.7), to obtain (see appendix B for further details)

$$\mathrm{SNR}_m = \left[\int_0^{\infty} df \Big(\sum_{i=1}^{M} \sum_{j=i+1}^{M} \sum_{OO'} \tilde{\gamma}_{ij,OO'}\left(f\right) \tilde{Q}_{ij,OO'}\left(f\right) + \sum_{i=1}^{M} \sum_{j=1}^{N} \sum_{O} \tilde{\gamma}_{ij,O}\left(f\right) \tilde{Q}_{ij,O}\left(f\right) + \right.$$
$$\left. + \sum_{i=1}^{N} \sum_{j=i+1}^{N} \tilde{\gamma}_{ij}\left(f\right) \tilde{Q}_{ij}\left(f\right) \Big) \right]^{\frac{1}{2}} \equiv \frac{16\pi\sqrt{2T}}{5} \sqrt{\int_0^{\infty} df R(f)} \tag{3.16}$$

where, after choosing the weight function in such a way as to maximize this expression (see Appendix B.3)

$$R\left(f\right) = \sum_{i=1}^{M} \sum_{j=i+1}^{M} \sum_{OO'} \frac{\left| \sum_{\lambda} H_{\lambda}\left(f\right) \sum_{\ell=|m|}^{\infty} p_{\ell m,\lambda}\, \gamma_{\ell m,ij,OO',\lambda}\left(f\right) \right|^2}{N_{i,O}\left(f\right) N_{j,O'}\left(f\right)} +$$
$$+ \sum_{i=1}^{M} \sum_{j=1}^{N} \sum_{O} \frac{\left| \sum_{\lambda} H_{\lambda}\left(f\right) \sum_{\ell=|m|}^{\infty} p_{\ell m,\lambda}\, \gamma_{\ell m,ij,O,\lambda}\left(f\right) \right|^2}{N_{i,O}\left(f\right) P_j\left(f\right)} +$$
$$+ \sum_{i=1}^{N} \sum_{j=i+1}^{N} \frac{\left| \sum_{\lambda} H_{\lambda}\left(f\right) \sum_{\ell=|m|}^{\infty} p_{\ell m,\lambda}\, \gamma_{\ell m,ij,\lambda}\left(f\right) \right|^2}{P_i\left(f\right) P_j\left(f\right)} \tag{3.17}$$

In the next chapter, we apply this result to the network of detectors introduced in the previous chapter.

Chapter 4

LIGO+Virgo+KAGRA+ET

In the following we consider a network constituted of the two Advanced LIGO interferometers in the two sites of Hanford and Livingston in USA, the Advanced Virgo interferometer near Cascina (Italy), KAGRA in Japan and ET, which we suppose to be located in the Sardinia site (coordinates 40.4°N; 9.45°E). This network is made of 4 L-shaped interferometers and one triangular-shaped. Therefore, we set N=4 and M=1[1].

For this network we have the following writing for the SNR from equation (3.16)

$$\begin{aligned}\mathrm{SNR}_m &= \left[\int_0^\infty df \left(\sum_{j=1}^{4}\sum_{O}\tilde{\gamma}_{1j,O}\,(f)\;\tilde{Q}_{1j,O}\,(f)+\sum_{i=1}^{4}\sum_{j=i+1}^{4}\tilde{\gamma}_{ij}\,(f)\;\tilde{Q}_{ij}\,(f)\right)\right]^{\frac{1}{2}}= \\ &= \frac{16\pi\sqrt{2T}}{5}\left[\int_0^\infty df\Big(\sum_{j=1}^{4}\sum_{O}\frac{\left|\sum_\lambda H_\lambda\,(f)\sum_{\ell=|m|}^{\infty}p_{\ell m,\lambda}\,\gamma_{\ell m,1j,O,\lambda}\,(f)\right|^2}{N_{1,O}\,(f)\,P_j\,(f)}+\right. \\ &\left.+\sum_{i=1}^{4}\sum_{j=i+1}^{4}\frac{\left|\sum_\lambda H_\lambda\,(f)\sum_{\ell=|m|}^{\infty}p_{\ell m,\lambda}\,\gamma_{\ell m,ij,\lambda}\,(f)\right|^2}{P_i\,(f)\,P_j\,(f)}\Big)\right]^{\frac{1}{2}}\end{aligned} \tag{4.1}$$

and after using (1.19)

$$\begin{aligned}\mathrm{SNR}_m &= \frac{3H_0^2\sqrt{2T}}{5\pi^2}\left[\int_0^\infty df\Big(\sum_{j=1}^{4}\sum_{O}\frac{\left|\sum_\lambda \Omega_{GW,\lambda}\,(f)\sum_{\ell=|m|}^{\infty}p_{\ell m,\lambda}\,\gamma_{\ell m,1j,O,\lambda}\,(f)\right|^2}{f^6\,N_{1,O}\,(f)\,Pj\,(f)}+\right. \\ &\left.+\sum_{i=1}^{4}\sum_{j=i+1}^{4}\frac{\left|\sum_\lambda \Omega_{GW,\lambda}\,(f)\sum_{\ell=|m|}^{\infty}p_{\ell m,\lambda}\,\gamma_{\ell m,ij,\lambda}\,(f)\right|^2}{f^6\,P_i\,(f)\,Pj\,(f)}\Big)\right]^{\frac{1}{2}}\end{aligned} \tag{4.2}$$

For definiteness, we identify Advanced LIGO-Hanford site as i=1, Advanced LIGO-Livingston as i=2 (which we assume to have the same PSD $P_1(f) = P_2(f)$), Virgo as i=3 (with PSD defined as $P_3(f)$) and KAGRA with i=4 (with PSD $P_4(f)$). We further assume that all multipoles of the SGWB anisotropies have the same degree of polarization. We implement this in eqs. (1.17) and

[1] In this chapter we will make also a comparison between the response of the present network to the SGWB and the same network without considering ET: in that case our equations must be restricted to the case M=0

(1.18) by taking the coefficient p_{lm}'s be polarization-independent, namely

$$p_{\ell m,1} = p_{\ell m,-1} \equiv p_{\ell m} \tag{4.3}$$

and by encoding the degree of polarization in the common factor

$$\begin{aligned} H_1(f) &\equiv H(f)(1+p) \\ H_{-1}(f) &\equiv H(f)(1-p) \end{aligned} \tag{4.4}$$

which implies

$$\begin{aligned} \Omega_{GW,1}(f) &\equiv \frac{1}{2}\Omega_{GW}(f)(1+p) \\ \Omega_{GW,-1}(f) &\equiv \frac{1}{2}\Omega_{GW}(f)(1-p) \end{aligned} \tag{4.5}$$

We also note that in writing eq. (4.4) we have also assumed that the degree of polarization is frequency-independent. The parameter p controlling the polarization is a real number that ranges from -1 to 1. The two extremes correspond to a fully chiral background, while $p = 0$ corresponds to an unpolarised SGWB. Under these assumptions eq. (4.2) becomes

$$\begin{aligned} \mathrm{SNR}_m = \frac{3H_0^2\sqrt{2T}}{10\pi^2}\Bigg[\int_0^\infty df \Omega_{GW}^2(f) \times \\ \times \Bigg(\sum_{j=1}^{4}\sum_{O}\frac{\left|\sum_{\ell=|m|}^{\infty} p_{\ell m}\left[(1+p)\gamma_{\ell m,1j,O,1}(f) + (1-p)\gamma_{\ell m,1j,O,-1}(f)\right]\right|^2}{f^6 N_{1,O}(f) P_j(f)} + \\ + \sum_{i=1}^{4}\sum_{j=i+1}^{4}\frac{\left|\sum_{\ell=|m|}^{\infty} p_{\ell m}\left[(1+p)\gamma_{\ell m,ij,1}(f) + (1-p)\gamma_{\ell m,ij,-1}(f)\right]\right|^2}{f^6 P_i(f) P_j(f)}\Bigg)\Bigg]^{\frac{1}{2}} \end{aligned} \tag{4.6}$$

To evaluate this quantity, we assume a power-law frequency dependence for the energy density:

$$\Omega_{\mathrm{GW}}(f) = \bar{\Omega}_{\mathrm{GW}}\left(\frac{f}{100\,\mathrm{Hz}}\right)^{\alpha} \tag{4.7}$$

where $\bar{\Omega}_{\mathrm{GW}}$ is the fractional energy density at the pivot scale of 100 Hz. Typical values considered for the spectral index are $\alpha = 0$, as for a cosmological inflationary signal (characterized by nearly scale-invariance) and $\alpha = 2/3$, as expected for the stochastic background due to black hole-black hole and black hole-neutron star binary system inspirals [24]. For our treatment we consider $\alpha \in [-2, 2]$, since the models we know from literature do not present values of α which lay outside this interval. We can then rewrite eq. (4.6) as

$$\mathrm{SNR}_m = \bar{\Omega}_{\mathrm{GW}} \sqrt{\frac{T}{(1\,\mathrm{Hz})^3} \frac{9H_0^4}{2\pi^4}} \Bigg[\sum_{i=1}^{4} \sum_{j=i+1}^{4} \int_{f_{\mathrm{min},ij}}^{f_{\mathrm{max},ij}} \frac{df}{1\,\mathrm{Hz}} \frac{10^{-4\alpha} \left(\frac{f}{1\,\mathrm{Hz}}\right)^{2\alpha-6}}{P_i(f)\ P_j(f)\ \mathrm{Hz}^2} \times$$
$$\times \left| \sum_{\ell=|m|}^{\infty} p_{\ell m} \left[(1+p)\, \gamma_{\ell m,ij,1}(f) + (1-p)\, \gamma_{\ell m,ij,-1}(f) \right] \right|^2 +$$
$$+ \sum_{j=1}^{4} \sum_{O=A,E} \int_{f_{\mathrm{min},j1}}^{f_{\mathrm{max},j1}} \frac{df}{1\,\mathrm{Hz}} \frac{10^{-4\alpha} \left(\frac{f}{1\,\mathrm{Hz}}\right)^{2\alpha-6}}{P_j(f)\ N_{1,O}(f)\ \mathrm{Hz}^2} \times$$
$$\times \left| \sum_{\ell=|m|}^{\infty} p_{\ell m} \left[(1+p)\, \gamma_{\ell m,1j,O,1}(f) + (1-p)\, \gamma_{\ell m,1j,O,-1}(f) \right] \right|^2 \Bigg]^{\frac{1}{2}} \tag{4.8}$$

where we define the set of minimum and maximum frequencies over which the PSDs $P_i(f)$ are defined: $\{f_{\mathrm{min},i}\}$, $\{f_{\mathrm{max},i}\}$ with $i = 1, ..., 4$ and

$$\begin{aligned} f_{\mathrm{min},ij} &= \max\{f_{\mathrm{min},i}, f_{\mathrm{min},j}\} \\ f_{\mathrm{max},ij} &= \min\{f_{\mathrm{max},i}, f_{\mathrm{max},j}\} \end{aligned} \tag{4.9}$$

since we want to integrate only the frequency range which is common to each of the two detectors, taken pair by pair.

This equation can be numerically approximated as

$$\mathrm{SNR}_m \simeq \bar{\Omega}_{\mathrm{GW}} \sqrt{\frac{T}{1\,\mathrm{year}}} \Bigg[\sum_{i=1}^{4} \sum_{j=i+1}^{4} \int_{f_{\mathrm{min},ij}}^{f_{\mathrm{max},ij}} \frac{df}{1\,\mathrm{Hz}} \frac{1.28 \times 10^{-66-4\alpha} \left(\frac{f}{1\,\mathrm{Hz}}\right)^{2\alpha-6}}{P_i(f)\ P_j(f)\ \mathrm{Hz}^2} \times$$
$$\times \left| \sum_{\ell=|m|}^{\infty} p_{\ell m} \left[(1+p)\, \gamma_{\ell m,ij,1}(f) + (1-p)\, \gamma_{\ell m,ij,-1}(f) \right] \right|^2 +$$
$$+ \sum_{j=1}^{4} \sum_{O=A,E} \int_{f_{\mathrm{min},j1}}^{f_{\mathrm{max},j1}} \frac{df}{1\,\mathrm{Hz}} \frac{1.28 \times 10^{-66-4\alpha} \left(\frac{f}{1\,\mathrm{Hz}}\right)^{2\alpha-6}}{P_j(f)\ N_{1,O}(f)\ \mathrm{Hz}^2} \times$$
$$\times \left| \sum_{\ell=|m|}^{\infty} p_{\ell m} \left[(1+p)\, \gamma_{\ell m,1j,O,1}(f) + (1-p)\, \gamma_{\ell m,1j,O,-1}(f) \right] \right|^2 \Bigg]^{\frac{1}{2}} \tag{4.10}$$

Finally, we assume that the SGWB is dominated by a single multipole (ℓ, m), giving an estimate of the threshold value of $\bar{\Omega}_{\mathrm{GW}} p_{\ell,m}$ necessary to obtain an $\mathrm{SNR}_m = 1$ during $T = 1\,\mathrm{year}$ of observation. Inverting equation (4.10) under our hypotheses, we have

$$\bar{\Omega}_{\rm GW} p_{\ell m}\Big|_{\rm thr,1y} = \Bigg[\sum_{i=1}^{4} \sum_{j=i+1}^{4} \int_{f_{\min,ij}}^{f_{\max,ij}} \frac{df}{1\,\mathrm{Hz}} \frac{1.28 \times 10^{-66-4\alpha} \left(\frac{f}{1\,\mathrm{Hz}}\right)^{2\alpha-6}}{P_i(f)\ P_j(f)\ \mathrm{Hz}^2} \times$$
$$\times \Big| \Big[(1+p)\,\gamma_{\ell m,ij,1}(f) + (1-p)\,\gamma_{\ell m,ij,-1}(f) \Big] \Big|^2 +$$
$$+ \sum_{i=1}^{4} \sum_{O=A,E} \int_{f_{\min,i1}}^{f_{\max,i1}} \frac{df}{1\,\mathrm{Hz}} \frac{1.28 \times 10^{-66-4\alpha} \left(\frac{f}{1\,\mathrm{Hz}}\right)^{2\alpha-6}}{P_i(f)\ N_{1,O}(f)\ \mathrm{Hz}^2} \times$$
$$\times \Big| \left[(1+p)\,\gamma_{\ell m,i1,O,1}(f) + (1-p)\,\gamma_{\ell m,i1,O,-1}(f) \right] \Big|^2 \Bigg]^{-\frac{1}{2}} \tag{4.11}$$

In appendix D we provide an explicit analytic writing for the response functions $\gamma_{\ell m,ij,\lambda}$ for the monopole ($\ell = 0$), dipole ($\ell = 1$) and quadrupole ($\ell = 2$).

We specify in appendix E our procedure for determining the detector-dependent elements d^{ab}_{1A}, d^{ab}_{1E} and d^{ab}_{i}, which encode the orientation of the arms of our interferometers.

In figures 5-15 we plot the threshold values of $\bar{\Omega}_{\rm GW} p_{\ell m}\Big|_{\rm thr,1y}$ of equation (4.11) for different values of p and α. In particular figure 5 considers the monopole ($\ell = 0$), figures 7-9 the dipoles ($\ell = 1$) and figures 11-15 the quadrupoles ($\ell = 2$). The thick lines correspond to the full network (which we recall is made of the two Advanced LIGO, Advanced Virgo, KAGRA and ET), while the dashed ones correspond to the values obtained by the same network without ET. The comparison of the two results quantifies the impact that ET can have for the study of the SGWB.

In figure 17 we combine the threshold values for all the coefficients, in the case of a scale invariant ($\alpha = 0$) and unpolarised ($p = 0$) SGWB.

As it is displayed in tables 6-16, the contribution of ET leads to a significant improvement on the value of the $\bar{\Omega}_{\rm GW} p_{\ell,m}|_{\rm thr,1y}$. Tables show the values of the ratio $\frac{\bar{\Omega}_{\rm GW} p_{\ell,m}|_{\rm thr,1y,ET}}{\bar{\Omega}_{\rm GW} p_{\ell,m}|_{\rm thr,1y,no\ ET}}$ between the threshold value of $\bar{\Omega}_{\rm GW} p_{\ell,m}$ obtained considering a network of the two Advanced LIGO, Advanced Virgo and KAGRA and ET over the same value considering the previous network without ET. The tables 6-16 refer to the values shown in each relative plot of figures 5-15.

In all the plots shown in this paragraph we consider only multipoles (ℓ, m) with $m > 0$, since in equation (4.11) we see that the functions $\gamma_{lm,ij,O,\lambda}(f)$ and $\gamma_{lm,ij,\lambda}(f)$ appear only with the square modulus of a linear combination of them. Therefore, looking at their explicit writing in (D.1) we can see that

$$\bar{\Omega}_{\rm GW} p_{\ell,m}\Big|_{\rm thr,1y} = \bar{\Omega}_{\rm GW} p_{\ell,-m}\Big|_{\rm thr,1y} \tag{4.12}$$

For all these accounts, we set the angle of the orientation of ET (as introduced in figure 23) $\beta = 0$. This assumption is arbitrary, since the instrument is not built yet and its direction arms still not defined, but we found by an explicit evaluation that all the values of $\bar{\Omega}_{GW} p_{\ell,m}\Big|_{\text{thr,1y}}$ do not depend on the value of β (see E for further details on the ET geometry definition)

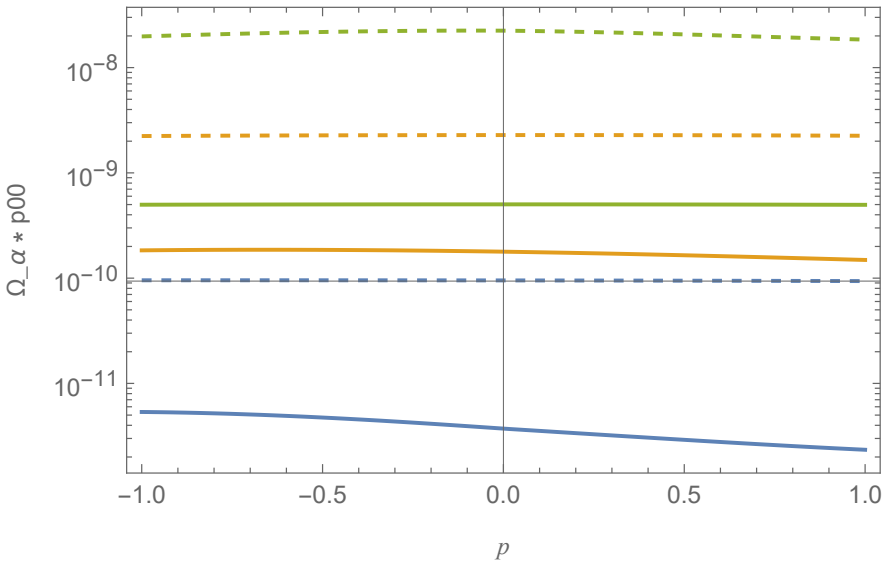

FIGURE 5: Sensitivity to a monopole of the SGWVB. The lines show the amplitude that the multipoles must have to produce SNR = 1 in one year of observation, whose scale is set on y-axis. On x-axis we show how the amplitude depends on the parameter p introduced in equation (4.4). The blue lines are drawn under the assumption of a red tilted power spectrum ($\alpha = -2$), the orange lines represent are plotted for a scale invariant one ($\alpha = 0$) while the green ones are made for a blue tilted one ($\alpha = 2$). A pivot frequency scale of 100 Hz is assumed. The thick lines correspond to the threshold values for the network of the two Advanced LIGO, Advanced Virgo and KAGRA interferometers. The dashed lines are the expected values for the same network + Einstein Telescope.

$(\ell = 0, m = 0)$	$p = -1$	$p = -0.5$	$p = 0$	$p = 0.5$	$p = 1$
$\alpha = -2$	0.0561	0.0497	0.0391	0.0308	0.025
$\alpha = 0$	0.082	0.0817	0.078	0.0724	0.0661
$\alpha = 2$	0.0252	0.023	0.0224	0.0242	0.0269

FIGURE 6: The values of the ratio $\frac{\bar{\Omega}_{GW} p_{\ell,m}|_{\text{thr,1y,ET}}}{\bar{\Omega}_{GW} p_{\ell,m}|_{\text{thr,1y,no ET}}}$ for the monopole $(\ell = 0, m = 0)$ at different values of α and p

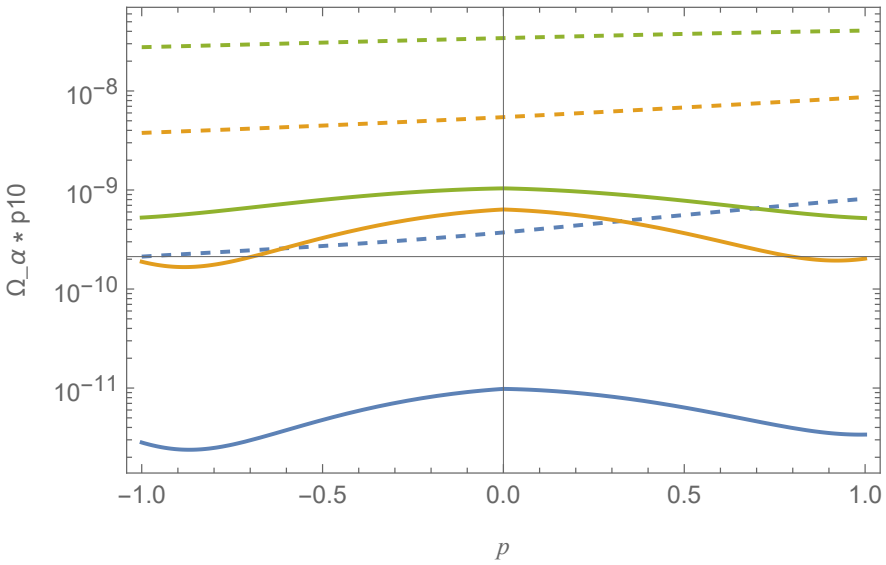

FIGURE 7: Sensitivity to a dipole ($(\ell, m) = 1, 0$) of the SGWVB. The lines show the amplitude that the multipoles must have to produce SNR = 1 in one year of observation, whose scale is set on y-axis. On x-axis we show how the amplitude depends on the parameter p introduced in equation (4.4). The blue lines are drawn under the assumption of a red tilted power spectrum ($\alpha = -2$), the orange lines represent are plotted for a scale invariant one ($\alpha = 0$) while the green ones are made for a blue tilted one ($\alpha = 2$). A pivot frequency scale of 100 Hz is assumed. The thick lines correspond to the threshold values for the network of the two Advanced LIGO, Advanced Virgo and KAGRA interferometers. The dashed lines are the expected values for the same network + Einstein Telescope.

$(\ell = 1, m = 0)$	$p = -1$	$p = -0.5$	$p = 0$	$p = 0.5$	$p = 1$
$\alpha = -2$	0.0133	0.0175	0.0263	0.0114	0.0041
$\alpha = 0$	0.05	0.0732	0.1169	0.0538	0.0234
$\alpha = 2$	0.019	0.0258	0.0304	0.0207	0.0128

FIGURE 8: The values of the ratio $\frac{\bar{\Omega}_{\rm GW} p_{\ell,m}|_{\rm thr,1y,ET}}{\bar{\Omega}_{\rm GW} p_{\ell,m}|_{\rm thr,1y,no\,ET}}$ for the dipole ($\ell = 1, m = 0$) at different values of α and p

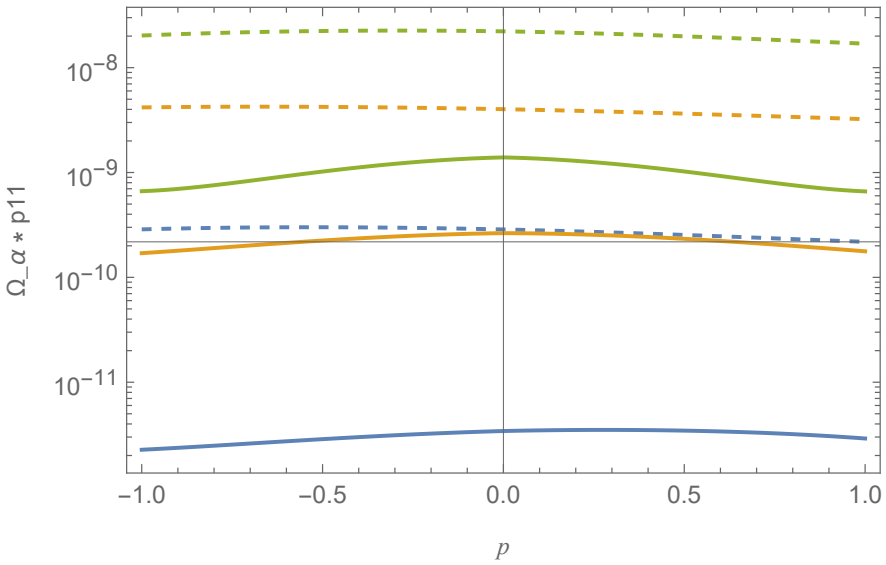

FIGURE 9: Sensitivity to a dipole ($(\ell, m) = 1, 1$) of the SGWVB. The lines show the amplitude that the multipoles must have to produce SNR = 1 in one year of observation, whose scale is set on y-axis. On x-axis we show how the amplitude depends on the parameter p introduced in equation (4.4). The blue lines are drawn under the assumption of a red tilted power spectrum ($\alpha = -2$), the orange lines represent are plotted for a scale invariant one ($\alpha = 0$) while the green ones are made for a blue tilted one ($\alpha = 2$). A pivot frequency scale of 100 Hz is assumed. The thick lines correspond to the threshold values for the network of the two Advanced LIGO, Advanced Virgo and KAGRA interferometers. The dashed lines are the expected values for the same network + Einstein Telescope.

$(\ell = 1, m = 1)$	$p = -1$	$p = -0.5$	$p = 0$	$p = 0.5$	$p = 1$
$\alpha = -2$	0.0079	0.0095	0.012	0.0136	0.0133
$\alpha = 0$	0.0407	0.0531	0.0657	0.064	0.0549
$\alpha = 2$	0.0328	0.0457	0.0627	0.0514	0.039

FIGURE 10: The values of the ratio $\frac{\bar{\Omega}_{GW} p_{\ell,m}|_{\text{thr,1y,ET}}}{\bar{\Omega}_{GW} p_{\ell,m}|_{\text{thr,1y,no ET}}}$ for the dipole ($\ell = 1, m = 1$) at different values of α and p

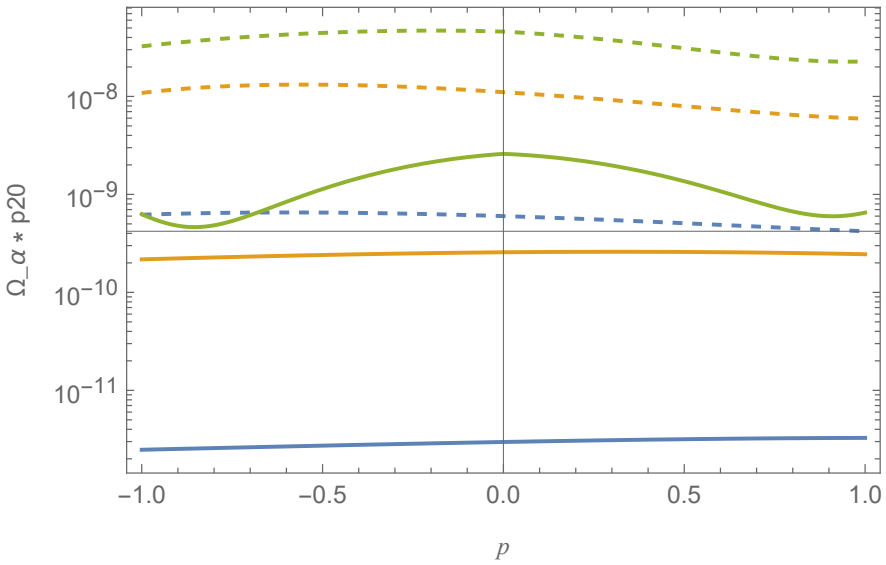

FIGURE 11: Sensitivity to a quadrupole ($(\ell, m) = 2, 0$) of the SGWVB. The lines show the amplitude that the multipoles must have to produce SNR = 1 in one year of observation, whose scale is set on y-axis. On x-axis we show how the amplitude depends on the parameter p introduced in equation (4.4). The blue lines are drawn under the assumption of a red tilted power spectrum ($\alpha = -2$), the orange lines represent are plotted for a scale invariant one ($\alpha = 0$) while the green ones are made for a blue tilted one ($\alpha = 2$). A pivot frequency scale of 100 Hz is assumed. The thick lines correspond to the threshold values for the network of the two Advanced LIGO, Advanced Virgo and KAGRA interferometers. The dashed lines are the expected values for the same network + Einstein Telescope.

$(\ell = 2, m = 0)$	$p = -1$	$p = -0.5$	$p = 0$	$p = 0.5$	$p = 1$
$\alpha = -2$	0.004	0.0042	0.005	0.0062	0.0078
$\alpha = 0$	0.02	0.0183	0.0232	0.0325	0.0414
$\alpha = 2$	0.0194	0.0255	0.0565	0.0439	0.0287

FIGURE 12: The values of the ratio $\frac{\bar{\Omega}_{GW} p_{\ell,m}|_{\text{thr,1y,ET}}}{\bar{\Omega}_{GW} p_{\ell,m}|_{\text{thr,1y,no ET}}}$ for the quadrupole ($\ell = 2, m = 0$) at different values of α and p

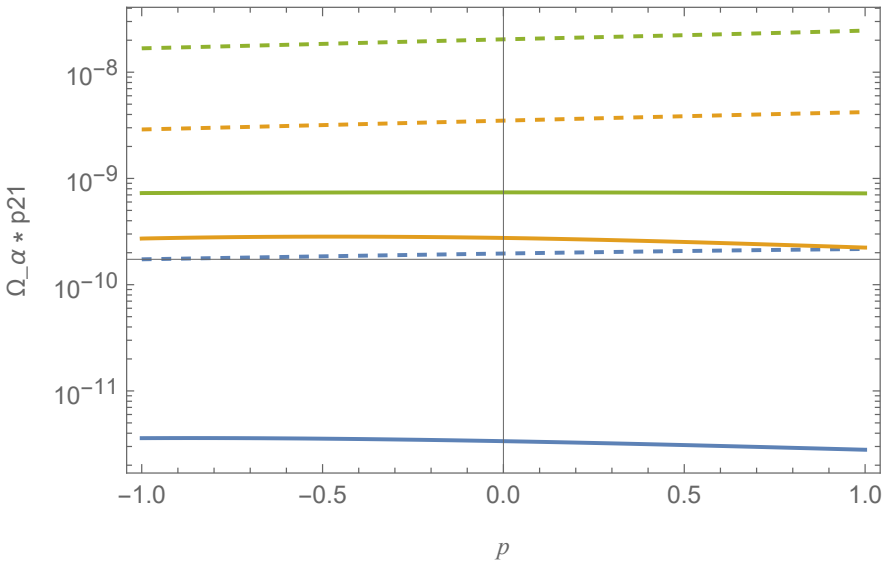

FIGURE 13: Sensitivity to a quadrupole ($(\ell, m) = 2, 1$) of the SGWVB. The lines show the amplitude that the multipoles must have to produce SNR = 1 in one year of observation, whose scale is set on y-axis. On x-axis we show how the amplitude depends on the parameter p introduced in equation (4.4). The blue lines are drawn under the assumption of a red tilted power spectrum ($\alpha = -2$), the orange lines represent are plotted for a scale invariant one ($\alpha = 0$) while the green ones are made for a blue tilted one ($\alpha = 2$). A pivot frequency scale of 100 Hz is assumed. The thick lines correspond to the threshold values for the network of the two Advanced LIGO, Advanced Virgo and KAGRA interferometers. The dashed lines are the expected values for the same network + Einstein Telescope.

$(\ell = 2, m = 1)$	$p = -1$	$p = -0.5$	$p = 0$	$p = 0.5$	$p = 1$
$\alpha = -2$	0.0207	0.0192	0.0171	0.0149	0.0129
$\alpha = 0$	0.094	0.0891	0.0787	0.0655	0.0531
$\alpha = 2$	0.0434	0.0399	0.0363	0.0329	0.0294

FIGURE 14: The values of the ratio $\frac{\bar{\Omega}_{\rm GW} p_{\ell,m}|_{\rm thr,1y,ET}}{\bar{\Omega}_{\rm GW} p_{\ell,m}|_{\rm thr,1y,no\,ET}}$ for the quadrupole ($\ell = 2, m = 1$) at different values of α and p

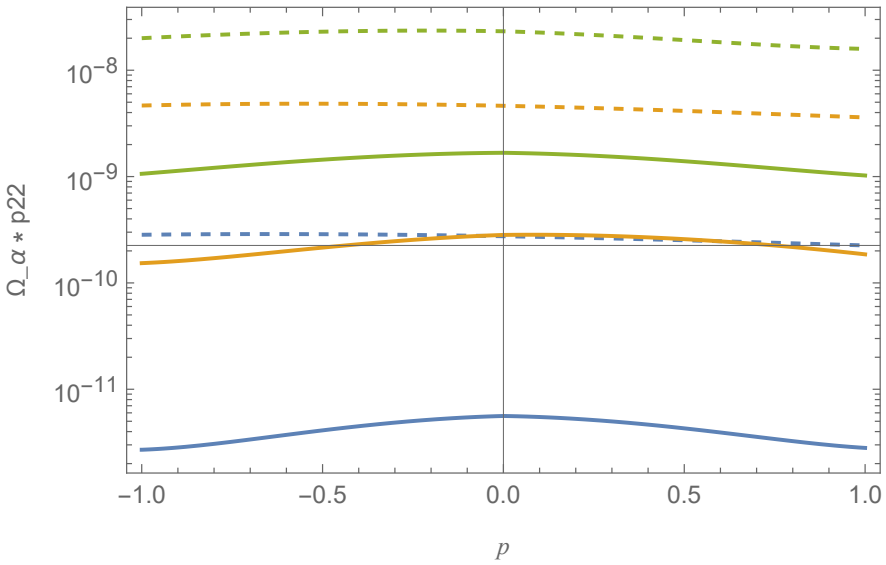

FIGURE 15: Sensitivity to a quadrupole ($(\ell, m) = 2, 2$) of the SGWVB. The lines show the amplitude that the multipoles must have to produce SNR = 1 in one year of observation, whose scale is set on y-axis. On x-axis we show how the amplitude depends on the parameter p introduced in equation (4.4). The blue lines are drawn under the assumption of a red tilted power spectrum ($\alpha = -2$), the orange lines represent are plotted for a scale invariant one ($\alpha = 0$) while the green ones are made for a blue tilted one ($\alpha = 2$). A pivot frequency scale of 100 Hz is assumed. The thick lines correspond to the threshold values for the network of the two Advanced LIGO, Advanced Virgo and KAGRA interferometers. The dashed lines are the expected values for the same network + Einstein Telescope.

$(\ell = 2, m = 2)$	$p = -1$	$p = -0.5$	$p = 0$	$p = 0.5$	$p = 1$
$\alpha = -2$	0.0095	0.0143	0.0204	0.017	0.0125
$\alpha = 0$	0.033	0.0444	0.0611	0.0622	0.0516
$\alpha = 2$	0.0531	0.0626	0.072	0.0726	0.0645

FIGURE 16: The values of the ratio $\frac{\bar{\Omega}_{GW} p_{\ell,m}|_{\text{thr,1y,ET}}}{\bar{\Omega}_{GW} p_{\ell,m}|_{\text{thr,1y,no ET}}}$ for the quadrupole ($\ell = 2, m = 2$) at different values of α and p

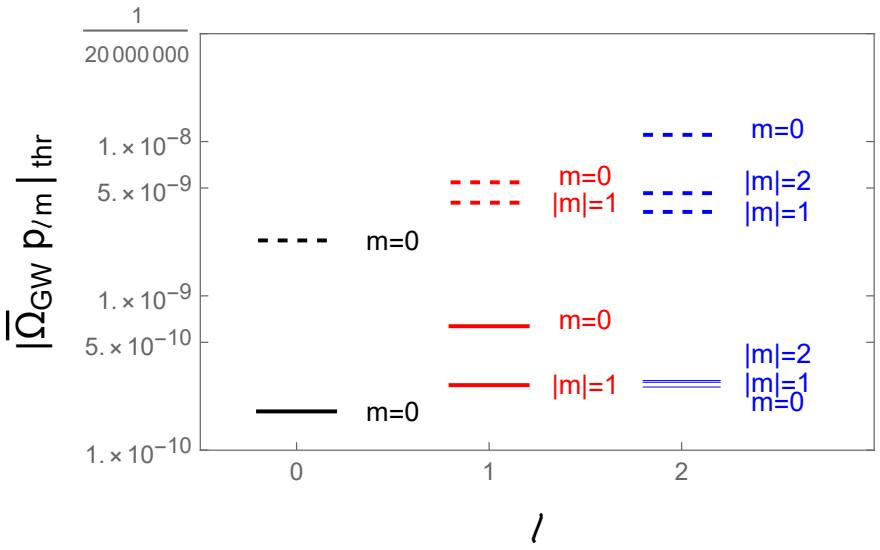

FIGURE 17: Sensitivity to a statistically invariant ($p = 0$ of equation (4.4)) monopole, dipole, and quadrupole of the SGWB. The lines show the amplitude that the multipoles must have to produce SNR = 1 in one year of observation. The thick lines correspond to the threshold values for the network of the two Advanced LIGO, Advanced Virgo and KAGRA interferometers. The dashed lines are the expected values for the same network + Einstein Telescope. A scale invariant Ω_{GW} is assumed ($\alpha = 0$ of equation (4.7)). A pivot frequency scale of 100 Hz is assumed.

4.1 – STATISTICALLY ISOTROPIC $p_{\ell,m}$

We can also consider the case of a statistically isotropically signal, in which the coefficients $p_{ell,m}$ satisfy

$$\langle p_{\ell m} p^*_{\ell' m'} \rangle = C_\ell \, \delta_{\ell\ell'} \, \delta_{mm'} \tag{4.13}$$

with a single C_ℓ dominating over the other ones. We obtain the following expectation from the $m = 0, 1, 2$ measurements from eq. (4.10)

$$\begin{aligned}
\left\langle \sum_m \mathrm{SNR}_m \right\rangle \simeq \bar{\Omega}_{\mathrm{GW}} C_\ell^{1/2} \sqrt{\frac{T}{1\,\mathrm{year}}} \Bigg[& \sum_{i=1}^{4} \sum_{j=i+1}^{4} \int_{f_{\mathrm{min},ij}}^{f_{\mathrm{max},ij}} \frac{df}{1\,\mathrm{Hz}} \frac{1.28 \times 10^{-66-4\alpha} \left(\frac{f}{1\,\mathrm{Hz}}\right)^{2\alpha-6}}{P_i(f)\; P_j(f)\; \mathrm{Hz}^2} \times \\
& \times \sum_m \left| (1+p)\, \gamma_{\ell m,ij,1}(f) + (1-p)\, \gamma_{\ell m,ij,-1}(f) \right|^2 + \\
& + \sum_{j=1}^{4} \sum_{O=A,E} \int_{f_{\mathrm{min},j1}}^{f_{\mathrm{max},j1}} \frac{df}{1\,\mathrm{Hz}} \frac{1.28 \times 10^{-66-4\alpha} \left(\frac{f}{1\,\mathrm{Hz}}\right)^{2\alpha-6}}{P_j(f)\; N_{1,O}(f)\; \mathrm{Hz}^2} \times \\
& \times \sum_m \left| (1+p)\, \gamma_{\ell m,1j,O,1}(f) + (1-p)\, \gamma_{\ell m,1j,O,-1}(f) \right|^2 \Bigg]^{\frac{1}{2}}
\end{aligned} \tag{4.14}$$

and the sensitivity to C_ℓ is then obtained from the sum over all m's

$$\begin{aligned}
\bar{\Omega}_{\mathrm{GW}} C_\ell^{1/2} \Big|_{\mathrm{thr,1y}} = \Bigg[& \sum_{i=1}^{4} \sum_{j=i+1}^{4} \int_{f_{\mathrm{min},ij}}^{f_{\mathrm{max},ij}} \frac{df}{1\,\mathrm{Hz}} \frac{1.28 \times 10^{-66-4\alpha} \left(\frac{f}{1\,\mathrm{Hz}}\right)^{2\alpha-6}}{P_i(f)\; P_j(f)\; \mathrm{Hz}^2} \times \\
& \times \sum_m \Big| \Big[(1+p)\, \gamma_{\ell m,ij,1}(f) + (1-p)\, \gamma_{\ell m,ij,-1}(f) \Big] \Big|^2 + \\
& + \sum_{i=1}^{4} \sum_{O=A,E} \int_{f_{\mathrm{min},i1}}^{f_{\mathrm{max},i1}} \frac{df}{1\,\mathrm{Hz}} \frac{1.28 \times 10^{-66-4\alpha} \left(\frac{f}{1\,\mathrm{Hz}}\right)^{2\alpha-6}}{P_i(f)\; N_{1,O}(f)\; \mathrm{Hz}^2} \times \\
& \times \sum_m \Big| \left[(1+p)\, \gamma_{\ell m,i1,O,1}(f) + (1-p)\, \gamma_{\ell m,i1,O,-1}(f) \right] \Big|^2 \Bigg]^{-\frac{1}{2}}
\end{aligned} \tag{4.15}$$

In figure 18 we plot the threshold values of $\bar{\Omega}_{\mathrm{GW}}\, C_\ell^{1/2}$ necessary to be detected to our network, with and without considering Einstein Telescope, under the assumption of isotropic statistics of the multipoles $p_{\ell,m}$.

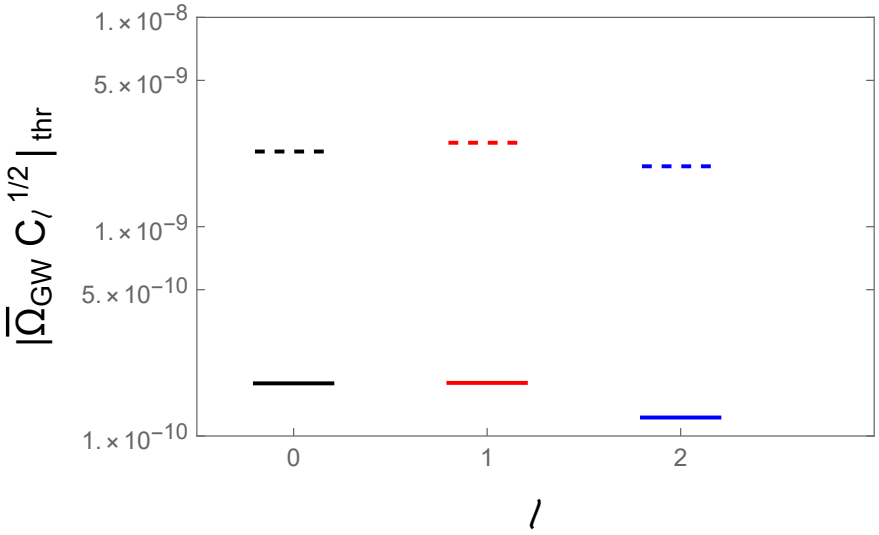

FIGURE 18: Sensitivity to a statistically invariant ($p = 0$ of equation (4.4)) monopole, dipole, and quadrupole of the SGWB under the hypothesis of statistically isotropic distribution of multipoles (ℓ, m) at fixed ℓ value. The lines show the amplitude that the multipoles must have to produce SNR = 1 in one year of observation. The thick lines correspond to the threshold values for the network of the two Advanced LIGO, Advanced Virgo and KAGRA interferometers. The dashed lines are the expected values for the same network + Einstein Telescope. A scale invariant Ω_{GW} is assumed ($\alpha = 0$ of equation (4.7)). A pivot frequency scale of 100 Hz is assumed.

Chapter 5

Two ETs in the short distance limit

Let us consider now a network made of two hypothetical Einstein Telescopes, located at the two sites under consideration for the actual ET detector. The first site is the Sos Enattos mine in Sardinia, at coordinates 40.4°N; 9.45°E. The second site is at the Belgium-Netherlands border. For definiteness, we choose the city of Maastricht, at coordinates 50.9°N; 5.69°E. Assuming the Earth to be a perfect sphere of radius RE = 6; 371 km, the length of the segment connecting these two locations is $d_{ET} \simeq 1.200$ km. For this choice, the argument in the phase of eq. (B.11) satisfies

$$\Phi \equiv \left|2\pi f \hat{n} \cdot \left(\boldsymbol{x}_{1\alpha} - \boldsymbol{x}_{2\beta}\right)\right| \leq 2\pi f \, |\boldsymbol{x}_1 - \boldsymbol{x}_2| \simeq 0.025 \, \frac{f}{\text{Hz}} \, \frac{|\boldsymbol{x}_1 - \boldsymbol{x}_2|}{1,200\,\text{km}} \tag{5.1}$$

As we discuss below (see Figure 19) this quantity is smaller than one at the frequency to which ET is most sensitive to. As an example, for a scale invariant GW signal (Ω_{GW} independent of frequency), the sensitivity is strongly peaked at $f \simeq 7\,\text{Hz}$. For this value, the product in eq. (5.1) evaluates to about 0.18. It is therefore meaningful to evaluate eq. (B.10) as an expansion series in Φ. As we show below, the response functions to the various multipoles $p_{\ell m}$ are suppressed by positive powers of Φ, with exception to those to the multipoles $\ell = 0$, 2, 4 and $|m| \leq \ell$ [12]. For this reason, in this chapter we evaluate only these unsuppressed contributions. As we show in Appendix C, correlators between even (odd) multipoles ℓ receive contributions only from even (odd) powers of Φ. Therefore, evaluating these coefficients at $\Phi = 0$ results in a $\text{O}\left(\Phi^2\right) \simeq 3\%$ inaccuracy at the most sensitive frequencies. Taking $\Phi = 0$ allows for a greater simplification of eq. (B.10). This is a major departure from the study of [12], where the much longer distance between the two LIGO interferometers did not allow for this simplification. As we show in this chapter, in this limit the detector response functions (to be defined shortly) acquire vey simple analytical expressions, which can be employed to determine the SNR, and hence the sensitivity to the anisotropy, almost fully analytically, only up to one numerical integration over frequency.

Proceeding in this way, we can readily go from the correlation of the signal at the three vertices to the correlator of the signal in the thee channels, and write the response functions in equations (3.9) as

$$\gamma_{\ell m,12,OO',\lambda} \equiv \frac{5}{8\pi} \int d^2\hat{n} \, Y_{\ell m}\left(\hat{n}\right) e^{*\lambda}_{ab}\left(\hat{n}\right) e^{\lambda}_{cd}\left(\hat{n}\right) \, d^{ab}_{1O} \, d^{cd}_{2O'} \tag{5.2}$$

We note that under this approximation the $\gamma_{\ell m,ij,OO',\lambda}$ are now just simple numbers, frequency-

independent. We can therefore define the frequency-independent coefficients

$$\gamma_{\ell m,\lambda,abcd} \equiv \frac{5}{8\pi} \int d^2\hat{n}\, Y_{\ell m}\left(\hat{n}\right) e^{*\lambda}_{ab}\left(\hat{n}\right) e^{\lambda}_{cd}\left(\hat{n}\right) \tag{5.3}$$

in terms of which

$$\gamma_{\ell m,12,OO',\lambda} \equiv \gamma_{\ell m,\lambda,abcd} \times d^{ab}_{1O}\, d^{cd}_{2O'} \tag{5.4}$$

For the present section (which recalls the main steps done in [18]) we assume an unpolarized background, i.e. $p = 0$. Therefore it turns out to be useful to introduce the new coefficients

$$\begin{aligned} \gamma_{\ell m,OO'} &\equiv \gamma_{\ell m,abcd} \times d^{ab}_{1O}\, d^{cd}_{2O'} \\ \gamma_{\ell m,abcd} &\equiv \sum_{\lambda} \gamma_{\ell m,\lambda,abcd} \end{aligned} \tag{5.5}$$

The coefficients $\gamma_{\ell m,abcd}$ are computed in Appendix F, where, integrating over the two angles,

we obtain simple expressions for the $\gamma_{0m,ab,cd}$, $\gamma_{2m,ab,cd}$, $\gamma_{4m,ab,cd}$ terms:

$$
\begin{aligned}
\gamma_{00,ab,cd} &\cong \frac{1}{2\sqrt{\pi}}\left(\delta_{ac}\,\delta_{bd}+\delta_{ad}\,\delta_{bc}\right)\\
\gamma_{20,ab,cd} &\cong \frac{1}{14}\sqrt{\frac{5}{\pi}}\left(\delta_{ac}\,A_{bd}+\delta_{ad}\,A_{bc}+\delta\leftrightarrow A\right)\\
\gamma_{2\pm1,ab,cd} &\cong \frac{3}{14}\sqrt{\frac{5}{6\pi}}\left(\delta_{ac}\,B_{bd\pm}+\delta_{ad}\,B_{bc\pm}+\delta\leftrightarrow B_{\pm}\right)\\
\gamma_{2\pm2,ab,cd} &\cong -\frac{3}{14}\sqrt{\frac{5}{6\pi}}\left(\delta_{ac}\,C_{bd\pm}+\delta_{ad}\,C_{bc\pm}+\delta\leftrightarrow C_{\pm}\right)\\
\gamma_{40,ab,cd} &\cong \frac{1}{756\sqrt{\pi}}\Bigg[-\delta_{ac}\,\delta_{bd}-\delta_{ad}\,\delta_{bc}-5\left(\delta_{ac}\,A_{bd}+\delta_{ad}\,A_{bc}+\delta\leftrightarrow A\right)\\
&\qquad +20\left(A_{ac}\,A_{bd}+A_{ad}\,A_{bc}-\frac{1}{4}A_{ab}\,A_{cd}\right)\Bigg]\\
\gamma_{4\pm1,ab,cd} &\cong \frac{1}{1512}\sqrt{\frac{5}{\pi}}\Bigg[2\left(\delta_{ac}\,B_{bd\pm}+\delta_{ab}\,B_{cd\pm}+\delta\leftrightarrow B_{\pm}\right)\\
&\qquad +7\left(A_{ac}\,B_{bd\pm}+A_{ad}\,B_{bc\pm}+A_{ab}\,B_{cd\pm}+A\leftrightarrow B_{\pm}\right)\Bigg]\\
\gamma_{4\pm2,ab,cd} &\cong -\frac{1}{504}\sqrt{\frac{5}{2\pi}}\Bigg[2\left(\delta_{ac}\,C_{bd\pm}+\delta_{ad}\,C_{bc\pm}+\delta\leftrightarrow C_{\pm}\right)\\
&\qquad +7\left(A_{ac}\,C_{bd\pm}+A_{ad}\,C_{bc\pm}+A\leftrightarrow C_{\pm}\right)\Bigg]\\
\gamma_{4\pm3,ab,cd} &= -\frac{1}{24}\sqrt{\frac{5}{7\pi}}\left(B_{ab\pm}\,C_{cd\pm}+B_{\pm}\leftrightarrow C_{\pm}\right)\\
\gamma_{4\pm4,ab,cd} &= \frac{1}{12}\sqrt{\frac{5}{14\pi}}C_{ab\pm}\,C_{cd\pm}
\end{aligned}
\tag{5.6}
$$

while all the other coefficients vanish. The symbol $\cong$ denotes the fact that we have disregarded terms proportional to δ_{ab} and to δ_{cd}, as they vanish when contracted with, respectively, the detector coefficients d^{1ab}_{O} and $d^{cd}_{2O'}$. Finally, in eq. (5.6) we have introduced the matrices

$$
A_{cd}=\begin{pmatrix}1&0&0\\0&1&0\\0&0&-2\end{pmatrix}\,,\quad B_{cd\pm}=\begin{pmatrix}0&0&\pm1\\0&0&i\\\pm1&i&0\end{pmatrix}\,,\quad C_{cd\pm}=\begin{pmatrix}1&\pm i&0\\\pm i&-1&0\\0&0&0\end{pmatrix}
\tag{5.7}
$$

The simple analytical expressions (5.6) are an original result of [18], and they can be used for any pair of detectors (since the geometry of the detectors is encoded in the $d^{ab}_{iO}\,d^{cd}_{jO'}$ terms), in the small frequency regime.

5.1 – SNR COMPUTATION

In terms of the original quantities, one can obtain also in this case the final expression for the signal-to-noise ratio

$$\mathrm{SNR}_m = \frac{3H_0^2\sqrt{2T}}{10\,\pi^2}\sqrt{\int_0^\infty df\,\frac{\Omega_{\mathrm{GW}}^2(f)}{f^6\,N^2(f)}} \times\left[\left|\sum_{\ell=|m|}^{\infty} p_{\ell m}\,\gamma_{\ell m,AA}\right|^2+\left|\sum_{\ell=|m|}^{\infty} p_{\ell m}\,\gamma_{\ell m,EE}\right|^2+\left|\sum_{\ell=|m|}^{\infty} p_{\ell m}\,\gamma_{\ell m,AE}\right|^2+\left|\sum_{\ell=|m|}^{\infty} p_{\ell m}\,\gamma_{\ell m,EA}\right|^2\right]^{1/2} \tag{5.8}$$

where we identify $N \equiv N_{A,i} = N_{E,i}$. We note that, assuming an unpolarized background ($p = 0$) we have $p_{\ell,m,\lambda} \equiv p_{\ell,m}$

To evaluate eq. (5.8) we assume a power-law signal in the ET observational window

$$\Omega_{\mathrm{GW}}(f) = \bar{\Omega}_{\mathrm{GW}}\left(\frac{f}{10\,\mathrm{Hz}}\right)^{\alpha} \tag{5.9}$$

where $\bar{\Omega}_{\mathrm{GW}}$ is the fractional energy density at the pivot scale equal to 10 Hz. We can then rewrite eq. (5.8) as

$$\begin{aligned}\mathrm{SNR}_m \;=\; &\sqrt{\frac{T}{1\,\mathrm{year}}}\,\mathcal{F}_\alpha \times\left[\left|\sum_{\ell=|m|}^{\infty}\bar{\Omega}_{\mathrm{GW}}\,p_{\ell m}\,\gamma_{\ell m,AA}\right|^2+\left|\sum_{\ell=|m|}^{\infty}\bar{\Omega}_{\mathrm{GW}}\,p_{\ell m}\,\gamma_{\ell m,EE}\right|^2\right.\\ &\left.+\left|\sum_{\ell=|m|}^{\infty}\bar{\Omega}_{\mathrm{GW}}\,p_{\ell m}\,\gamma_{\ell m,AE}\right|^2+\left|\sum_{\ell=|m|}^{\infty}\bar{\Omega}_{\mathrm{GW}}\,p_{\ell m}\,\gamma_{\ell m,EA}\right|^2\right]^{1/2}\end{aligned} \tag{5.10}$$

where we have normalized the total observation time to one year, and where we have defined the dimensionless factor

$$\begin{aligned}\mathcal{F}_\alpha &\equiv \sqrt{\frac{1\,\mathrm{year}}{(1\,\mathrm{Hz})^3}\,\frac{9H_0^4}{50\pi^4}\int_{f_{\min}}^{f_{\max}}\frac{df}{1\,\mathrm{Hz}}\,\frac{10^{-2\alpha}\left(\frac{f}{1\,\mathrm{Hz}}\right)^{2\alpha-6}}{N^2(f)\;\mathrm{Hz}^2}} \simeq\\ &\simeq\sqrt{\int_{\mathrm{Hz}}^{10^4\,\mathrm{Hz}}\frac{df}{1\,\mathrm{Hz}}\,\frac{1.28\times10^{-66-2\alpha}\left(\frac{f}{1\,\mathrm{Hz}}\right)^{2\alpha-6}}{N^2(f)\;\mathrm{Hz}^2}}\end{aligned} \tag{5.11}$$

In the evaluation we have taken a year of 365.25 days, the value of the current Hubble

rate $H_0 \simeq 67\,\mathrm{km\,s^{-1}\,Mpc^{-1}}$ indicated by Planck [25], and the minimum and maximum ET frequencies given in [26].

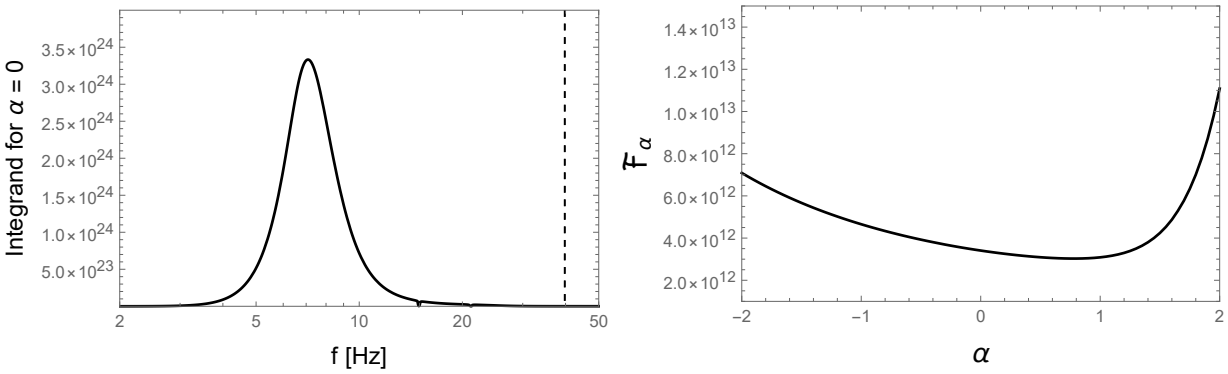

FIGURE 19: Left panel: integrand of the quantity $\mathcal{F}_\alpha$ introduced in eqs. (5.10) and (5.11), for a scale-invariant $\Omega_{\rm GW}$. The vertical dashed line is the threshold (5.12) for the low frequency / short separation condition, in the hypothesis in which two ET-like instruments are placed at the sites currently under consideration for ET. We see that the ET sensitivity is completely dominated by frequencies that satisfy this condition. Right panel: Value of $\mathcal{F}_\alpha$ for α ranging between -2 and 2.

In the left panel of Figure 19 we show the integrand of eq. (5.11) for the choice of $\alpha = 0$. As discussed after eq. (5.1), our results are valid for frequencies

$$f \ll \frac{1}{2\pi\, d_{\rm ET}} \simeq 40\,\mathrm{Hz}\frac{1,200\,\mathrm{km}}{d_{ET}} \tag{5.12}$$

where $d_{ET} = 1,200\,\mathrm{Km}$ is the distance of the segment connecting the two sites under consideration for ET. We see that the sensitivity is completely dominated by frequencies that satisfy the condition (5.12). As already remarked, disregarding the phase in eq. (B.10) amounts in a $\mathrm{O}\left(\frac{f}{40\,\mathrm{Hz}}\right)^2$ mistake, that, evaluated at the peak frequency visible in the figure, is about 0.03. In the right panel of Figure 19 we plot the value of $\mathcal{F}_\alpha$ for α ranging between -2 and 2. The two cases $\alpha = 0, 2/3$ mentioned above correspond, respectively, to $\mathcal{F}_0 \simeq 6.8 \times 10^{11}$ and $\mathcal{F}_{2/3} \simeq 6 \times 10^{11}$.

5.2 – Sensitivity of the ET pair to multipoles of the SGWB

Also for this subsection we first assume that only one multiple $p_{\ell m}$ dominates the SGWB, so that

$$\mathrm{SNR}_m = \mathcal{F}_\alpha \sqrt{\frac{T}{1\,\mathrm{year}}}\,\bar{\Omega}_{\rm GW}\,|p_{\ell m}|\left[\left|\gamma_{\ell m,AA}\right|^2 + \left|\gamma_{\ell m,EE}\right|^2 + \left|\gamma_{\ell m,AE}\right|^2 + \left|\gamma_{\ell m,EA}\right|^2\right]^{1/2} \tag{5.13}$$

The threshold amplitude to give SNR = 1 is therefore

$$\bar{\Omega}_{\rm GW}\,|p_{\ell m}|\,\Big|_{\rm threshold} = \sqrt{\frac{1\,\text{year}}{T}}\,\frac{1}{\mathcal{F}_\alpha\;\;\gamma_{\ell m,\rm combined}} \tag{5.14}$$

where [1]

$$\gamma_{\ell m,\rm combined} \equiv \left[\left|\gamma_{\ell m,AA}\right|^2 + \left|\gamma_{\ell m,EE}\right|^2 + \left|\gamma_{\ell m,AE}\right|^2 + \left|\gamma_{\ell m,EA}\right|^2\right]^{1/2} \tag{5.15}$$

As expected, the threshold value decreases as the inverse of the square root of the observation time. For definiteness, we fix T to one year in the following computations.

To evaluate the threshold value, we need to compute the overlap function elements according to eq. (5.3). In eq. (5.6) we provided simple analytic results for the detector-independent $\gamma_{\ell m,ab,cd}$ coefficients. We now need to determine the detector-dependent elements d^{ab}_{iA} and d^{ab}_{iE}, which encode the orientation of the arms of the ET pair.

From the definition (3.9), and from the property (A.4), we see that $\gamma_{\ell m,OO'}$ transforms as $Y_{\ell m}$ under a rotation. Namely,

$$\begin{aligned}\gamma_{\ell m,RORO'} &= \frac{5}{8\pi}\int d^2\hat{n}\,Y_{\ell m}\left(\hat{n}\right)\sum_P e^P_{ab}\left(\hat{n}\right)e^P_{cd}\left(\hat{n}\right)\;R^a_{a'}R^b_{b'}d^{a'b'}_{1O}\;R^c_{c'}R^d_{d'}d^{c'd'}_{2O'}\\ &= \frac{5}{8\pi}\int d^2\hat{n}\,Y_{\ell m}\left(R\hat{n}\right)\sum_P e^P_{ab}\left(\hat{n}\right)e^P_{cd}\left(\hat{n}\right)d^{ab}_{1O}d^{cd}_{2O'}\end{aligned} \tag{5.16}$$

Therefore, for a rotation of angle φ about the $z-$axis, $\gamma_{\ell m,OO'} \to \mathrm{e}^{im\varphi}\,\gamma_{\ell m,OO'}$. It follows that $\left|\gamma_{\ell m,OO'}\right|^2$ is invariant under such rotation. With our choice of frame, a rotation about the $z-$axis connects two locations on Earth that have the same latitude, and different longitude. It follows that the sensitivity to the various multipoles does not depend on the individual longitudes of the two sites, but only on their difference.

We specify the position and orientation of the two ET-like detectors accordingly to what has been done in appendix E, denoting the latitude and longitude of each site with θ_i and φ_i, respectively and β_i the angles of rotation of the two instruments accordingly with figure 23 (we recall that $i = 1, 2$ denote the first or the second detector). We find that (see [18] for further details) the combination (5.15) depends only on the latitude of the detectors, θ_1 and θ_2, and on the difference of their longitudes, $\varphi_2 - \varphi_1$. Furthermore, (5.15) does not depend on the angles of rotation β_i of the two ETs. Evaluating the coefficients between the two sites currently under consideration for ET produces the sensitivities shown in Figure 20.

Finally, to give a measure of the sensitivity to a given multipole number ℓ, we consider the case of a statistically isotropically signal, as in equation (4.13), obtaining the following

[1] We note that $\gamma_{\ell,-m,OO'} = (-1)^m\,\gamma^*_{\ell,-m,OO'}$, due to the property of the spherical harmonics in eq. (3.9). Therefore the value of $\gamma_{\ell m,\rm combined}$ does not depend on the sign of m.

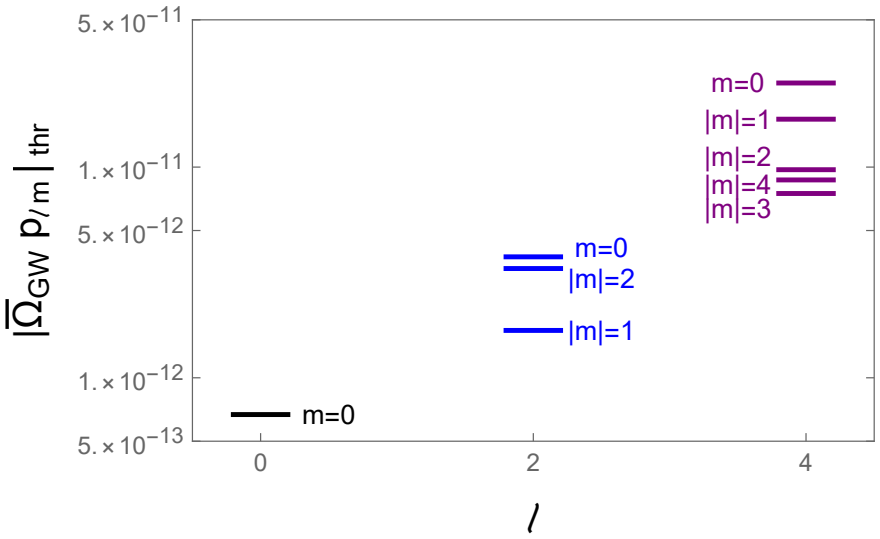

FIGURE 20: Sensitivity to the monopole and to the various quadrupole and hexadecapole moments. The solid lines shows the amplitude that the multipoles must have to produce SNR = 1 in one year of observation ot two ET-like detectors placed at the two sites currently under consideration for ET. A scale invariant $\Omega_{\rm GW}$ is assumed ($\alpha = 0$).

expectation from the $m = 0, 2, 4$ measurements

$$\begin{aligned}
\left\langle \sum_m \mathrm{SNR}_m \right\rangle &= \sqrt{\frac{T}{1\,\mathrm{year}}\, \mathcal{F}_\alpha^2\, \bar{\Omega}_{\rm GW}^2 \sum_m \langle p_{\ell m} p^*_{\ell m} \rangle \sum_{O=A,E} \sum_{O'=A,E} \gamma_{\ell m, OO'}\, \gamma^*_{\ell m, OO'}} \\
&= \sqrt{\frac{T}{1\,\mathrm{year}}}\, \mathcal{F}_\alpha\, C_\ell^{1/2}\, \bar{\Omega}_{\rm GW} \left[\sum_m \left(|\gamma_{\ell m, AA}|^2 + |\gamma_{\ell m, AE}|^2 + |\gamma_{\ell m, EA}|^2 + |\gamma_{\ell m, EE}|^2 \right) \right]^{1/2} \\
&= \sqrt{\frac{T}{1\,\mathrm{year}}}\, \mathcal{F}_\alpha\, C_\ell^{1/2}\, \bar{\Omega}_{\rm GW} \left[\sum_m \gamma^2_{\ell m, \mathrm{combined}} \right]^{1/2} \\
&\equiv \sqrt{\frac{T}{1\,\mathrm{year}}}\, \mathcal{F}_\alpha\, C_\ell^{1/2}\, \bar{\Omega}_{\rm GW}\, \gamma_{\ell, \mathrm{tot}}
\end{aligned} \tag{5.17}$$

and the sensitivity to C_ℓ is then obtained from the sum over all m's

$$\bar{\Omega}_{\rm GW}\, C_\ell^{1/2} \Big|_{\mathrm{threshold,1year}} = \frac{1}{\mathcal{F}_\alpha \left[\sum_{m=-\ell}^{\ell} \gamma^2_{\ell m, \mathrm{combined}} \right]^{1/2}} \tag{5.18}$$

Given what we proved in eq. (5.16), summing over m results in a quantity that is invariant under rotations [27]. Therefore, the sensitivity (5.18) only depends on the opening angle ψ formed by the two radial vectors that, starting from the centre of the Earth, point in the directions of the

two sites. Or, equivalently, on the distance $R_E\,\psi$ between the two sites. [2] An explicit evaluation gives

$$\begin{aligned}\gamma^2_{0,\mathrm{tot}} &= \frac{1+6\cos^2\psi+\cos^4\psi}{16\pi}\\ \gamma^2_{2,\mathrm{tot}} &= \frac{5\left[13-6\cos^2\psi+\cos^4\psi\right]}{196\pi}\\ \gamma^2_{4,\mathrm{tot}} &= \frac{321+246\cos^2\psi+\cos^4\psi}{28224\pi}\end{aligned} \tag{5.19}$$

We show the corresponding threshold values in Figure 21.

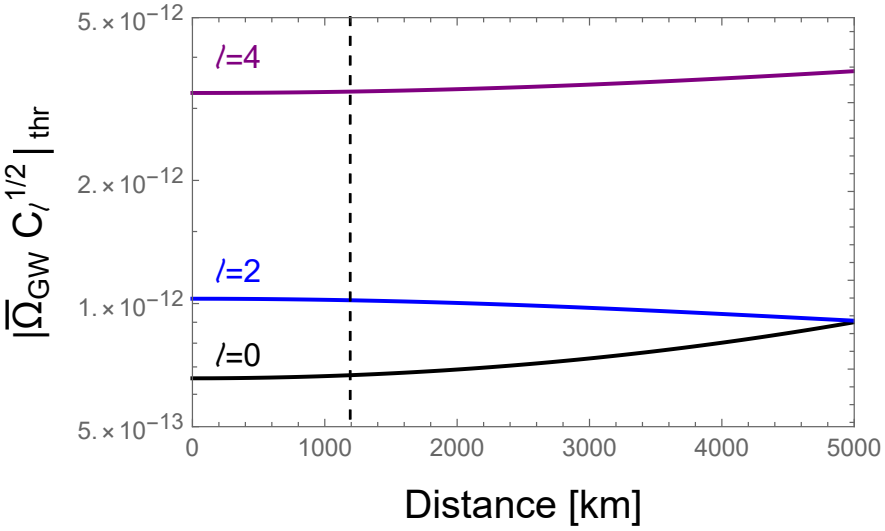

FIGURE 21: Sensitivity to a statistically invariant monopole, quadruple, and hexadecapole multipole of the SGWB. The lines show the amplitude that the multipoles must have to produce SNR = 1 in one year of observation. The horizontal axis is the distance between the two sites. The vertical dashed line corresponds to the distance between the two sites under consideration for ET. A scale invariant Ω_{GW} is assumed ($\alpha = 0$).

[2] This distance is the length of the arc on the Earth surface between the two sites. The angle between the two sites under considerations for ET is $\psi \simeq 0.19$. For this angle, the length of the arc is only about 0.15 % greater than the length of the segment joining the two sites, that is the distance that should be used in the condition (5.12).

Chapter 6

Conclusions

In this work we studied the sensitivity of a network of L-shaped and triangular-shaped ground based detectors to a Stochastic Gravitational Wave background. We followed the computation of ref. [12], that provided the formalism to study the response functions to the anisotropic SGWB from ground-based detectors, that have a well defined scanning pattern related to the daily rotation of the Earth. We also followed [17], that provided a simple procedure to write the overlap functions for a pair of detectors at any frequency. We extended their results in several ways.

Firstly, we extended the procedure of [12] to a generic network of detectors, not restricting our treatment to just a pair of instruments. Furthermore, we went beyond the assumption of a non polarized background, taking into account the possibility that the SGWB can bring a net amount of polarization. Thirdly, we considered the presence in the network of triangular-shape detectors, where multiple measurements can be performed at the same location, that we diagonalised using the formalism developed for the LISA constellation [20].

We applied this formalism to a network made of the two Advanced LIGOs, Advanced Virgo, KAGRA and ET, which is assumed to be built in the site under current consideration in Sardinia (Italy). In this case we provided the threshold values of Ω_{GW} necessary to the SGWB to be detected by this network of instruments. We paid particular attention to the impact provided by ET, by comparing the threshold levels of this network with and without the inclusion of this instrument. Our analysis has been done under the assumption that the SGWB is dominated by a single multipole, in an expansion of the signal in spherical harmonics. We provided explicit results for the first three multipoles, namely the monopole, dipole, and the quadrupole). For these multipoles, we provided analytic expressions for the (frequency-dependent) overlap functions of any detector pairs [1].

Averaging over the possible values of m within each ℓ, we obtained that the threshold values of $\overline{\Omega_{GW} p_\ell}$ for the monopole, dipole and quadrupole to be detected over 1 year of observation are presented in table 22 (in the first line we show the values for the network of the two Advanced LIGOs, Advanced Virgo and KAGRA interferometers; in the second line we consider the same network with Einstein Telescope). We found that the contribution of ET for the measurement of a SGWB amounts to an improvement of a factor $\sim$10 to the sensitivity with respect to the existing network of instruments in their *Advanced* configuration.

[1] The analytic expression for the quadrupole case is an original result of this thesis.

We were also interested in quantifying the SGWB that ET can reach on its own, without correlating it with LIGO, Virgo, and KAGRA. Multiple measurements can be performed at ET instrument (combining the measurements by the detectors placed in the three vertices). However, measurements performed at the same site have correlated noise, which substantially impacts our ability to detect a SGWB signal. We therefore considered the (speculative) possibility that two ET-detectors are constructed in the two sites currently under consideration for ET (one in Sardinia and one at the Belgium-Netherlands border). The distance between these two sites is such that the overlap functions can be evaluated by simply setting the GW frequency to zero, where they acquire particularly simple expressions [18].

Therefore, in table 22 we compared also the threshold values of $\bar{\Omega}_{GW} C_\ell^{1/2}$ for the monopole, dipole and quadrupole necessary to be detected over 1 year of observation by the full network of section 4 with the ones for the network made of the two ETs, as in section 5. The result are shown on the second and third line respectively. In this case, we see that the introduction of a second instrument ET-like can improve the detectability of a SGWB of a factor $\sim$100 with respect to the network with only one Einstein Telescope and the other existing instruments.

$\bar{\Omega}_{GW} C_\ell^{1/2}$	$\ell = 0$	$\ell = 1$	$\ell = 2$
LIGOs+Virgo+KAGRA	2.3×10^{-9}	2.5×10^{-9}	1.9×10^{-9}
LIGOs+Virgo+KAGRA+ET	1.8×10^{-10}	1.8×10^{-10}	1.2×10^{-10}
ET (Sardinia)+ET (Netherlands)	7.6×10^{-13}	8.4×10^{-12}	1.1×10^{-12}

FIGURE 22: Averaged threshold values of $\bar{\Omega}_{GW} C_\ell^{1/2}$ for monopole, dipole and quadrupole necessary to produce SNR=1 in the network of instruments considered. The computation are done assuming scale invariant power spectrum, unpolarized background and one year of observation.

As a last remark, we know from theory [28] that the predicted energy density for the monopole of an unpolarized astrophysical background (the models predict $\alpha = \frac{2}{3}$ as remarked before) is $\bar{\Omega}^{\rm th}_{GW,\rm mon} \simeq 3 \times 10^{-9}$, while an explicit evaluation for the network made of Advanced LIGOs + Advanced Virgo + KAGRA leads to a threshold value necessary to produce SNR=1 (over 1 year of observation) of $\bar{\Omega}^{\rm LVK}_{GW,\rm mon} \simeq 1.5 \times 10^{-9}$. The same computation taking into account also the Einstein Telescope contribution leads to $\bar{\Omega}^{\rm LVK+ET}_{GW,\rm mon} \simeq 9.5 \times 10^{-11}$, from which it becomes evident the benefit of Einstein Telescope to study the SGWB.

The present thesis can be extended in several directions. For example, one can go beyond the assumption of having the angular and the frequency dependence factorized for the power spectrum of the SGWB. Another possibility is to consider simultaneously more than a single multipole (ℓ, m) for the anisotropies of the SGWB, understanding how to disentangle their independent contributions. It can be also interesting to understand how to prove, in the case of a non chiral symmetric background, the presence of a net amount of polarized gravitational waves with the present network of interferometers.

Appendix A

Polarization operators

We consider the two polarization tensors defined in (1.4). It can be proven that

$$\begin{aligned} e^r_{ab}(\hat{n})\, e^s_{ab}(\hat{n}) &= 2\,\delta^{rs} \\ \sum_{s=+,\times} e^s_{ab}(\hat{n})\, e^s_{cd}(\hat{n}) &= \bar{Q}_{ac}\,\bar{Q}_{bd} + \bar{Q}_{ad}\,\bar{Q}_{bc} - \bar{Q}_{ab}\,\bar{Q}_{cd} \quad , \quad \bar{Q}_{ab} \equiv \delta_{ab} - \hat{n}_a\,\hat{n}_b \\ \sum_{s=+,\times} \int d^2\hat{n}\, e^s_{ab}(\hat{n})\, e^s_{cd}(\hat{n}) &= \frac{8\pi}{5}\left(\delta_{ac}\delta_{bd} + \delta_{ad}\delta_{bc} - \frac{2}{3}\delta_{ab}\delta_{cd}\right) \end{aligned} \tag{A.1}$$

Moreover, we can introduce the helicity operators

$$\tilde{e}_{ab,R} \equiv \frac{e^+_{ab} + i\, e^\times_{ab}}{\sqrt{2}} \equiv \tilde{e}_{ab,1} \quad , \quad \tilde{e}_{ab,L} \equiv \frac{e^+_{ab} - i\, e^\times_{ab}}{\sqrt{2}} \equiv \tilde{e}_{ab,-1} \tag{A.2}$$

As shown in Appendix A of [29], under a rotation $\hat{n} \to R\hat{n}$, the helicity operators transform as

$$\tilde{e}_{ab,\lambda}(R\hat{n}) = \mathrm{e}^{-2i\lambda\,\gamma[\hat{n},R]}\, R_{ac} R_{bd}\, \tilde{e}_{cd,\lambda}(\hat{n}) \tag{A.3}$$

where γ is a real quantity whose precise expression is not relevant for the present discussion (see [29] for the precise expression). By combining the last two expressions one finds that

$$\sum_{s=+,\times} e^s_{ab}(R\hat{n})\, e^s_{cd}(R\hat{n}) = R_{aa'} R_{bb'} R_{cc'} R_{dd'} \sum_{s=+,\times} e^s_{ab}(\hat{n})\, e^s_{cd}(\hat{n}) \tag{A.4}$$

namely the quantity $\sum_{s=+,\times} e^s_{ab}(R\hat{n})\, e^s_{cd}(R\hat{n})$ is a tensor under rotations, while the individual polarization operator is not. Therefore, using equation (A.2) we find that

$$e^{*\lambda}_{ab}(\hat{n})\, e^\lambda_{cd}(\hat{n}) = \sum_{s=+,\times} e^s_{ab}(\hat{n})\, e^s_{cd}(\hat{n}) \tag{A.5}$$

and from equation (A.4) it follows immediately that also the quantity $e^{*\lambda}_{ab}(R\hat{n})\, e^\lambda_{cd}(R\hat{n})$ is a tensor under rotations.

Appendix B

Evaluation of signal expectation value and variance in chapter 3

B.1 – Signal expectation value

As we discussed in section 3, the different measurements are noise-uncorrelated. Therefore, the expectation value of the estimator $\mathcal{C}_m$ in (3.6) contains only the contribution from the signal

$$\begin{aligned}\langle \mathcal{C}_m \rangle = \frac{1}{T}\int_0^T dt\, \mathrm{e}^{-im\omega_e t} \int_{-\infty}^{+\infty} df \sum_{i=1}^{M}\sum_{j=i+1}^{M}\sum_{O,O'} \left\langle \tilde{s}^*_{iO}(f,t)\, \tilde{s}_{jO'}(f,t)\right\rangle \tilde{Q}_{ij,OO'}(f) + \\ + \sum_{i=1}^{M}\sum_{j=1}^{N}\sum_{O} \left\langle \tilde{s}^*_{iO}(f,t)\, \tilde{s}_{j}(f,t)\right\rangle \tilde{Q}_{ij,O} + \\ + \sum_{i=1}^{N}\sum_{j=i+1}^{N}\sum_{O} \left\langle \tilde{s}^*_{i}(f,t)\, \tilde{s}_{j}(f,t)\right\rangle \tilde{Q}_{ij}\end{aligned} \tag{B.1}$$

To compute the signal we recall that, to first order in the GW, light starting from $\boldsymbol{x}$ at the unperturbed time $t-2L$, arriving at $\boldsymbol{x}+L\,\hat{l}$, and returning back to $\boldsymbol{x}$ at the unperturbed time time t completes this flight in the time

$$T_{\text{return}} = 2L + \frac{\hat{l}^a\,\hat{l}^b}{2}\int_0^L ds\, h_{ab}\left(t-2L+s,\, \boldsymbol{x}+s\,\hat{l}\right) + \frac{\hat{l}^a\,\hat{l}^b}{2}\int_0^L ds\, h_{ab}\left(t-L+s,\, \boldsymbol{x}+L\,\hat{l}-s\,\hat{l}\right) \tag{B.2}$$

where we note that $T_0 = 2L$ is the unperturbed time for a return travel. We work in the regime of short arm, namely $2\pi f L \ll 1$. This applies to existing ground-based interferometers, and to the ones which are planned to be built in the next decades (we explicitly verify that this condition applies to our study in Chapter 5). In this case, we can approximate the GW appearing in (B.2) as $h_{ab}(t,\boldsymbol{x})$, which is constant along the line integral, and therefore

$$T_{\text{ret}} = 2L + \frac{\hat{l}^a\,\hat{l}^b}{2}\times 2\,L\,h_{ab}(t,\boldsymbol{x}) \tag{B.3}$$

We denote by $\boldsymbol{x}_{i\alpha}(t)$ the location of the vertex α of the $i-$th triangular-shaped detector, and by $\boldsymbol{x}_j(t)$ the location of the $j-$th L-shaped detector of the network. We denote by $\hat{u}_{i\alpha}(t)$

and $\hat{v}_{i\alpha}(t)$ the unit vectors in the directions of the two arms that start from this vertex of each triangular-shaped detector, as indicated in Figure 23. We note that these quantities are time-dependent due to the rotation of the Earth about its axis. With this conventions, the signal at the time t at the vertex α of the i-th triangular-shaped detector, located at $\boldsymbol{x}_{i\alpha}(t)$, is

$$s_{i\alpha}(t) = d^{ab}_{i\alpha}(t) h_{ab}(t, \boldsymbol{x}_i(t)) \quad , \quad d^{ab}_{i\alpha}(t) \equiv \frac{\hat{u}^a_{i\alpha}(t)\hat{u}^b_{i\alpha}(t) - \hat{v}^a_{i\alpha}(t)\hat{v}^b_{i\alpha}(t)}{2} \tag{B.4}$$

Analogously, being $\hat{u}_{j\alpha}(t)$ and $\hat{v}_{j\alpha}(t)$ the unit vectors in the directions of the two arms that start from the $j-$th L-shaped interferometer, the signal at the time t at the j-th L-shaped detector, located at $\boldsymbol{x}_j(t)$, is

$$s_j(t) = d^{ab}_j(t) h_{ab}(t, \boldsymbol{x}_i(t)) \quad , \quad d^{ab}_j(t) \equiv \frac{\hat{u}^a_j(t)\hat{u}^b_j(t) - \hat{v}^a_j(t)\hat{v}^b_j(t)}{2} \tag{B.5}$$

By using (B.4), (B.5) and (1.9) one finds

$$\tilde{s}_{i\alpha}(f, t) = \sum_{\lambda=R,L} \int d^2\hat{n} \int_{-\infty}^{+\infty} df' \mathrm{e}^{-2\pi i(f-f')t} \delta_\tau(f - f') \, \mathrm{e}^{-2\pi i f' \hat{n}\cdot\boldsymbol{x}_{i\alpha}(t)} h_\lambda(f', \hat{n}) \, e^\lambda_{ab}(\hat{n}) \, d^{ab}_{i\alpha}(t) \tag{B.6}$$

$$\tilde{s}_j(f, t) = \sum_{\lambda=R,L} \int d^2\hat{n} \int_{-\infty}^{+\infty} df' \mathrm{e}^{-2\pi i(f-f')t} \delta_\tau(f - f') \, \mathrm{e}^{-2\pi i f' \hat{n}\cdot\boldsymbol{x}_j(t)} h_\lambda(f', \hat{n}) \, e^\lambda_{ab}(\hat{n}) \, d^{ab}_{i\alpha}(t) \tag{B.7}$$

where, as we mentioned after (3.2), the interferometer location and arms directions can be treated as constant in the time integration of length τ. In analogy to [12] we have introduced the notation

$$\delta_\tau(f) \equiv \frac{\sin(\pi\tau f)}{\pi f} \quad , \quad \lim_{\tau\to\infty} \delta_\tau(f) = \delta_D(f) \tag{B.8}$$

We then compute the correlators

$$\begin{aligned}
\left\langle \tilde{s}^*_{i\alpha}\left(f,\,t\right)\tilde{s}_{j\beta}\left(f',\,t\right)\right\rangle &= \sum_{\lambda=R,L}\int_{-\infty}^{+\infty} df'\,\delta^2_\tau\left(f-f'\right)H_\lambda\left(\left|f'\right|\right)\int d^2\hat{n}\mathrm{e}^{2\pi i f'\hat{n}\cdot\left(\boldsymbol{x}_{i\alpha}(t)-\boldsymbol{x}_{j\beta}(t)\right)}\\
&\quad\times\sum_{\ell m}p_{\ell m,\lambda}Y_{\ell m}\left(\hat{n}\right)\,e^{*\lambda}_{ab}\left(\hat{n}\right)e^{\lambda}_{cd}\left(\hat{n}\right)d^{ab}_{i\alpha}\left(t\right)d^{cd}_{j\beta}\left(t\right)\\
\left\langle \tilde{s}^*_{i\alpha}\left(f,\,t\right)\tilde{s}_{j}\left(f',\,t\right)\right\rangle &= \sum_{\lambda=R,L}\int_{-\infty}^{+\infty} df'\,\delta^2_\tau\left(f-f'\right)H_\lambda\left(\left|f'\right|\right)\int d^2\hat{n}\mathrm{e}^{2\pi i f'\hat{n}\cdot\left(\boldsymbol{x}_{i\alpha}(t)-\boldsymbol{x}_{j}(t)\right)}\\
&\quad\times\sum_{\ell m}p_{\ell m,\lambda}Y_{\ell m}\left(\hat{n}\right)\,e^{*\lambda}_{ab}\left(\hat{n}\right)e^{\lambda}_{cd}\left(\hat{n}\right)d^{ab}_{i\alpha}\left(t\right)d^{cd}_{j}\left(t\right)\\
\left\langle \tilde{s}^*_{i}\left(f,\,t\right)\tilde{s}_{j}\left(f',\,t\right)\right\rangle &= \sum_{\lambda=R,L}\int_{-\infty}^{+\infty} df'\,\delta^2_\tau\left(f-f'\right)H_\lambda\left(\left|f'\right|\right)\int d^2\hat{n}\mathrm{e}^{2\pi i f'\hat{n}\cdot\left(\boldsymbol{x}_{i}(t)-\boldsymbol{x}_{j}(t)\right)}\\
&\quad\times\sum_{\ell m}p_{\ell m,\lambda}Y_{\ell m}\left(\hat{n}\right)\,e^{*\lambda}_{ab}\left(\hat{n}\right)e^{\lambda}_{cd}\left(\hat{n}\right)d^{ab}_{i}\left(t\right)d^{cd}_{j}\left(t\right)
\end{aligned}\tag{B.9}$$

As the integration time τ is chosen to be much greater than the inverse of the typical measured frequencies, one of the two δ_τ in this expression can be substituted with a Dirac $\delta-$function, while the other one evaluates to the integration time, obtaining

$$\begin{aligned}
\left\langle \tilde{s}^*_{i\alpha}\left(f,\,t\right)\tilde{s}_{j\beta}\left(f,\,t\right)\right\rangle &= \tau\sum_{\lambda=R,L}H_\lambda\left(\left|f\right|\right)\int d^2\hat{n}\,\mathrm{e}^{2\pi i f\hat{n}\cdot\left(\boldsymbol{x}_{i\alpha}(t)-\boldsymbol{x}_{j\beta}(t)\right)}\\
&\quad\times\sum_{\ell m}p_{\ell m,\lambda}Y_{\ell m}\left(\hat{n}\right)\,e^{*\lambda}_{ab}\left(\hat{n}\right)e^{\lambda}_{cd}\left(\hat{n}\right)d^{ab}_{i\alpha}\left(t\right)d^{cd}_{j\beta}\left(t\right)\\
\left\langle \tilde{s}^*_{i\alpha}\left(f,\,t\right)\tilde{s}_{j}\left(f,\,t\right)\right\rangle &= \tau\sum_{\lambda=R,L}H_\lambda\left(\left|f\right|\right)\int d^2\hat{n}\,\mathrm{e}^{2\pi i f\hat{n}\cdot\left(\boldsymbol{x}_{i\alpha}(t)-\boldsymbol{x}_{j}(t)\right)}\\
&\quad\times\sum_{\ell m}p_{\ell m,\lambda}Y_{\ell m}\left(\hat{n}\right)\,e^{*\lambda}_{ab}\left(\hat{n}\right)e^{\lambda}_{cd}\left(\hat{n}\right)d^{ab}_{i\alpha}\left(t\right)d^{cd}_{j}\left(t\right)\\
\left\langle \tilde{s}^*_{i}\left(f,\,t\right)\tilde{s}_{j}\left(f,\,t\right)\right\rangle &= \tau\sum_{\lambda=R,L}H_\lambda\left(\left|f\right|\right)\int d^2\hat{n}\,\mathrm{e}^{2\pi i f\hat{n}\cdot\left(\boldsymbol{x}_{i}(t)-\boldsymbol{x}_{j}(t)\right)}\\
&\quad\times\sum_{\ell m}p_{\ell m,\lambda}Y_{\ell m}\left(\hat{n}\right)\,e^{*\lambda}_{ab}\left(\hat{n}\right)e^{\lambda}_{cd}\left(\hat{n}\right)d^{ab}_{i}\left(t\right)d^{cd}_{j}\left(t\right)
\end{aligned}\tag{B.10}$$

Proceeding in this way, we can readily go from the correlation of the signal at the three vertices to the correlator of the signal in the thee channels, and rewrite the first equation of (B.10) as

$$\begin{aligned}
\left\langle \tilde{s}^*_{iO}\left(f,\,t\right)\tilde{s}_{jO'}\left(f,\,t\right)\right\rangle &= \tau\sum_{\lambda=R,L}H_\lambda\left(\left|f\right|\right)\int d^2\hat{n}\mathrm{e}^{2\pi i f\hat{n}\cdot\left(\boldsymbol{x}_{i}(t)-\boldsymbol{x}_{j}(t)\right)}\\
&\quad\times\sum_{\ell m}p_{\ell m,\lambda}Y_{\ell m}\left(\hat{n}\right)e^{*\lambda}_{ab}\left(\hat{n}\right)e^{\lambda}_{cd}\left(\hat{n}\right)d^{ab}_{iO}\left(t\right)d^{cd}_{jO'}\left(t\right)
\end{aligned}\tag{B.11}$$

where $d^{ab}_{iO}\equiv c_{O\alpha}d^{ab}_{i\alpha}$. Evaluating these linear combinations we find

$$d^{ab}_{iA}=\frac{2}{\sqrt{3}}d^{ab}_{iX}\quad,\quad d^{ab}_{iE}=-\frac{2}{3}\left(d^{ab}_{iX}+2d^{ab}_{iY}\right)\quad,\quad d^{ab}_{iT}=0\tag{B.12}$$

namely only the two channels A and E are non vanishing in the short arm approximation. Inserting all this in (B.1), we obtain

$$\begin{aligned}\langle C_m\rangle =& \frac{\tau}{T}\int_0^T dt\, \mathrm{e}^{-im\omega_e t}\sum_{\lambda=R,L}\int_{-\infty}^{+\infty} df\, H_\lambda\left(|f|\right)\int d^2\hat{n}\, e^{*\lambda}_{ab}\left(\hat{n}\right) e^{\lambda}_{cd}\left(\hat{n}\right)\sum_{\ell m'} p_{\ell m',\lambda}\, Y_{\ell m'}\left(\hat{n}\right)\\ &\times\Bigg[\sum_{i=1}^{M}\sum_{j=i+1}^{M}\sum_{O=A,E}\sum_{O'=A,E} d^{ab}_{iO}\left(t\right) d^{cd}_{jO'}\left(t\right) Q_{ij,OO'}\left(f\right)\mathrm{e}^{2\pi i f\hat{n}\cdot\left(\boldsymbol{x}_i(t)-\boldsymbol{x}_j(t)\right)}+\\ &+\sum_{i=1}^{M}\sum_{j=1}^{N}\sum_{O=A,E} d^{ab}_{iO}\left(t\right) d^{cd}_{j}\left(t\right) Q_{ij,O}\left(f\right)\mathrm{e}^{2\pi i f\hat{n}\cdot\left(\boldsymbol{x}_i(t)-\boldsymbol{x}_j(t)\right)}+\\ &+\sum_{i=1}^{N}\sum_{j=i+1}^{N} d^{ab}_{i}\left(t\right) d^{cd}_{j}\left(t\right) Q_{ij}\left(f\right)\mathrm{e}^{2\pi i f\hat{n}\cdot\left(\boldsymbol{x}_i(t)-\boldsymbol{x}_j(t)\right)}\Bigg]\end{aligned} \tag{B.13}$$

As we mentioned, the quantities $d^{ab}_{i,A/E}\left(t\right)$ and $d^{ab}_{i}\left(t\right)$ are time dependent because of the rotation of the Earth in the frame of the fixed stars. Denoting by $d^{ab}_{i,A/E}$ and d^{ab}_{i} the same quantities in a frame that is fixed with respect to the Earth,

$$\begin{aligned} d^{ab}_{i,A/E}\left(t\right) &= R_{aa'}\left(t\right) R_{bb'}\left(t\right) d^{a'b'}_{i,A/E}\\ d^{ab}_{i}\left(t\right) &= R_{aa'}\left(t\right) R_{bb'}\left(t\right) d^{a'b'}_{i}\end{aligned} \tag{B.14}$$

where $R\left(t\right)$ is a rotation matrix of period T_e around the $z-$axis. We can reabsorb this rotation by changing integration variable $\hat{n}\to R\hat{n}$ in eq. (B.13). Using then eq. (A.5) we see that the rotation matrix disappears from everywhere apart from the argument of the spherical harmonic, where it produces $Y_{\ell m'}\left(R\hat{n}\right)=\mathrm{e}^{im'\omega_e t}Y_{\ell m'}\left(\hat{n}\right)$. Then we define the position of the i-th interferometer in this reference frame as $\boldsymbol{x}_i$, in such a way that we can set, as in (3.13)

$$\Delta\boldsymbol{x}_{ij}=\boldsymbol{x}_i-\boldsymbol{x}_j \tag{B.15}$$

It is then immediate to see that the integration in time then forces $m'=m$, and

$$\begin{aligned}\langle C_m\rangle =& \tau\sum_{\lambda=R,L}\int_{-\infty}^{+\infty} df\, H_\lambda\left(|f|\right)\int d^2\hat{n}\, e^{*\lambda}_{ab}\left(\hat{n}\right) e^{\lambda}_{cd}\left(\hat{n}\right)\sum_{\ell=|m|}^{\infty} p_{\ell m,\lambda}\, Y_{\ell m}\left(\hat{n}\right)\\ &\times\Bigg[\sum_{i=1}^{M}\sum_{j=i+1}^{M}\sum_{O,O'} d^{ab}_{iO}d^{cd}_{jO'}Q_{ij,OO'}\left(f\right)\mathrm{e}^{2\pi i f\hat{n}\cdot\Delta\boldsymbol{x}_{ij}}+\sum_{i=1}^{M}\sum_{j=i+1}^{N}\sum_{O} d^{ab}_{iO}d^{cd}_{j}Q_{ij,O}\left(f\right)\mathrm{e}^{2\pi i f\hat{n}\cdot\Delta\boldsymbol{x}_{ij}}+\\ &+\sum_{i=1}^{N}\sum_{j=1}^{N} d^{ab}_{i}d^{cd}_{j}Q_{ij}\left(f\right)\mathrm{e}^{2\pi i f\hat{n}\cdot\Delta\boldsymbol{x}_{ij}}\Bigg]\end{aligned} \tag{B.16}$$

which leads to (3.8) in the main text.

B.2 – Variance of the noise

For what concerns the variance of the noise, we start from the denominator of (3.7), evaluating

$$\begin{aligned}\left\langle |\mathcal{C}_m|^2 \right\rangle = \frac{1}{T^2}\int_0^T dt \int_0^T dt' \mathrm{e}^{im\omega_e(t-t')} \int_{-\infty}^{+\infty} df \int_{-\infty}^{+\infty} df' \\ \times \left\langle \left[\sum_{O,O'} \sum_{i=1}^{M} \sum_{j=i+1}^{M} Q^*_{ij,OO'}(f)\, \tilde{n}_{i,O}(f,t)\, \tilde{n}^*_{j,O'}(f,t) + \right.\right. \\ + \sum_{O} \sum_{i=1}^{M} \sum_{j=1}^{N} Q^*_{ij,O}(f)\, \tilde{n}_{i,O}(f,t)\, \tilde{n}^*_{j}(f,t) + \left.\left. \sum_{i=1}^{N} \sum_{j=i+1}^{N} Q^*_{ij}(f)\, \tilde{n}_{i}(f,t)\, \tilde{n}^*_{j}(f,t) \right] \right. \\ \times \left[\sum_{O'',O'''} \sum_{k=1}^{M} \sum_{l=k+1}^{M} Q_{kl,O''O'''}(f')\, \tilde{n}^*_{k,O''}(f',t')\, \tilde{n}_{l',O'''}(f',t') + \right. \\ \left. \left. + \sum_{O''} \sum_{k=1}^{M} \sum_{l=1}^{N} Q_{kl,O''}(f')\, \tilde{n}^*_{k,O''}(f',t')\, \tilde{n}_{l}(f',t') + \sum_{k=1}^{N} \sum_{l=k+1}^{N} Q_{kl}(f)\, \tilde{n}^*_{k}(f',t')\, \tilde{n}_{l}(f',t') \right] \right\rangle\end{aligned} \tag{B.17}$$

Some useful intermediate quantities for this computation are

$$\begin{aligned}\left\langle \tilde{n}^*_{iO}(f,t)\, \tilde{n}_{jO'}(f',t') \right\rangle = \frac{\delta_{ij}\,\delta_{OO'}}{2} \int_{-\infty}^{+\infty} df_1\, \mathrm{e}^{2\pi i t(f-f_1) - 2\pi i t'(f'-f_1)} \times \\ \times\, \delta_\tau(f-f_1)\, \delta_\tau(f'-f_1)\, N_{i,O}(|f_1|)\end{aligned} \tag{B.18}$$

$$\begin{aligned}\left\langle \tilde{n}^*_{iO}(f,\,t)\, \tilde{n}_j(f',\,t') \right\rangle = 0 \\ \left\langle \tilde{n}^*_{i}(f,\,t)\, \tilde{n}_j(f',\,t') \right\rangle = \frac{\delta_{ij}}{2} \int_{-\infty}^{+\infty} df_1\, \mathrm{e}^{2\pi i t(f-f_1) - 2\pi i t'(f'-f_1)} \delta_\tau(f-f_1)\, \delta_\tau(f'-f_1)\; P_i(|f_1|)\end{aligned} \tag{B.19}$$

which follows from combining eq. (3.2) and (3.1) for the noise with eq. (2.9) and (2.4). It is also useful to recall that reality of $n_{i,O}(t)$ and $n_i(t)$ imposes that $\tilde{n}_{i,O}(f) = \tilde{n}^*_{i,O}(-f)$ and $\tilde{n}_i(f) = \tilde{n}^*_i(-f)$. Inserting this into eq. (B.17), evaluating the expectation values under the

assumption that the noise is Gaussian, and integrating over the times, results in

$$\begin{aligned}\left\langle |\mathcal{C}_m|^2 \right\rangle = \frac{1}{4T^2}\int_{-\infty}^{+\infty} df df' df_1 df_2 \delta_\tau\left(f-f_1\right)\delta_\tau\left(f-f_2\right)\delta_\tau\left(f'-f_1\right)\delta_\tau\left(f'-f_2\right)\times \\ \times\,\delta_T^2\left(f_1-f_2+\frac{m\omega_e}{2\pi}\right)\Bigg[\sum_{i=1}^{M}\sum_{j=i+1}^{M}\sum_{OO'} N_{i,O}\left(|f_1|\right)N_{j,O'}\left(|f_2|\right)Q^*_{ij,OO'}\left(f\right)\,Q_{ij,OO'}\left(f'\right)+ \\ +\sum_{i=1}^{M}\sum_{j=1}^{N}\sum_{O} N_{i,O}\left(|f_1|\right)P_j\left(|f_2|\right)Q^*_{ij,O}\left(f\right)\,Q_{ij,O}\left(f'\right)+ \\ +\sum_{i=1}^{N}\sum_{j=i+1}^{N} P_i\left(|f_1|\right)P_j\left(|f_2|\right)Q^*_{ij}\left(f\right)\,Q_{ij}\left(f'\right)\Bigg]\end{aligned} \tag{B.20}$$

The integration time T is much greater than the inverse of the argument of δ_T, so we can treat that term as a Dirac $\delta-$function times T. Moreover, we can disregard $\frac{m\,\omega_e}{2\pi}$ in the argument, as it is much smaller than the frequencies in the ET window. This results in

$$\begin{aligned}\left\langle |\mathcal{C}_m|^2 \right\rangle = \frac{1}{4T}\int_{-\infty}^{+\infty} df df' df_1 \delta_\tau^2\left(f-f_1\right)\delta_\tau^2\left(f'-f_1\right) \\ \times\Bigg[\sum_{i=1}^{M}\sum_{j=i+1}^{M}\sum_{OO'} N_{i,O}\left(|f_1|\right)N_{j,O'}\left(|f_1|\right)Q^*_{ij,OO'}\left(f\right)\,Q_{ij,OO'}\left(f'\right)+ \\ +\sum_{i=1}^{M}\sum_{j=1}^{N}\sum_{O} N_{i,O}\left(|f_1|\right)P_j\left(|f_1|\right)Q^*_{ij,O}\left(f\right)\,Q_{ij,O}\left(f'\right)+ \\ +\sum_{i=1}^{N}\sum_{j=i+1}^{N} P_i\left(|f_1|\right)P_j\left(|f_1|\right)Q^*_{ij}\left(f\right)\,Q_{ij}\left(f'\right)\Bigg]\end{aligned} \tag{B.21}$$

We treat the δ_τ quantities analogously, and we obtain equation (3.15) in the main text.

B.3 – The SNR

Starting from (3.7) with (3.8) and (3.15) we obtain the following expression

$$\begin{aligned}\mathrm{SNR}_m = \frac{16\pi\sqrt{2T}}{5}\Bigg[\sum_\lambda \int_0^{+\infty} df H_\lambda(f) \sum_{\ell=|m|}^{\infty} p_{\ell m,\lambda}\Bigg(\sum_{i=1}^{M}\sum_{j=i+1}^{M}\sum_{O,O'}\gamma_{\ell m,ij,OO',\lambda}(f)\,Q_{ij,OO'}(f) + \\ + \sum_{i=1}^{M}\sum_{j=1}^{N}\sum_{O}\gamma_{\ell m,ij,O,\lambda}(f)\,Q_{ij,O}(f) + \sum_{i=1}^{N}\sum_{j=i+1}^{N}\gamma_{\ell m,ij,\lambda}(f)\,Q_{ij}(f)\Bigg)\Bigg]\times \\ \times\Bigg[\int_0^{+\infty} df\Bigg(\sum_{i=1}^{M}\sum_{j=i+1}^{M}\sum_{OO'} N_{i,O}(|f|)\,N_{j,O'}(|f|)\left|Q_{ij,OO'}(f)\right|^2 + \\ + \sum_{i=1}^{M}\sum_{j=1}^{N}\sum_{O} N_{i,O}(|f|)\,P_j(|f|)\left|Q_{ij,O}(f)\right|^2 + \sum_{i=1}^{N}\sum_{j=i+1}^{N} P_i(|f|)\,P_j(|f|)\left|Q_{ij}(f)\right|^2\Bigg)\Bigg]^{-\frac{1}{2}}\end{aligned} \tag{B.22}$$

where we have restricted the domain of integration to positive frequencies only. By relabelling

$$\begin{aligned}&\frac{16\pi\sqrt{2T}}{5}\sum_\lambda \frac{H_\lambda(f)}{\sqrt{N_{i,O}(f)\,N_{j,O'}(f)}}\sum_{\ell=|m|}^{\infty} p_{\ell m,\lambda}\,\gamma_{\ell m,ij,OO',\lambda}(f) \equiv \tilde{\gamma}_{ij,OO'}(f) \\ &\frac{16\pi\sqrt{2T}}{5}\sum_\lambda \frac{H_\lambda(f)}{\sqrt{N_{i,O}(f)\,P_j(f)}}\sum_{\ell=|m|}^{\infty} p_{\ell m,\lambda}\,\gamma_{\ell m,ij,O,\lambda}(f) \equiv \tilde{\gamma}_{ij,O}(f) \\ &\frac{16\pi\sqrt{2T}}{5}\sum_\lambda \frac{H_\lambda(f)}{\sqrt{P_i(f)\,P_j(f)}}\sum_{\ell=|m|}^{\infty} p_{\ell m,\lambda}\,\gamma_{\ell m,ij,\lambda}(f) \equiv \tilde{\gamma}_{ij}(f)\end{aligned} \tag{B.23}$$

and

$$\begin{aligned}&\sqrt{N_{i,O}(f)\,N_{j,O'}(f)}Q_{ij,OO'}(f) \equiv \tilde{Q}_{ij,OO'}(f) \\ &\sqrt{N_{i,O}(f)\,P_j(f)}Q_{ij,O}(f) \equiv \tilde{Q}_{ij,O}(f) \\ &\sqrt{P_i(f)\,P_j(f)}Q_{ij}(f) \equiv \tilde{Q}_{ij}(f)\end{aligned} \tag{B.24}$$

we can rewrite

$$\mathrm{SNR}_m = \left[\int_0^\infty df \Big(\sum_{i=1}^{M} \sum_{j=i+1}^{M} \sum_{OO'} \tilde{\gamma}_{ij,OO'}(f)\, \tilde{Q}_{ij,OO'}(f) + \sum_{i=1}^{M} \sum_{j=1}^{N} \sum_{O} \tilde{\gamma}_{ij,O}(f)\, \tilde{Q}_{ij,O}(f) + \right.$$
$$\left. + \sum_{i=1}^{N} \sum_{j=i+1}^{N} \tilde{\gamma}_{ij}(f)\, \tilde{Q}_{ij}(f) \Big) \right] \times \left[\int_0^\infty df \Big(\sum_{i=1}^{M} \sum_{j=i+1}^{M} \sum_{OO'} |\tilde{Q}_{ij,OO'}(f)|^2 + \right.$$
$$\left. + \sum_{i=1}^{M} \sum_{j=1}^{N} \sum_{O} |\tilde{Q}_{ij,O}(f)|^2 + \sum_{i=1}^{N} \sum_{j=i+1}^{N} |\tilde{Q}_{ij}(f)|^2 \Big) \right]^{-\frac{1}{2}} \tag{B.25}$$

which is maximized by $\tilde{Q}_{ij,OO'}(f) = c\,\tilde{\gamma}^*_{ij,OO'}(f)$, $\tilde{Q}_{ij,O}(f) = c\,\tilde{\gamma}^*_{ij,O}(f)$ and $\tilde{Q}_{ij}(f) = c\,\tilde{\gamma}^*_{ij}(f)$ where c is an arbitrary real constant that can be set to one. In terms of the original quantities, this gives (3.16) in the main text

Appendix C

Impact of a non vanishing phase Φ

In this appendix we estimate the impact of neglecting the phase Φ in eq. (B.10). Specifically we show that, once reintroduced in (B.13), this phase changes the result only to second order. To see this, we Taylor expand to first order eq. (B.13) with the phase inserted into it

$$\begin{aligned}\langle C_m\rangle \simeq & \frac{\tau}{T}\int_0^T dt\, \mathrm{e}^{-im\omega_e t}\sum_{\lambda=R,L}\int_{-\infty}^{+\infty} df\, H_\lambda\left(|f|\right)\int d^2\hat{n}\, e^{*\lambda}_{ab}\left(\hat{n}\right) e^{\lambda}_{cd}\left(\hat{n}\right)\sum_{\ell m'} p_{\ell m',\lambda}\, Y_{\ell m'}\left(\hat{n}\right)\\ &\times\Bigg[\sum_{i=1}^{M}\sum_{j=i+1}^{M}\sum_{O=A,E}\sum_{O'=A,E} d^{ab}_{iO}\left(t\right) d^{cd}_{jO'}\left(t\right) Q_{ij,OO'}\left(f\right)\left(1+2\pi i f\hat{n}\cdot\Delta\boldsymbol{x}_{ij}(t)\right)+\\ &+\sum_{i=1}^{M}\sum_{j=1}^{N}\sum_{O=A,E} d^{ab}_{iO}\left(t\right) d^{cd}_{j}\left(t\right) Q_{ij,O}\left(f\right)\left(1+2\pi i f\hat{n}\cdot\Delta\boldsymbol{x}_{ij}(t)\right)+\\ &+\sum_{i=1}^{N}\sum_{j=i+1}^{N} d^{ab}_{i}\left(t\right) d^{cd}_{j}\left(t\right) Q_{ij}\left(f\right)\left(1+2\pi i f\hat{n}\cdot\Delta\boldsymbol{x}_{ij}(t)\right)\Bigg]\\ &\equiv\left\langle C^{(0)}_m\right\rangle+\left\langle C^{(1)}_m\right\rangle\end{aligned}\tag{C.1}$$

where $C^{(i)}_m$ denotes the order Φ^i term in the Taylor expansion, and where we have defined $\Delta\boldsymbol{x}_{ij}(t)=\boldsymbol{x}_i(t)-\boldsymbol{x}_j(t)$. In the following, we denote by L the length of this vector.

We denote the first order correction of the coefficients (3.14) analogously,

$$\gamma^{(1)}_{\ell m,abcd,\lambda}(\Delta\boldsymbol{x}_{ij},f,t)\equiv\frac{5}{8\pi}\int d^2\hat{n}\, 2\pi i f\hat{n}\cdot\Delta\boldsymbol{x}_{ij}(t)\, Y_{\ell m}\left(\hat{n}\right) e^{\lambda}_{ab}\left(\hat{n}\right) e^{\lambda}_{cd}\left(\hat{n}\right)\tag{C.2}$$

Differently from the zeroth-order expressions evaluated in the man text, the quantities $\gamma^{(1)}_{\ell m,abcd,\lambda}(\Delta\boldsymbol{x}_{ij},f,t)$ depend on time. For this reason, we first define a new variable $\alpha\equiv\omega_e\, t$ and we compute $\gamma^{(1)}_{\ell m,abcd,\lambda}(\Delta\boldsymbol{x}_{ij},f,t)$ in a set of new reference systems with coordinates (θ',φ'), co-rotating with the Earth, and defined in such a way that each vector $\Delta\boldsymbol{x}'_{ij}$ is oriented along the $z'-$axis [12]

$$\hat{n}'\cdot\Delta\boldsymbol{x}'_{ij}(\alpha)=L\,\cos\theta'\tag{C.3}$$

We choose the fixed frame such that $\Delta\boldsymbol{x_{ij}}$ has no $y-$component at the initial time. The change of coordinate $(\theta,\,\varphi)\to(\theta',\,\varphi')$ is then obtained from two consecutive rotations. The first rotation is by an angle α about the $z-$axis, so that, after this rotation, $\Delta\boldsymbol{x_{ij}}$ has vanishing $y-$component

at all times. The second rotation is along the new $y-$axis (the one emerging from the first rotation), so to eliminate the $x-$component of $\Delta \boldsymbol{x}_{ij}$. We denote by β the angle of this second rotation, and by R the matrix that encodes the product of these two rotations. Accounting for the change of the polarization operator given by combining eq. (A.4) and (A.5) and for the change of the spherical harmonics under a rotation, we see that the change of variable results in

$$\begin{cases} Y_{\ell m}(\theta,\varphi) = \sum_{k=-\ell}^{l} D^{\ell *}_{mk}(\alpha,\beta,0) Y_{\ell k}(\theta',\varphi') = \sum_{k=-\ell}^{\ell} e^{im\alpha} d^{\ell}_{mk}(\beta) Y_{\ell k}(\theta',\varphi') \\ \hat{n}\cdot\Delta \boldsymbol{x}_{ij}(\alpha) = L\,\cos\theta' \\ e^{*\lambda}_{ab}\,(\hat{n})\, e^{\lambda}_{cd}\,(\hat{n}) = R_{aa'}\,R_{bb'}\,R_{cc'}\,R_{dd'}\,e^{*\lambda}_{a'b'}\,(\hat{n}')\, e^{\lambda}_{c'd'}\,(\hat{n}') \\ d^2\hat{n} = d^2\hat{n}' \end{cases} \tag{C.4}$$

where the explicit form for the coefficients $d^{l}_{mk}(\beta)$, which is however irrelevant for our purposes, can be found in [12]. With these substitution, and setting $u \equiv \cos\theta'$, one finds

$$\gamma^{(1)}_{\ell m,abcd,\lambda}(\alpha,f) = 2\pi i f\,\frac{5}{8\pi} R_{aa'}\,R_{bb'}\,R_{cc'}\,R_{dd'} \sum_{k=-\ell}^{\ell} e^{im\alpha} d^{\ell}_{mk}(\beta) N^{k}_{\ell} \int_{-1}^{1} du\, P^{k}_{\ell}(u)\, L\, u\, I^{k,\lambda}_{a'b'c'd'}\,(u) \tag{C.5}$$

where we have used $Y_{\ell k}(\theta',\varphi') = \sqrt{\frac{2\ell+1}{4\pi}\frac{(\ell-k)!}{(\ell+k)!}} P^{k}_{\ell}(\cos\theta') e^{ik\varphi'} \equiv N^{k}_{\ell} P^{k}_{\ell}(\cos\theta') e^{ik\varphi'}$, and where we have introduced

$$I^{k,\lambda}_{a'b'c'd'}\,(u) \equiv \int_{0}^{2\pi} d\varphi' e^{ik\varphi'} e^{*\lambda}_{a'b'}\,(\hat{n}')\, e^{\lambda}_{c'd'}\,(\hat{n}') \tag{C.6}$$

One can verify that $I^{k,\lambda}_{a'b'c'd'}\,(u)$ has parity $(-1)^k$ as $u \to -u$. The associated Legendre polynomials $P^{k}_{\ell}\,(u)$ have instead parity $(-1)^{k+\ell}$. Therefore, the integrand of the $\int_{-1}^{+1} du$ integration in (C.5) has parity $(-1)^{\ell+1}$. As the integration is on an even domain, it vanishes for even ℓ, and, as a consequence,

$$\gamma^{(1)}_{lm,abcd,\lambda}(\alpha,f) = 0 \quad \text{for even } \ell \tag{C.7}$$

This concludes the proof that the terms $\gamma^{(0)}_{0m,abcd}$, $\gamma^{(0)}_{2m,abcd}$, $\gamma^{(0)}_{4m,abcd}$ evaluated in chapter 5, do not receive corrections to linear order in Φ. Therefore, our results for these coefficients are accurate up to $\mathrm{O}\left(\Phi^2\right)$ corrections. To conclude this appendix is worth noting that the same steps outlined here allow to see that only even (odd) powers of Φ contribute to even (odd) ℓ correlators.

Appendix D

Evaluation of the functions $\Gamma^{M,D,Q}_{abcd,\lambda}(\kappa,\hat{s})$

In this appendix, we show that the explicit writing of (3.14) for the monopole, dipole and quadrupole is

$$\begin{aligned}
\gamma_{00,abcd,\lambda}(\kappa,\hat{s}) &= \frac{5}{2\sqrt{\pi}}\Gamma^{M}_{abcd,\lambda}(\kappa,\hat{s}) \\
\gamma_{10,abcd,\lambda}(\kappa,\hat{s}) &= -\frac{5i}{2}\sqrt{\frac{3}{\pi}}\Gamma^{D}_{abcd,\lambda}(\kappa,\hat{s},\hat{z}) \\
\gamma_{1\pm1,abcd,\lambda}(\kappa,\hat{s}) &= \frac{5i}{2}\sqrt{\frac{3}{2\pi}}\left[\pm\Gamma^{D}_{abcd,\lambda}(\kappa,\hat{s},\hat{x})+i\Gamma^{D}_{abcd,\lambda}(\kappa,\hat{s},\hat{y})\right] \\
\gamma_{20,abcd,\lambda}(\kappa,\hat{s}) &= \frac{5}{4}\sqrt{\frac{5}{\pi}}\left[-3\Gamma^{Q}_{abcd,\lambda}(\kappa,\hat{s},\hat{z},\hat{z})-\Gamma^{M}_{abcd,\lambda}(\kappa,\hat{s})\right] \\
\gamma_{2\pm1,abcd,\lambda}(\kappa,\hat{s}) &= \frac{5}{2}\sqrt{\frac{15}{2\pi}}\left[\pm\Gamma^{Q}_{abcd,\lambda}(\kappa,\hat{s},\hat{x},\hat{z})+i\Gamma^{Q}_{abcd,\lambda}(\kappa,\hat{s},\hat{y},\hat{z})\right] \\
\gamma_{2\pm2,abcd,\lambda}(\kappa,\hat{s}) &= \frac{5}{4}\sqrt{\frac{15}{2\pi}}\left[-\Gamma^{Q}_{abcd,\lambda}(\kappa,\hat{s},\hat{x},\hat{x})\mp 2i\Gamma^{Q}_{abcd,\lambda}(\kappa,\hat{s},\hat{x},\hat{y})+\Gamma^{Q}_{abcd,\lambda}(\kappa,\hat{s},\hat{y},\hat{y})\right]
\end{aligned} \tag{D.1}$$

where we introduced the following functions:

$$\begin{aligned}
\Gamma^{M}_{abcd,\lambda}(\kappa,\hat{s}) &= \frac{1}{8\pi}\int d^2\hat{n}\, e^{i\kappa\hat{n}\cdot\hat{s}}\, e^{*\lambda}_{ab}(\hat{n})\, e^{\lambda}_{cd}(\hat{n}) \\
\Gamma^{D}_{abcd,\lambda}(\kappa,\hat{s},\hat{v}) &= \frac{1}{8\pi}\int d^2\hat{n}\, e^{i\kappa\hat{n}\cdot\hat{s}}\, e^{*\lambda}_{ab}(\hat{n})\, e^{\lambda}_{cd}(\hat{n})\, (i\hat{v}\cdot\hat{n}) \\
\Gamma^{Q}_{ab,cd,\lambda}(\kappa,\hat{s},\hat{v},\hat{w}) &= \frac{1}{8\pi}\int d^2\hat{n}\, e^{i\kappa\hat{n}\cdot\hat{s}}\, e^{*\lambda}_{ab}(\hat{n})\, e^{\lambda}_{cd}(\hat{n})\, (i\hat{v}\cdot\hat{n})\,(i\hat{w}\cdot\hat{n})
\end{aligned} \tag{D.2}$$

In [17] it has been proven that the last expressions can be rewritten in the form of

$$\begin{aligned}
\Gamma^{M}_{abcd,\lambda}(\kappa,\hat{s}) &= \Gamma_{abcd,\lambda}(\kappa,\boldsymbol{s})_{|s=1} \\
\Gamma^{D}_{abcd,\lambda}(\kappa,\hat{s},\hat{v}) &= \left[\frac{1}{\kappa}\hat{v}_i\frac{\partial}{\partial s_i}\Gamma_{abcd,\lambda}(\kappa,\boldsymbol{s})\right]_{|s=1} \\
\Gamma^{Q}_{ab,cd,\lambda}(\kappa,\hat{s},\hat{v},\hat{w}) &= \left[\frac{1}{\kappa^2}\hat{v}_i\hat{w}_j\frac{\partial^2}{\partial s_i\partial s_j}\Gamma_{abcd,\lambda}(\kappa,\boldsymbol{s})\right]_{|s=1}
\end{aligned} \tag{D.3}$$

with

$$\begin{aligned}\Gamma_{abcd,\lambda}(\kappa,\boldsymbol{s}) = f_A(\kappa s)\frac{\delta_{ac}\delta_{bd}+\delta_{ad}\delta_{bc}}{2} + \frac{f_B(\kappa s)}{s^2}\frac{\delta_{ac}s_b s_d+\delta_{bd}s_a s_c+\delta_{ad}s_b s_c+\delta_{bc}s_a s_d}{4}+\\ + \frac{f_C(\kappa s)}{s^4}s_a s_b s_c s_d + \lambda\frac{f_D(\kappa s)}{s}\frac{\delta_{ac}s_e\varepsilon_{bde}+\delta_{bd}s_e\varepsilon_{ace}+\delta_{ad}s_e\varepsilon_{bce}+\delta_{bc}s_e\varepsilon_{ade}}{4}+\\ + \lambda\frac{f_E(\kappa s)}{s^3}\frac{s_a s_c s_e\varepsilon_{bde}+s_b s_d s_e\varepsilon_{ace}+s_a s_d s_e\varepsilon_{bce}+s_b s_c s_e\varepsilon_{ade}}{4}\end{aligned} \tag{D.4}$$

and

$$\begin{aligned}f_A(y) &= \frac{j_1(y)}{2y}+\frac{1-y^2}{2y^2}j_2(y)\\ f_B(y) &= \frac{j_1(y)}{y}+\frac{5-y^2}{y^2}j_2(y)\\ f_C(y) &= -7\frac{j_1(y)}{4y}+\frac{35-y^2}{y^2}j_2(y)\\ f_D(y) &= \frac{j_1(y)}{2}-\frac{j_2(y)}{2y}\\ f_E(y) &= -\frac{j_1(y)}{2}+\frac{5j_2(y)}{2y}\end{aligned} \tag{D.5}$$

where $j_1(y)$ and $j_2(y)$ are the Bessel Functions, respectively of the first and the second type. The authors of [17] provided for a couple of L-shaped interferometers the explicit form of the quantities

$$\begin{aligned}\mathcal{M}^{\lambda}_{ij}(k,\hat{s}) &= \Gamma^{M}_{abcd,\lambda}(\kappa,\hat{s})d^{ab}_i d^{cd}_j\\ \mathcal{D}^{\lambda}_{ij}(k,\hat{s},\hat{v}) &= \Gamma^{D}_{abcd,\lambda}(\kappa,\hat{s},\hat{v})d^{ab}_i d^{cd}_j\end{aligned} \tag{D.6}$$

which we recall to be:

$$\begin{aligned}\mathcal{M}^{\lambda}_{ij}(k) = f_A(\kappa)\,\mathrm{tr}\left[d_i d_j\right] + f_B(\kappa)\left(d_i\hat{s}_{ij}\right)^a\left(d_j\hat{s}_{ij}\right)^a + f_C(\kappa)\left(d_i\hat{s}_{ij}\hat{s}_{ij}\right)\left(d_j\hat{s}_{ij}\hat{s}_{ij}\right)\\ + \lambda f_D(\kappa)\left[d_i d_j\right]^{ab}\varepsilon_{abc}\hat{s}^c_{ij} + \lambda f_E(\kappa)\left(d_i\hat{s}_{ij}\right)^a\left(d_j\hat{s}_{ij}\right)^b\varepsilon_{abc}\hat{s}^c_{ij}\end{aligned} \tag{D.7}$$

and

$$\begin{aligned}
\mathcal{D}_{ij,\lambda}(\kappa,\hat{s},\hat{v}) &= f'_A(\kappa)(\hat{v}\hat{s})\left(d_i d_j\right)^{aa} \\
&+ \left[f'_B(\kappa) - \frac{2f_B(\kappa)}{\kappa}\right](\hat{v}\hat{s})\left(d_i\hat{s}\right)^a\left(d_j\hat{s}\right)^a + \frac{f_B(\kappa)}{\kappa}\left[\left(d_i\hat{v}\right)^a\left(d_j\hat{s}\right)^a + \left(d_i\hat{s}\right)^a\left(d_j\hat{v}\right)^a\right] \\
&+ \left[f'_C(\kappa) - \frac{4f_C(\kappa)}{\kappa}\right](\hat{v}\hat{s})\left(d_i\hat{s}\hat{s}\right)\left(d_j\hat{s}\hat{s}\right) + \frac{2f_C(\kappa)}{\kappa}\left[\left(d_i\hat{v}\hat{s}\right)\left(d_j\hat{s}\hat{s}\right) + \left(d_i\hat{s}\hat{s}\right)\left(d_j\hat{v}\hat{s}\right)\right] \\
&+ \lambda(\hat{v}\hat{s})\left[f'_D(\kappa) - \frac{f_D(\kappa)}{\kappa}\right]\left(d_i d_j\times\hat{s}\right) + \lambda\frac{f_D(\kappa)}{\kappa}\left(d_i d_j\times\hat{v}\right) \\
&+ \lambda\left[f'_E(\kappa) - \frac{3f_E(\kappa)}{\kappa}\right](\hat{v}\hat{s})\left[\left(d_i\hat{s}\right)\left(d_j\hat{s}\right)\times\hat{s}\right] \\
&+ \lambda\frac{f_E(\kappa)}{\kappa}\left\{\left[\left(d_i\hat{v}\right)\left(d_j\hat{s}\right)\times\hat{s}\right] + \left[\left(d_i\hat{s}\right)\left(d_j\hat{v}\right)\times\hat{s}\right] + \left[\left(d_i\hat{s}\right)\left(d_j\hat{s}\right)\times\hat{v}\right]\right\}
\end{aligned} \tag{D.8}$$

with

$$\begin{aligned}
\left(d_i d_j\right)^{ab} &\equiv d_i^{ac} d_j^{cb} \\
\left(d_i\hat{s}\right)^a &\equiv d_i^{ab}\hat{s}^b \\
\left(d_i\hat{s}\hat{s}\right) &\equiv d_i^{ab}\hat{s}^a\hat{s}^b \\
\left(d_i d_j\times\hat{s}\right) &\equiv d_i^{ae} d_j^{eb}\varepsilon_{abc}\hat{s}_c \\
\left[\left(d_i\hat{s}\right)\left(d_j\hat{s}\right)\times\hat{s}\right] &\equiv \left(d_i\hat{s}\right)^a\left(d_j\hat{s}\right)^b\varepsilon_{abc}\hat{s}_c \\
\left(\hat{v}\hat{s}\right) &\equiv \hat{v}^i\hat{s}^i \\
\left(d_i\hat{v}\right)^a &\equiv d_i^{ab}\hat{v}^b \\
\left(d_i\hat{v}\hat{s}\right) &\equiv d_i^{ab}\hat{v}^a\hat{s}^b \\
\left(d_i d_j\times\hat{v}\right) &\equiv d_i^{ae} d_j^{eb}\varepsilon_{abc}\hat{v}_c \\
\left[\left(d_i\hat{v}\right)\left(d_j\hat{s}\right)\times\hat{s}\right] &\equiv \left(d_i\hat{v}\right)^a\left(d_j\hat{s}\right)^b\varepsilon_{abc}\hat{s}_c \\
\left[\left(d_i\hat{s}\right)\left(d_j\hat{v}\right)\times\hat{s}\right] &\equiv \left(d_i\hat{s}\right)^a\left(d_j\hat{v}\right)^b\varepsilon_{abc}\hat{s}_c \\
\left[\left(d_i\hat{s}\right)\left(d_j\hat{s}\right)\times\hat{v}\right] &\equiv \left(d_i\hat{s}\right)^a\left(d_j\hat{s}\right)^b\varepsilon_{abc}\hat{v}_c
\end{aligned} \tag{D.9}$$

We went on following the procedure proved in equation (D.3) and we found the explicit analytic writing of the functions $\Gamma^{Q}_{abcd,\lambda}(\kappa,\hat{s},\hat{v},\hat{w})$

$$
\begin{aligned}
\Gamma^{Q}_{abcd,\lambda}(\kappa,\hat{s},\hat{v},\hat{w}) = {} & \left[f''_A(\kappa)\hat{v}_e\hat{s}_e\ \hat{w}_f\hat{s}_f + \frac{f'_A(\kappa)}{\kappa}\hat{v}_e\hat{w}_e - \frac{f'_A(\kappa)}{\kappa}\hat{v}_e\hat{s}_e\ w_f\hat{s}_f\right]\frac{1}{2}\left(\delta_{ac}\delta_{bd}+\delta_{aa}\delta_{bc}\right)+\\
& + \left[f''_B(\kappa) - \frac{2f'_B(\kappa)}{\kappa} + \frac{2f_B(\kappa)}{\kappa^2}\right]\hat{v}_e\hat{s}_e\hat{w}_f\hat{s}_f\frac{1}{4}\left(\delta_{ac}\hat{s}_b\hat{s}_d+\text{perm.}\right)+\\
& + \left[f'_B(\kappa) - \frac{2f_B(\kappa)}{\kappa}\right]\frac{1}{\kappa}(\hat{v}_e\hat{w}_e - \hat{v}_e\hat{s}_e\hat{w}_f\hat{s}_f)\frac{1}{4}\left(\delta_{ac}\hat{s}_b\hat{s}_d+\text{perm.}\right)+\\
& + \left[f'_B(\kappa) - \frac{2f_B(\kappa)}{\kappa}\right]\hat{v}_e\hat{s}_e\frac{1}{\kappa}\frac{1}{4}\{\delta_{ac}(\hat{w}_b\hat{s}_d+\hat{w}_d\hat{s}_b-2\hat{w}_f\hat{s}_f\hat{s}_b\hat{s}_d)+\text{perm.}\}+\\
& + \left[\frac{f'_B(\kappa)}{\kappa} - \frac{f_B(\kappa)}{\kappa^2}\right]\hat{w}_e\hat{s}_e\frac{1}{4}\{\delta_{ad}(\hat{v}_b\hat{s}_c+\hat{v}_c\hat{s}_b)+\text{perm.}\}+\\
& + \frac{f_B(\kappa)}{\kappa^2}\frac{1}{4}\{\delta_{ad}(\hat{v}_b\hat{w}_c+\hat{v}_c\hat{w}_b-\hat{w}_e\hat{s}_e\hat{v}_b\hat{s}_c-\hat{w}_e\hat{s}_e\hat{v}_c\hat{s}_b)+\text{perm.}\}+\\
& + \left[f''_C(\kappa) - \frac{4f'_C(\kappa)}{\kappa} + \frac{4f_C(\kappa)}{\kappa^2}\right]\hat{v}_e\hat{s}_e\hat{w}_f\hat{s}_f\hat{s}_a\hat{s}_b\hat{s}_c\hat{s}_d+\\
& + \left[f'_C(\kappa) - \frac{4f_C(\kappa)}{\kappa}\right]\frac{1}{\kappa}\hat{v}_e\{\hat{w}_a\hat{s}_b\hat{s}_c\hat{s}_d\hat{s}_e+\text{perm.}-5\hat{s}_a\hat{s}_b\hat{s}_c\hat{s}_d\hat{s}_e\hat{w}_f\hat{s}_f\}+\\
& + 2\left[\frac{f'_C(\kappa)}{\kappa} - \frac{f_C(\kappa)}{\kappa^2}\right]\hat{w}_e\hat{s}_e\frac{1}{2}\{\hat{v}_a\hat{s}_b\hat{s}_c\hat{s}_d+\text{perm.}\}+\\
& + \frac{2f_C(\kappa)}{\kappa^2}\frac{1}{2}\{\hat{v}_d(\hat{w}_a\hat{s}_b\hat{s}_c+\text{perm.}-3\hat{w}_e\hat{s}_e\hat{s}_a\hat{s}_b\hat{s}_c)+\text{perm.}\}+\\
& + \lambda\left[f''_D(\kappa) - \frac{f'_D(\kappa)}{\kappa} + \frac{f_D(\kappa)}{\kappa^2}\right]\hat{v}_e\hat{s}_e\hat{w}_f\hat{s}_f\frac{1}{4}(\delta_{ac}\varepsilon_{bdg}+\text{perm.})\hat{s}_g+\\
& + \lambda\left[f'_D(\kappa) - \frac{f_D(\kappa)}{\kappa}\right]\frac{1}{\kappa}\hat{v}_e\frac{1}{4}(\delta_{ac}\varepsilon_{bdg}+\text{perm.})(\hat{w}_e\hat{s}_g+\hat{w}_g\hat{s}_e-2\hat{w}_f\hat{s}_f\hat{s}_e\hat{s}_g)+\\
& + \lambda\left[\frac{f'_D(\kappa)}{\kappa} - \frac{f_D(\kappa)}{\kappa^2}\right]\hat{w}_f\hat{s}_f\frac{1}{4}(\delta_{ac}\varepsilon_{bdg}+\text{perm.})\hat{v}_g+\\
& + \lambda\left[f''_E(\kappa) - \frac{3f'_E(\kappa)}{\kappa} + \frac{3f_E(\kappa)}{\kappa^2}\right]\hat{w}_f\hat{s}_f\hat{v}_e\hat{s}_e\hat{s}_g\frac{1}{4}\left[\hat{s}_b\hat{s}_d\varepsilon_{acg}+\text{perm.}\right]+\\
& + \lambda\left[f'_E(\kappa) - \frac{3f_E(\kappa)}{\kappa}\right]\frac{1}{\kappa}\hat{v}_e\frac{1}{4}\{\varepsilon_{acg}(\hat{w}_e\hat{s}_b\hat{s}_d\hat{s}_g+\text{perm.}-4\hat{s}_e\hat{s}_b\hat{s}_d\hat{s}_g\hat{w}_f\hat{s}_f)+\text{perm.}\}+\\
& + \lambda\left[\frac{f'_E(\kappa)}{\kappa} - \frac{f_E(\kappa)}{\kappa^2}\right]\hat{w}_f\hat{s}_f\frac{1}{4}\{\left[(\hat{v}_b\hat{s}_d+\hat{s}_b\hat{v}_d)\hat{s}_g+\hat{s}_b\hat{s}_d\hat{v}_g\right]\varepsilon_{acg}+\text{perm.}\}+\\
& + \lambda\frac{f_E(\kappa)}{\kappa^2}\frac{1}{4}\Big\{\Big[\Big(\hat{w}_b\hat{v}_d+\hat{v}_b\hat{w}_d-2\hat{w}_f\hat{s}_f(\hat{v}_b\hat{s}_d+\hat{v}_d\hat{s}_b)\Big)\hat{s}_g+(\hat{s}_b\hat{v}_d+\hat{s}_d\hat{v}_b)\hat{w}_g+\\
& \qquad +(\hat{w}_b\hat{s}_d+\hat{s}_b\hat{w}_d-2\hat{s}_b\hat{s}_d\hat{w}_f\hat{s}_f)\hat{v}_g\Big]\varepsilon_{acg}+\text{perm.}\Big\} \qquad \text{(D.10)}
\end{aligned}
$$

and after being projected on the geometry of the couple of the detectors we define

$$
\mathcal{Q}^{\lambda}_{ij}(\kappa,\hat{s},\hat{v},\hat{w}) = \Gamma^{Q}_{abcd,\lambda}(\kappa,\hat{s},\hat{v},\hat{w})d^{ab}_i d^{cd}_j \qquad \text{(D.11)}
$$

where we identify the two contributes:

$$\mathcal{Q}_{ij,\lambda}(\kappa,\hat{s},\hat{v},\hat{w}) = \mathcal{Q}_{ij,\lambda}(\kappa,\hat{s},\hat{v},\hat{w})\big|_{\text{Parity invariant}} + \mathcal{Q}_{ij,\lambda}(\kappa,\hat{s},\hat{v},\hat{w})\big|_{\text{Parity violating}} \tag{D.12}$$

with

$$\begin{aligned}
&\mathcal{Q}_{ij,\lambda}(\kappa,\hat{s},\hat{v},\hat{w})\big|_{\text{Parity invariant}} = \\
&\left\{\frac{f'_A(\kappa)}{\kappa}(\hat{v}\hat{w}) + \left[f''_A(\kappa) - \frac{f'_A(\kappa)}{\kappa}\right](\hat{v}\hat{s})(\hat{w}\hat{s})\right\}\left(d_i d_j\right)^{aa} \\
&+\left\{\left[\frac{f'_B(\kappa)}{\kappa} - \frac{2f_B(\kappa)}{\kappa^2}\right](\hat{v}\hat{w}) + \left[f''_B(\kappa) - \frac{5f'_B(\kappa)}{\kappa} + \frac{8f_B(\kappa)}{\kappa^2}\right](\hat{v}\hat{s})(\hat{w}\hat{s})\right\}\left(d_i\hat{s}\right)^a\left(d_j\hat{s}\right)^a \\
&+\left[\frac{f'_B(\kappa)}{\kappa} - \frac{2f_B(\kappa)}{\kappa^2}\right](\hat{v}\hat{s})\left[\left(d_i\hat{w}\right)^a\left(d_j\hat{s}\right)^a + \left(d_i\hat{s}\right)^a\left(d_j\hat{w}\right)^a\right] \\
&+\left[\frac{f'_B(\kappa)}{\kappa} - \frac{2f_B(\kappa)}{\kappa^2}\right](\hat{w}\hat{s})\left[\left(d_i\hat{v}\right)^a\left(d_j\hat{s}\right)^a + \left(d_i\hat{s}\right)^a\left(d_j\hat{v}\right)^a\right] \\
&+\frac{f_B(\kappa)}{\kappa^2}\left[\left(d_i\hat{v}\right)^a\left(d_j\hat{w}\right)^a + \left(d_i\hat{w}\right)^a\left(d_j\hat{v}\right)^a\right] \\
&+\left\{\left[\frac{f'_C(\kappa)}{\kappa} - \frac{4f_C(\kappa)}{\kappa^2}\right](\hat{v}\hat{w}) + \left[f''_C(\kappa) - \frac{9f'_C(\kappa)}{\kappa} + \frac{24f_C(\kappa)}{\kappa^2}\right](\hat{v}\hat{s})(\hat{w}\hat{s})\right\}\left(d_i\hat{s}\hat{s}\right)\left(d_j\hat{s}\hat{s}\right) \\
&\quad+2\left[\frac{f'_C(\kappa)}{\kappa} - \frac{4f_C(\kappa)}{\kappa^2}\right](\hat{v}\hat{s})\left[\left(d_i\hat{w}\hat{s}\right)\left(d_j\hat{s}\hat{s}\right) + \left(d_i\hat{s}\hat{s}\right)\left(d_j\hat{w}\hat{s}\right)\right] \\
&\quad+2\left[\frac{f'_C(\kappa)}{\kappa} - \frac{4f_C(\kappa)}{\kappa^2}\right](\hat{w}\hat{s})\left[\left(d_i\hat{v}\hat{s}\right)\left(d_j\hat{s}\hat{s}\right) + \left(d_i\hat{s}\hat{s}\right)\left(d_j\hat{v}\hat{s}\right)\right] \\
&\qquad+\frac{2f_C(\kappa)}{\kappa^2}\left[\left(d_i\hat{v}\hat{w}\right)\left(d_j\hat{s}\hat{s}\right) + \left(d_i\hat{s}\hat{s}\right)\left(d_j\hat{v}\hat{w}\right) + 2\left(d_i\hat{v}\hat{s}\right)\left(d_j\hat{w}\hat{s}\right) + 2\left(d_i\hat{w}\hat{s}\right)\left(d_j\hat{v}\hat{s}\right)\right]
\end{aligned} \tag{D.13}$$

and

$$\begin{aligned}
&\mathcal{Q}_{ij,\lambda}(\kappa,\hat{s},\hat{v},\hat{w})\big|_{\text{Parity violating}} = \\
&\lambda\left\{\left[\frac{f'_D(\kappa)}{\kappa} - \frac{f_D(\kappa)}{\kappa^2}\right](\hat{v}\hat{w}) + \left[f''_D(\kappa) - \frac{3f'_D(\kappa)}{\kappa} + \frac{3f_D(\kappa)}{\kappa^2}\right](\hat{v}\hat{s})(\hat{w}\hat{s})\right\}\left(d_i d_j\times\hat{s}\right) \\
&+\lambda\left[\frac{f'_D(\kappa)}{\kappa} - \frac{f_D(\kappa)}{\kappa^2}\right](\hat{v}\hat{s})\left(d_i d_j\times\hat{w}\right) + \lambda\left[\frac{f'_D(\kappa)}{\kappa} - \frac{f_D(\kappa)}{\kappa^2}\right](\hat{w}\hat{s})\left(d_i d_j\times\hat{v}\right) \\
&+\lambda\left\{\left[\frac{f'_E(\kappa)}{\kappa} - \frac{3f_E(\kappa)}{\kappa^2}\right](\hat{v}\hat{w}) + \left[f''_E(\kappa) - \frac{7f'_E(\kappa)}{\kappa} + \frac{15f_E(\kappa)}{\kappa^2}\right](\hat{v}\hat{s})(\hat{w}\hat{s})\right\}\left[\left(d_i\hat{s}\right)\left(d_j\hat{s}\right)\times\hat{s}\right] \\
&+\lambda\left[\frac{f'_E(\kappa)}{\kappa} - \frac{3f_E(\kappa)}{\kappa^2}\right](\hat{v}\hat{s})\left\{\left[\left(d_i\hat{w}\right)\left(d_j\hat{s}\right)\times\hat{s}\right] + \left[\left(d_i\hat{s}\right)\left(d_j\hat{w}\right)\times\hat{s}\right] + \left[\left(d_i\hat{s}\right)\left(d_j\hat{s}\right)\times\hat{w}\right]\right\}
\end{aligned}$$

$$
\begin{aligned}
&+\lambda\left[\frac{f_E'(\kappa)}{\kappa}-\frac{3f_E(\kappa)}{\kappa^2}\right](\hat{w}\hat{s})\left\{\left[(d_i\hat{v})\left(d_j\hat{s}\right)\times\hat{s}\right]+\left[(d_i\hat{s})\left(d_j\hat{v}\right)\times\hat{s}\right]+\left[(d_i\hat{s})\left(d_j\hat{s}\right)\times\hat{v}\right]\right\}\\
&+\lambda\frac{f_E'(\kappa)}{\kappa^2}\Bigg\{\left[(d_i\hat{v})\left(d_j\hat{s}\right)\times\hat{w}\right]+\left[(d_i\hat{s})\left(d_j\hat{v}\right)\times\hat{w}\right]+\left[(d_i\hat{w})\left(d_j\hat{s}\right)\times\hat{v}\right]+\left[(d_i\hat{s})\left(d_j\hat{w}\right)\times\hat{v}\right]\\
&+\left[(d_i\hat{v})\left(d_j\hat{w}\right)\times\hat{s}\right]+\left[(d_i\hat{w})\left(d_j\hat{v}\right)\times\hat{s}\right]\Bigg\}
\end{aligned}
\tag{D.14}
$$

in doing this we also had to define

$$
\begin{aligned}
(\hat{v}\hat{w}) &\equiv \hat{v}^i\hat{w}^i\\
(d_i\hat{v}\hat{w}) &\equiv d_i^{ab}\hat{v}^a\hat{w}^b\\
\left[(d_i\hat{v})\left(d_j\hat{s}\right)\times\hat{w}\right] &\equiv (d_i\hat{v})^a\left(d_j\hat{s}\right)^b\varepsilon_{abc}\hat{w}_c\\
\left[(d_i\hat{s})\left(d_j\hat{v}\right)\times\hat{w}\right] &\equiv (d_i\hat{s})^a\left(d_j\hat{v}\right)^b\varepsilon_{abc}\hat{w}_c\\
\left[(d_i\hat{v})\left(d_j\hat{w}\right)\times\hat{s}\right] &\equiv (d_i\hat{v})^a\left(d_j\hat{w}\right)^b\varepsilon_{abc}\hat{s}_c
\end{aligned}
\tag{D.15}
$$

For completeness, one may introduce in an analogous way of (D.6) and (D.11) some useful quantities for studying a network made of both L-shaped and triangular-shaped interferometers:

$$
\begin{aligned}
\mathcal{M}^{\lambda}_{ij,O}(k,\hat{s}) &= \Gamma^{M}_{abcd,\lambda}(\kappa,\hat{s})d^{ab}_{i,O}d^{cd}_{j}\\
\mathcal{D}^{\lambda}_{ij,O}(k,\hat{s},\hat{v}) &= \Gamma^{D}_{abcd,\lambda}(\kappa,\hat{s},\hat{v})d^{ab}_{i,O}d^{cd}_{j}\\
\mathcal{Q}^{\lambda}_{ij,O}(\kappa,\hat{s},\hat{v},\hat{w}) &= \Gamma^{Q}_{abcd,\lambda}(\kappa,\hat{s},\hat{v},\hat{w})d^{ab}_{i,O}d^{cd}_{j}\\
\mathcal{M}^{\lambda}_{ij,OO'}(k,\hat{s}) &= \Gamma^{M}_{abcd,\lambda}(\kappa,\hat{s})d^{ab}_{i,O}d^{cd}_{j,O'}\\
\mathcal{D}^{\lambda}_{ij,OO'}(k,\hat{s},\hat{v}) &= \Gamma^{D}_{abcd,\lambda}(\kappa,\hat{s},\hat{v})d^{ab}_{i,O}d^{cd}_{j,O'}\\
\mathcal{Q}^{\lambda}_{ij,OO'}(\kappa,\hat{s},\hat{v},\hat{w}) &= \Gamma^{Q}_{abcd,\lambda}(\kappa,\hat{s},\hat{v},\hat{w})d^{ab}_{i,O}d^{cd}_{j,O'}
\end{aligned}
\tag{D.16}
$$

Appendix E

Geometry of the detectors

We specify the position and orientation of each detector as follows. We denote the latitude and longitude of the site with θ and φ, respectively. Following standard convention, the north pole is at latitude $\theta = 0$, while the equator is at latitude $\theta = \pi/2$. Let us consider a Cartesian system centred at the center of the Earth (assumed to be a perfect sphere), with the $x-$ axis pointing toward the location of 0 longitude on the equator, with the $y-$ axis pointing toward the location of $\pi/2$ longitude on the equator, and with the $z-$axis pointing toward the north pole. In this coordinate system, at the $\{\theta, \varphi\}$ location, the north direction is given by

$$\hat{v}_{\text{north}} = \{-\sin\theta\,\cos\varphi, -\sin\theta\,\sin\varphi, \cos\theta\} \tag{E.1}$$

while the east direction is given by

$$\hat{v}_{\text{east}} = \{-\sin\varphi, \cos\varphi, 0\} \tag{E.2}$$

we note that these vectors are a basis for the tangent space to the Earth surface at the $\{\theta, \varphi\}$ location, and they can therefore be employed to specify the directions of the arms of the detector. In our computations we specify the orientation by the angle β that the arm direction $\hat{u}_X$ forms with the north direction,

$$\hat{u}_X = \cos(\beta)\ \hat{v}_{\text{north}} + \sin(\beta)\ \hat{v}_{\text{east}} \tag{E.3}$$

for what concerns the L-shaped detectors, we have

$$\hat{u}_Y = -\sin(\beta)\ \hat{v}_{\text{north}} + \cos(\beta)\ \hat{v}_{\text{east}} \tag{E.4}$$

while for $\hat{u}_Y$ and $\hat{u}_Z$ in triangular-shaped interferometers we follow the conventions indicated in Figure 23.

E.1 – Geometry of ET adopted in Sections 4-5

For the case of a single ET (like the one considered in section 4 and section 5), an explicit evaluation of the d^{ab}_{1A} and d^{ab}_{1E} coefficients show that the $A-$ and the $E-$ channels can be

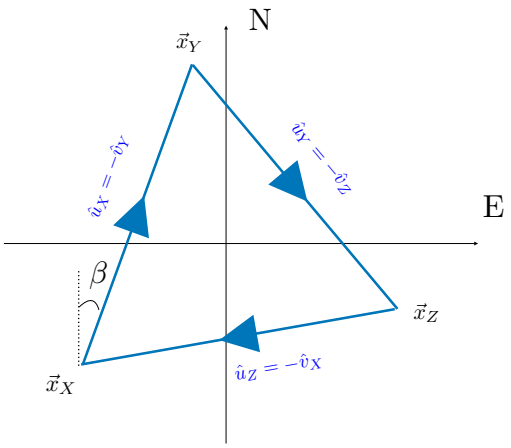

FIGURE 23: Our convention for the orientation of the three ET arms, with the labels "N" and "E" indicating, respectively, the north and east direction at the location of the interferometer, and with β being the angle formed by the direction $\hat{u}_X$ of the "first" arm and the north direction.

understood as two 90° interferometers that are shifted by 45° with respect to each other. To see this, we can imagine placing one interferometer to the north pole ($\theta = 0$), arriving to it from the meridian that joins the equator along the negative $y-$axis ($\varphi = -\frac{\pi}{2}$). In this way the $\hat{v}_{\text{east}}$ and the $\hat{v}_{\text{north}}$ directions are unit vectors oriented, respectively, along the $x-$ and $y-$ axis (as a conventional $2d$ Cartesian system in Figure 23) . One then finds that

$$d^{ab}_{1,A}(\beta) = d^{ab}_{90^\circ}\left(\frac{7\pi}{12} - \beta\right) \quad , \quad d^{ab}_{1,E}(\beta) = d^{ab}_{1,A}\left(\beta + \frac{\pi}{4}\right) \tag{E.5}$$

where $d^{ab}_{90^\circ}(\alpha)$ is the element in eq. (B.4) resulting from a 90° interferometer with the $\hat{u}$ arm (resp., $\hat{v}$ arm) oriented at a counter-clockwise angle α (resp., $\alpha + 90^\circ$) with respect to the $x-$axis.

As a consequence of the first of (E.5), $d^{ab}_{1,A}\left(\beta + \frac{\pi}{2}\right) = -d^{ab}_{1,A}(\beta)$. Combining this with the second of (E.5) results in $d^{ab}_{1,A}(\beta) = -d^{ab}_{1,E}\left(\beta + \frac{\pi}{4}\right)$. Therefore, the quantity (4.11) in section 4 and (5.15) in section 5 are at least invariant under the variation $\beta \to \beta + \frac{\pi}{4}$. One also expects that any physical result, such as the optimal SNR, should be invariant under a different labelling of the three arms. Therefore (4.11) and (5.15) should also be invariant under the variation $\beta \to \beta + \frac{2\pi}{3}$. Combining these two periodicities, we see that (4.11) and (5.15) should at least be invariant for $\beta \to \beta + \frac{\pi}{12}$. In fact, an explicit evaluation of these coefficients shows that (4.11) and (5.15) are independent of β.

E.2 – Positions and arms of existing and planned interferometers

To summarize, the table 24 displays the actual locations of the existing interferometers LIGO, Virgo and KAGRA, with the proposed ones for ET in the two sites (the one in Sardinia and the one in the Netherlands). In the table we consider $\beta = 0$, with β defined in (E.3) for both the ETs.

LIGO Hanford	Central location	$\{-0.338, -0.600, 0.725\}$
	First Arm	$\{-0.224, 0.799, 0.557\}$
	Second Arm	$\{-0.914, 0.0261, -0.405\}$
LIGO Livingston	Central location	$\{-0.0116, -0.861, 0.508\}$
	First Arm	$\{-0.953, -0.144, -0.266\}$
	Second Arm	$\{0.302, -0.488, -0.819\}$
Virgo	Central location	$\{0.712, 0.132, 0.690\}$
	First Arm	$\{-0.701, 0.201, 0.684\}$
	Second Arm	$\{-0.0485, -0.971, 0.236\}$
KAGRA	Central location	$\{-0.591, 0.546, 0.594\}$
	First Arm	$\{-0.390, -0.838, 0.382\}$
	Second Arm	$\{0.706, -0.00580, 0.709\}$
ET - Sardinia	Central location	$\{0.750734, 0.124943, 0.648682\}$
	First Arm	$\{-0.639881, -0.106494, 0.76106\}$
	Second Arm	$\{0.177765, 0.907522, -0.38053\}$
	Third Arm	$\{0.462115, -0.801028, -0.38053\}$
ET - Netherlands	Central location	$\{0.627568, 0.062529, 0.776046\}$
	First Arm	$\{-0.772223, -0.076942, 0.630676\}$
	Second Arm	$\{0.300248, 0.900229, -0.315338\}$
	Third Arm	$\{0.471974, -0.823287, -0.315338\}$

Figure 24: Cartesian coordinates of the unit-vectors specifying the positions of the interferometers and the direction of their arms, in the coordinate system described in this Appendix. For ET, we consider the configuration with $\beta = 0$, with β defined in (E.3).

Appendix F

Evaluation of the coefficients $\gamma_{\ell m,ab,cd}$

In this Appendix we evaluate the coefficients $\gamma_{\ell m,ab,cd}$. We start from eq. (5.3), where we insert the expression for the spherical harmonics,

$$Y_{\ell m}(\theta,\varphi) = \sqrt{\frac{2l+1}{4\pi}\frac{(l-m)!}{(l+m)!}}\, P_\ell^m(\cos\theta)\, e^{im\varphi} \equiv N_\ell^m\, P_\ell^m(\cos\theta)\, e^{im\varphi} \tag{F.1}$$

(θ and φ are the polar angles that specify the direction $\hat{n}$, and P_ℓ^m are the associated Legendre polynomials) and where we use the second of (A.1), to write

$$\begin{aligned}\gamma_{\ell m,ab,cd} = \frac{5}{8\pi}\int_0^\pi d\theta \sin\theta\, N_\ell^m P_\ell^m(\cos\theta) \int_0^{2\pi} d\varphi\, e^{im\varphi} \\ \times\Big\{\delta_{ac}\delta_{bd}+\delta_{ad}\delta_{bc}-\delta_{ab}\delta_{cd} \\ +\delta_{ab}\,\hat{n}_c\,\hat{n}_d+\delta_{cd}\,\hat{n}_a\,\hat{n}_b-[\delta_{ac}\,\hat{n}_b\,\hat{n}_d+\delta_{bd}\,\hat{n}_a\,\hat{n}_c+\delta_{ad}\,\hat{n}_b\,\hat{n}_c+\delta_{bc}\,\hat{n}_a\,\hat{n}_d] \\ +\hat{n}_a\,\hat{n}_b\,\hat{n}_c\,\hat{n}_d\Big\}.\end{aligned} \tag{F.2}$$

Let us first discuss the integration over the angle φ. We notice the presence of three structures, characterized by, respectively, zero, two, and four elements $\hat{n}$.

The terms with no $\hat{n}$ give

$$\int_0^{2\pi} d\varphi\, e^{im\varphi}\,\delta_{ab}\delta_{cd} = \begin{cases} 2\pi\delta_{ab}\delta_{cd} & \text{if } m=0\,, \\ 0 & \text{if } |m|>0\,, \end{cases} \tag{F.3}$$

(and identically for the other two structures in the second line of eq. (F.2)). An explicit evaluation of the terms with two $\hat{n}$ results in

$$\int_0^{2\pi} d\varphi' e^{im\varphi'}\,\delta_{ab}\hat{n}_c\hat{n}_d = \pi\delta_{ab}\begin{cases} \tilde{A}_{cd}(\theta) & \text{if } m=0\,, \\ \tilde{B}_{cd\pm}(\theta) & \text{if } m=\pm1\,, \\ \tilde{C}_{cd\pm}(\theta) & \text{if } m=\pm2\,, \\ 0 & \text{if } |m|>2\,, \end{cases} \tag{F.4}$$

where we have introduced the matrices

$$\tilde{A}_{cd}(\theta) \equiv \begin{pmatrix} \sin^2\theta & 0 & 0 \\ 0 & \sin^2\theta & 0 \\ 0 & 0 & 2\cos^2\theta \end{pmatrix} \tag{F.5}$$

$$\tilde{B}_{cd\pm}(\theta) \equiv \begin{pmatrix} 0 & 0 & \sin\theta\cos\theta \\ 0 & 0 & \pm i\sin\theta\cos\theta \\ \sin\theta\cos\theta & \pm i\sin\theta\cos\theta & 0 \end{pmatrix} \tag{F.6}$$

$$\tilde{C}_{cd\pm}(\theta) \equiv \frac{1}{2}\begin{pmatrix} \sin^2\theta & \pm i\sin^2\theta & 0 \\ \pm i\sin^2\theta & -\sin^2\theta & 0 \\ 0 & 0 & 0 \end{pmatrix} \tag{F.7}$$

Finally, an explicit evaluation of the terms with four $\hat{n}$ results in

$$\int_0^{2\pi} d\varphi e^{im\varphi}\hat{n}_a\hat{n}_b\hat{n}_c\hat{n}_d = \pi \begin{cases} \tilde{D}_{abcd} + \cos^2\theta\tilde{E}_{abcd} + \cos^4\theta\tilde{F}_{abcd} & \text{if } m = 0 \\ \sin\theta\,\cos\theta\left[\tilde{G}_{abcd\pm} + \cos^2\theta\,\tilde{H}_{abcd\pm}\right] & \text{if } m = \pm 1 \\ \left(1-\cos^4\theta\right)\tilde{I}_{abcd\pm} + \cos^2\theta\,\sin^2\theta\tilde{J}_{abcd\pm} & \text{if } m = \pm 2 \\ \cos\theta\,\sin^3\theta\,\tilde{K}_{abcd\pm} & \text{if } m = \pm 3 \\ \sin^4\theta\,\tilde{L}_{abcd\pm} & \text{if } m = \pm 4 \\ 0 & \text{if } |m| > 4 \end{cases} \tag{F.8}$$

where the matrices $D, \ldots M_\pm$ are constant (and where the $+$ and $-$ matrices are conjugate of each other). Their explicit form is not illuminating, and we do not report it here. We use the results (F.3), (F.4), and (F.8) in eq. (F.2) and we perform the remaining integration. Considering only the θ dependences, we have the following integrals (where $x = \cos\theta$)

$$\begin{aligned} N_\ell^0 \int_{-1}^{1} dx\, P_\ell(x) &= \frac{1}{\sqrt{\pi}}\delta_{\ell 0} \\ N_\ell^0 \int_{-1}^{1} dx\, P_\ell(x)\, x^2 &= \frac{1}{3\sqrt{\pi}}\delta_{\ell 0} + \frac{2}{3\sqrt{5\pi}}\delta_{\ell 2} \\ N_\ell^0 \int_{-1}^{1} dx\, P_\ell(x)\, x^4 &= \frac{1}{5\sqrt{\pi}}\delta_{\ell 0} + \frac{4}{7\sqrt{5\pi}}\delta_{\ell 2} + \frac{8}{105\sqrt{\pi}}\delta_{\ell 4} \end{aligned} \tag{F.9}$$

for the coefficient $m = 0$,

$$\begin{aligned} N_\ell^{\pm 1} \int_{-1}^{1} dx\, P_\ell^{\pm 1}(x)\, x\sqrt{1-x^2} &= \mp\sqrt{\frac{2}{15\,\pi}}\delta_{\ell 2} \\ N_\ell^{\pm 1} \int_{-1}^{1} dx\, P_\ell^{\pm 1}(x)\, x^3\sqrt{1-x^2} &= \mp\frac{1}{7}\sqrt{\frac{6}{5\pi}}\delta_{\ell 2} \mp \frac{4}{21\sqrt{5\,\pi}}\delta_{\ell 4} \end{aligned} \tag{F.10}$$

for the coefficient $m = \pm 1$,

$$\begin{aligned} N_\ell^{\pm 2} \int_{-1}^{1} dx\, P_\ell^{\pm 2}(x) \left(1 - x^2\right) &= 2\sqrt{\frac{2}{15\,\pi}}\,\delta_{\ell 2} \\ N_\ell^{\pm 2} \int_{-1}^{1} dx\, P_\ell^{\pm 2}(x) \left(1 - x^4\right) &= \frac{16}{7}\sqrt{\frac{2}{15\,\pi}}\,\delta_{\ell 2} + \frac{4}{21}\sqrt{\frac{2}{5\,\pi}}\,\delta_{\ell 4} \\ N_\ell^{\pm 2} \int_{-1}^{1} dx\, P_\ell^{\pm 2}(x)\, x^2 \left(1 - x^2\right) &= \frac{2}{7}\sqrt{\frac{2}{15\,\pi}}\,\delta_{\ell 2} + \frac{4}{21}\sqrt{\frac{2}{5\,\pi}}\,\delta_{\ell 4} \end{aligned} \tag{F.11}$$

for the coefficient $m = \pm 2$,

$$N_\ell^{\pm 3} \int_{-1}^{1} dx\, P_\ell^{\pm 3}(x)\, x \left(1 - x^2\right)^{3/2} = \mp \frac{4}{3\sqrt{35\,\pi}}\,\delta_{\ell 4} \tag{F.12}$$

for the coefficient $m = \pm 2$, and, finally

$$N_\ell^{\pm 4} \int_{-1}^{1} dx\, P_\ell^{\pm 4}(x) \left(1 - x^2\right)^2 = \frac{8}{3}\sqrt{\frac{2}{35\,\pi}}\,\delta_{\ell 4} \tag{F.13}$$

for the coefficient $m = \pm 3$.

Inserting these results, together with eqs. (F.3), (F.4), and (F.8), in eq. (F.2), we obtain the expressions given in eq. (5.6) of the main text.

F.1 – The coefficients $\gamma_{\ell m,ab,cd}$ as a low-frequency limit of (3.14)

In this appendix we derived the values of the coefficients $\gamma_{\ell m,ab,cd}$ by neglecting the value of the phase (5.1) as a first step of the treatment, and secondly computing the angular integrations in eq. (5.2), eventually obtaining (5.6). We can achieve the same results of (5.6) by considering the values of (3.14), summing over $\lambda = -1, 1$ and eventually taking the limit $\kappa \to 0$, namely

$$\gamma_{\ell m,ab,cd} = \lim_{\kappa \to 0} \sum_{\lambda = -1,1} \gamma_{\ell m,abcd}(\kappa, \hat{s}) \tag{F.14}$$

The proof of this equation is straightforward. First we consider the limit of (D.7), (D.8) and (D.12) for $\kappa \to 0$, obtaining

$$\begin{aligned}
\mathcal{M}_{ij,\lambda}(0,\hat{s}) =& \frac{\delta_{ac}\delta_{bd}+\delta_{ad}\delta_{bc}}{10} \times d_i^{ab} d_j^{cd} \\
\mathcal{D}_{iJ,\lambda}(0,\hat{s},\hat{v}) =& \frac{\lambda}{30}\left(\delta_{ac}\varepsilon_{bde}+\delta_{ad}\varepsilon_{bce}+\delta_{bc}\varepsilon_{ade}+\delta_{bd}\varepsilon_{ace}\right)\hat{v}_e \times d_i^{ab} d_j^{cd} \\
\mathcal{Q}_{ij,\lambda}(0,\hat{s},\hat{v},\hat{w}) =& \frac{1}{70}\Bigg[-\frac{11}{3}\hat{v}_e\hat{w}_e\left(\delta_{ac}\delta_{bd}+\delta_{ad}\delta_{bc}\right) + \\
&+\delta_{ac}\left(\hat{v}_b\hat{w}_d+\hat{w}_b\hat{v}_d\right)+\delta_{ad}\left(\hat{v}_b\hat{w}_c+\hat{w}_b\hat{v}_c\right)+ \\
&+\delta_{bc}\left(\hat{v}_a\hat{w}_d+\hat{w}_a\hat{v}_d\right)+\delta_{bd}\left(\hat{v}_a\hat{w}_c+\hat{w}_a\hat{v}_c\right)\Bigg] \times d_i^{ab} d_j^{cd}
\end{aligned} \tag{F.15}$$

Therefore

$$\begin{aligned}
\Gamma^M_{ab,cd}(0) &= \sum_\lambda \Gamma^M_{ab,cd,\lambda} = \frac{\delta_{ac}\delta_{bd}+\delta_{ad}\delta_{bc}}{5} \\
\Gamma^D_{ab,cd}(0,\hat{v}) &= \sum_\lambda \Gamma^D_{ab,cd,\lambda} = 0 \\
\Gamma^Q_{ab,cd}(0,\hat{v},\hat{w}) &= \sum_\lambda \Gamma^Q_{ab,cd,\lambda} = \frac{1}{35}\Bigg[-\frac{11}{3}\hat{v}_e\hat{w}_e\left(\delta_{ac}\delta_{bd}+\delta_{ad}\delta_{bc}\right) \\
&\qquad +\delta_{ac}\left(\hat{v}_b\hat{w}_d+\hat{w}_b\hat{v}_d\right)+\delta_{ad}\left(\hat{v}_b\hat{w}_c+\hat{w}_b\hat{v}_c\right) \\
&\qquad +\delta_{bc}\left(\hat{v}_a\hat{w}_d+\hat{w}_a\hat{v}_d\right)+\delta_{bd}\left(\hat{v}_a\hat{w}_c+\hat{w}_a\hat{v}_c\right)\Bigg]
\end{aligned} \tag{F.16}$$

and implementing those results into (D.1) we find back the same expressions of (5.6).

Bibliography

[1] Abbott et al. "Observation of Gravitational Waves from a Binary Black Hole Merger". In: *Phys. Rev. Lett.* 116 (6 Feb. 2016), page 061102. DOI: 10.1103/PhysRevLett.116.061102. URL: https://link.aps.org/doi/10.1103/PhysRevLett.116.061102.

[2] M Chiara Guzzetti et al. "Gravitational waves from inflation". In: *La Rivista del Nuovo Cimento* 39.9 (2016).

[3] Nicola Bartolo et al. "Science with the space-based interferometer LISA. IV: Probing inflation with gravitational waves". In: *Journal of Cosmology and Astroparticle Physics* 2016.12 (2016).

[4] Chiara Caprini and Daniel G Figueroa. "Cosmological backgrounds of gravitational waves". In: *Classical and Quantum Gravity* 35.16 (2018).

[5] Giulia Cusin et al. "Properties of the stochastic astrophysical gravitational wave background: astrophysical sources dependencies". In: *Physical Review D* 100.6 (2019).

[6] Alexander C Jenkins et al. "Anisotropies in the astrophysical gravitational-wave background: Predictions for the detection of compact binaries by LIGO and Virgo". In: *Physical Review D* 98.6 (2018).

[7] Giulia Cusin, Cyril Pitrou, and Jean-Philippe Uzan. "Anisotropy of the astrophysical gravitational wave background: Analytic expression of the angular power spectrum and correlation with cosmological observations". In: *Physical Review D* 96.10 (2017).

[8] Michael Geller et al. "Primordial anisotropies in the gravitational wave background from cosmological phase transitions". In: *Physical review letters* 121.20 (2018).

[9] Nicola Bartolo et al. "Gravitational wave anisotropies from primordial black holes". In: *Journal of Cosmology and Astroparticle Physics* 2020.02 (2020).

[10] Vasyl Alba and Juan Maldacena. "Primordial gravity wave background anisotropies". In: *arXiv preprint arXiv:1512.01531* (2015).

[11] N Bartolo et al. "Anisotropies and non-Gaussianity of the cosmological gravitational wave background". In: *Physical Review D* 100.12 (2019).

[12] Bruce Allen and Adrian C Ottewill. "Detection of anisotropies in the gravitational-wave stochastic background". In: *Physical Review D* 56.2 (1997).

[13] Neil J Cornish. "Mapping the gravitational-wave background". In: *Classical and Quantum Gravity* 18.20 (2001).

[14] Carlo Ungarelli and Alberto Vecchio. "Studying the anisotropy of the gravitational wave stochastic background with LISA". In: *Physical Review D* 64.12 (2001).

[15] Chiara MF Mingarelli et al. "Characterizing gravitational wave stochastic background anisotropy with pulsar timing arrays". In: *Physical Review D* 88.6 (2013).

[16] Matt Abernathy et al. "Einstein gravitational wave Telescope conceptual design study". In: (2011).

[17] Valerie Domcke et al. "Measuring the net circular polarization of the stochastic gravitational wave background with interferometers". In: *Journal of Cosmology and Astroparticle Physics* 2020.05 (2020).

[18] Giorgio Mentasti and Marco Peloso. "ET sensitivity to the anisotropic Stochastic Gravitational Wave Background". In: *Journal of Cosmology and Astroparticle Physics* 2021.03 (2021), page 080.

[19] Michele Maggiore. "Gravitational waves: Volume 1: Theory and experiments". In: 1 (2008).

[20] Matthew R Adams and Neil J Cornish. "Discriminating between a stochastic gravitational wave background and instrument noise". In: *Physical Review D* 82.2 (2010).

[21] Tristan L Smith and Robert R Caldwell. "LISA for cosmologists: calculating the signal-to-noise ratio for stochastic and deterministic sources". In: *Physical Review D* 100.10 (2019).

[22] S Hild et al. "Sensitivity studies for third-generation gravitational wave observatories". In: *Classical and Quantum Gravity* 28.9 (2011).

[23] "Unofficial sensitivity curves (ASD) for aLIGO, Kagra, Virgo, Voyager, Cosmic Explorer, and Einstein Telescope". In: (2020). URL: https://dcc.ligo.org/LIGO-T1500293/public.

[24] B. P. et al. Abbott. "GW170817: Implications for the Stochastic Gravitational-Wave Background from Compact Binary Coalescences". In: *Phys. Rev. Lett.* 120 (9 Feb. 2018). DOI: 10.1103/PhysRevLett.120.091101. URL: https://link.aps.org/doi/10.1103/PhysRevLett.120.091101.

[25] Nabila Aghanim et al. "Planck 2018 results-VI. Cosmological parameters". In: *Astronomy & Astrophysics* 641 (2020).

[26] "ET sensitivities page". In: (2018). URL: http://www.et-gw.eu/index.php/etsensitivities.

[27] Hideaki Kudoh and Atsushi Taruya. "Probing anisotropies of gravitational-wave backgrounds with a space-based interferometer: Geometric properties of antenna patterns and their angular power". In: *Physical Review D* 71.2 (2005).

[28] A. I. Renzini and C. R. Contaldi. "Improved limits on a stochastic gravitational-wave background and its anisotropies from Advanced LIGO O1 and O2 runs". In: *Phys. Rev. D* 100 (6 Sept. 2019), page 063527. DOI: 10.1103/PhysRevD.100.063527. URL: https://link.aps.org/doi/10.1103/PhysRevD.100.063527.

[29] Nicola Bartolo et al. "Probing non-Gaussian stochastic gravitational wave backgrounds with LISA". In: *Journal of Cosmology and Astroparticle Physics* 2018.11 (2018).

[30] M Punturo et al. "The Einstein Telescope: a third-generation gravitational wave observatory". In: *Classical and Quantum Gravity* 27.19 (2010).

[31] Michele Maggiore et al. "Science case for the Einstein telescope". In: *Journal of Cosmology and Astroparticle Physics* 2020.03 (2020).

[32] Yonadav Barry Ginat et al. "Probability distribution of astrophysical gravitational-wave background fluctuations". In: *Physical Review D* 102.8 (2020).

[33] Alexander C Jenkins et al. "Anisotropies in the astrophysical gravitational-wave background: The impact of black hole distributions". In: *Physical review letters* 122.11 (2019).

[34] Alexander C Jenkins et al. "Response to Cusin et al's comment on arXiv: 1810.13435". In: *arXiv preprint arXiv:1901.01078* (2019).

[35] Daniele Bertacca et al. "Projection effects on the observed angular spectrum of the astrophysical stochastic gravitational wave background". In: *Physical Review D* 101.10 (2020).

[36] Suvodip Mukherjee and Joseph Silk. "Time dependence of the astrophysical stochastic gravitational wave background". In: *Monthly Notices of the Royal Astronomical Society* 491.4 (2020).

[37] Giulia Cusin et al. "First predictions of the angular power spectrum of the astrophysical gravitational wave background". In: *Physical review letters* 120.23 (2018).

[38] Guadalupe Cañas-Herrera, Omar Contigiani, and Valeri Vardanyan. "Cross-correlation of the astrophysical gravitational-wave background with galaxy clustering". In: *Physical Review D* 102.4 (2020).

[39] Carlo R Contaldi. "Anisotropies of gravitational wave backgrounds: a line of sight approach". In: *Physics Letters B* 771 (2017).

[40] Nicola Bartolo et al. "Characterizing the cosmological gravitational wave background: Anisotropies and non-Gaussianity". In: *Physical Review D* 102.2 (2020).

[41] Valerie Domcke, Ryusuke Jinno, and Henrique Rubira. "Deformation of the gravitational wave spectrum by density perturbations". In: *Journal of Cosmology and Astroparticle Physics* 2020.06 (2020).

[42] L Valbusa Dall'Armi et al. "Imprint of relativistic particles on the anisotropies of the stochastic gravitational-wave background". In: *Physical Review D* 103.2 (2021).

[43] Eric Thrane et al. "Probing the anisotropies of a stochastic gravitational-wave background using a network of ground-based laser interferometers". In: *Physical Review D* 80.12 (2009).

[44] Joseph D Romano and Neil J Cornish. "Detection methods for stochastic gravitational-wave backgrounds: a unified treatment". In: *Living reviews in relativity* 20.1 (2017).

[45] B. P. et al. Abbott. "Directional Limits on Persistent Gravitational Waves from Advanced LIGO's First Observing Run". In: *Phys. Rev. Lett.* 118 (12 2017). DOI: 10.1103/PhysRevLett.118.121102. URL: https://link.aps.org/doi/10.1103/PhysRevLett.118.121102.

[46] Anirban Ain, Jishnu Suresh, and Sanjit Mitra. "Very fast stochastic gravitational wave background map making using folded data". In: *Physical Review D* 98.2 (2018).

[47] Abhishek Parida et al. "Component separation map-making for stochastic gravitational wave background". In: *arXiv preprint arXiv:1904.05056* (2019).

[48] Sambit Panda et al. "Stochastic gravitational wave background mapmaking using regularized deconvolution". In: *Physical Review D* 100.4 (2019).

[49] AI Renzini and CR Contaldi. "Improved limits on a stochastic gravitational-wave background and its anisotropies from Advanced LIGO O1 and O2 runs". In: *Physical Review D* 100.6 (2019).

[50] Yu-Kuang Chu, Guo-Chin Liu, and Kin-Wang Ng. "Spherical harmonic analysis of stochastic gravitational wave background anisotropies in interferometry experiments". In: *arXiv e-prints* (2020).

[51] Atsushi Taruya. "Probing anisotropies of gravitational-wave backgrounds with a space-based interferometer. III. Reconstruction of a high-frequency sky map". In: *Physical Review D* 74.10 (2006).

[52] David Alonso et al. "Noise angular power spectrum of gravitational wave background experiments". In: *Physical Review D* 101.12 (2020).

[53] Carlo R Contaldi et al. "Maximum likelihood map making with the Laser Interferometer Space Antenna". In: *Physical Review D* 102.4 (2020).

[54] Stephen R Taylor and Jonathan R Gair. "Searching for anisotropic gravitational-wave backgrounds using pulsar timing arrays". In: *Physical Review D* 88.8 (2013).

[55] Selim C. Hotinli, Marc Kamionkowski, and Andrew H. Jaffe. "The search for anisotropy in the gravitational-wave background with pulsar-timing arrays". In: *Open J. Astrophys.* 2.1 (2019). DOI: 10.21105/astro.1904.05348. arXiv: 1904.05348 [astro-ph.CO].

[56] Naoki Seto and Asantha Cooray. "LISA measurement of gravitational wave background anisotropy: Hexadecapole moment via a correlation analysis". In: *Physical Review D* 70.12 (2004).

[57] Hideaki Kudoh et al. "Detecting a gravitational-wave background with next-generation space interferometers". In: *Physical Review D* 73.6 (2006).

[58] Atsushi Taruya and Hideaki Kudoh. "Probing anisotropies of gravitational-wave backgrounds with a space-based interferometer. II. Perturbative reconstruction of a low-frequency skymap". In: *Physical Review D* 72.10 (2005).

[59] David Reitze et al. "Cosmic explorer: the US contribution to gravitational-wave astronomy beyond LIGO". In: *arXiv preprint arXiv:1907.04833* (2019).

[60] "Gravitational Wave Detectors and Sources". In: (2019). URL: http://www.gwplotter.com.

[61] Christopher J Moore, Robert H Cole, and Christopher PL Berry. "Gravitational-wave sensitivity curves". In: *Classical and Quantum Gravity* 32.1 (2014).

[62] SG Crowder et al. "Measurement of parity violation in the early universe using gravitational-wave detectors". In: *Physics Letters B* 726.1-3 (2013).